Towards Hydrogel-Capped Metal Implants for Cartilage Repair

by

Jiacheng Zhao

Department of Chemistry
Duke University

Date:_____

Approved:

_____
Benjamin J. Wiley, Supervisor

_____
Kenneth Gall

_____
Jie Liu

_____
Stefan Zauscher

Dissertation submitted in partial fulfillment of
the requirements for the degree of Doctor
of Philosophy in the Department of
Chemistry in the Graduate School
of Duke University

2022

ABSTRACT

Towards Hydrogel-Capped Metal Implants for Cartilage Repair

by

Jiacheng Zhao

Department of Chemistry
Duke University

Date:_____

Approved:

_____

Benjamin J. Wiley, Supervisor

_____

Kenneth Gall

_____

Jie Liu

_____

Stefan Zauscher

An abstract of a dissertation submitted in partial fulfillment of the requirements for the degree of Doctor of Philosophy in the Department of Chemistry in the Graduate School of Duke University

2022

Abstract

There are approximately 900,000 people in the US suffering from damage to the articular cartilage, with the knee being most commonly affected. Articular cartilage lacks a vasculature and has a limited ability to heal. A variety of surgical treatments have been developed to repair cartilage lesions. Current strategies for cartilage repair include microfracture, autologous chondrocyte implantation (ACI) and osteochondral allograft transfer (OAT). These strategies suffer from high failure rates (25-50% at 10 years), long rehabilitation times (more than 12 months) and decreasing efficacy in patients older than 40-50 years. Focal joint resurfacing with traditional orthopedic materials is being explored as an alternative strategy, but due to their high stiffness and coefficient of friction relative to cartilage, these implants may ultimately contribute to joint degeneration through abnormal stress and wear. A focal joint resurfacing method that is widely available, allows immediate weight bearing, has short recovery times and has low long-term failure rates remains an unmet need.

This thesis explores a strategy to address this need. There are two major criteria within this strategy: 1) develop a material that mimics the properties of cartilage and 2) attach this material to an orthopedic base to enable integration with bone.

I developed the first hydrogel to achieve the strength and modulus of cartilage in both tension and compression properties. This hydrogel also exhibits cartilage-equivalent tensile fatigue at 100,000 cycles. The hydrogel was created by infiltrating a PVA-PAMPS double-network hydrogel into a bacterial cellulose (BC) nanofiber network. The BC fibers provide tensile strength in a manner analogous to collagen in cartilage. The PAMPS

provides a fixed negative charge and osmotic restoring force similar to the role of aggrecan in cartilage.

Subsequently, I further improved and developed the hydrogel to reach a strength that exceeds that of cartilage. The high strength was achieved through reinforcement of crystallized PVA with BC. Experimental results show that reinforcement of annealed PVA with BC leads to a 3.2-fold improvement in the tensile strength (from 15.6 to 50.5 MPa) and a 1.7-fold increase in the compressive strength (from 56.7 to 95.4 MPa). The BC-reinforced PVA was also 3 times more wear resistant than cartilage over 1 million cycles and exhibited the same coefficient of friction. These properties make the BC-reinforced BC hydrogel an excellent candidate material for replacement of damaged cartilage.

Current strategies for adhering hydrogel to a surface are 10 times weaker than the shear strength with which cartilage is attached to bone. The osteochondral junction is characterized by mineralized collagen nanofibers anchoring cartilage to bone. I sought to mimic this strategy by bonding freeze-dried BC to porous titanium with a hydroxyapatite-forming cement. The cement penetrates about 10 microns into the bacterial cellulose, forming a nanofiber-reinforced zone of adhesion. The PVA-PAMPS hydrogel is then infiltrated into the bonded bacterial cellulose. This strategy achieved a shear strength of attachment three times greater than the state of the art.

I soon proposed an important enhancement of the attaching strategy by introducing shape memory alloy ring to change the direction of shear load bearing. It is the first method for attaching a hydrogel to metal with the same shear strength as the cartilage-bone interface. The average shear strength of the junction between 1.2-mm-thick hydrogel and

metal made in this manner exceeded the shear strength of porcine cartilage-bone interface. The shear strength of attachment increased with the number of bacterial cellulose layers and with the addition of cement between the bacterial cellulose layers. Such improved strategies for attaching hydrogels to a metal surface with sufficient strength to allow for weight-bearing can enable the creation of hydrogel-capped titanium implants for cartilage repair.

Contents

List of Tables

List of Figures

Acknowledgements

First, I would like to say thank you to my PI, Prof. Benjamin Wiley. His support and guidance helped me all the way through the past four years, enlightened my research and made me a much better person compared to where I started. Alongside with his help on my research, he also provided me with rare chances to work on real-life application projects which allowed me to greatly broaden my eyesight and be much more prepared for my career after graduation. I also would want to thank all of my committee members, Prof. Ken Gall, Prof. Jie Liu and Prof. Stefan Zauscher for your help and advice during the past four years. Prof. Zauscher also sacrificed his off time to attend my thesis defense and I would want to express my additional gratitude to him.

Second, I would like to thank all my collaborators including Dr. Feichen Yang, Dr. Huayu Tong, Heng, Shichen, Andrew from our lab, Dr. Will Koshut, Dr. Alina kirillova, Dr. Cambre Kelly from Ken's lab and Natasha from Becker's lab. My accomplishments cannot be made possible without your help, and it was my greatest pleasure to have the chance to work with you all.

Third, I want to thank all of my friends Xu Han, Mary Lu, Siyuan Zhu, Yun Tang, Shuai Li, Xinye Qian and many more for the highs and lows we experienced together, for the time we spent together and most importantly, for being with me for the past four years.

Last but not least, I would like to say a special thank you to my parents. I have not got the chance to see you in person for the past three years due to COVID travel restriction. I know you missed me just as much as I missed you. Now I am reaching a special and

important milestone of my life, I really hope what I achieved today can make you smile and be proud of me at the same time.

1. Introduction

1.1 Cartilage Repair

Articular cartilage is a thin layer (2-4 mm) of specialized tissue that lines the ends of bones in joints[1] such as the shoulder, elbow, wrist, fingers, hip, knee, ankle, and toes. Every year, approximately 900,000 people in the United States suffer from damage to the articular cartilage that lines the ends of the bones, with the knee being most commonly affected.[2] Articular cartilage has great mechanical properties to support our body weight and reduce the shock brought by our movements. However, cartilage also has a limited ability to heal due to the lack of blood vessels and nerves and is strongly associated with joint pain, disability, and osteoarthritis.[3, 4] Thus, the restoration of malfunctioned articular cartilage has become more popular and demanding so that a complete knee replacement can be prevented or delayed.

Current strategies for cartilage restoration include bone marrow stimulation (microfracture), autologous cartilage cell implantation, and osteochondral transplantation. These methods typically have high failure rates (25-50% at 10 years), prolonged rehabilitation times (> 12 months), can be very costly, and show decreasing efficacy in patients older than 40-50 years.[4, 5]

Focal joint resurfacing with traditional orthopedic materials is being explored as an alternative strategy, but these implants have limited ability to biologically integrate, and there are concerns they may contribute to joint degeneration through abnormal stress and wear.[6, 7]

Thus, an all-new cartilage repair method combining the strength of traditional strategies and focal joint resurfacing is in great need to improve[8] the quality of life for millions of people, while mitigating the $100 billion per year economic burden imposed by osteoarthritis in the USA alone.

1.2 Hydrogel for Cartilage Focal Resurfacing

Hydrogels are a promising solution for cartilage repair because, like cartilage, they mostly consist of water and thus have a surface with a low coefficient of friction. The first hydrogel implant, which consisted of polyvinyl alcohol (PVA) and was developed by Cartiva, was approved by the Food and Drug Administration (FDA) in July 2016 for treating arthritis in the big toe joint. However, nearly all hydrogels currently lack the mechanical strength, stiffness, and durability under cyclic load to be a suitable replacement for cartilage in load-bearing joints.

To act as a replacement for cartilage defects and serve all the key functions of cartilage, the ideal hydrogel materials need to have similar or better properties in mechanical strength and stiffness, dynamic modulus, tribology and fatigue. In addition, it obviously must be biocompatible, and similar to focal resurfacing devices should integrate with surrounding tissue to enable long-term integration in the defect site.

Failure to reach similar properties comparing to cartilage will lead to increased damage of the hydrogel and/or the surrounding tissue. If the mechanical strength, wear resistance or fatigue strength of a hydrogel replacement is inferior to natural cartilage, by definition, it will undergo excess damage during repetitive normal activities[9, 10]. If the COF of the hydrogel is too high, it will cause damage to the opposing cartilage surface.

Ideally, the goal is to create a material that can be implanted into a defect site and stay functional for more than 10 years delaying or preventing degradation of the surrounding native cartilage. This material would also need to be adhered to the bone or a substate that can integrate with the bone with the same shear-strength as the natural osteochondral junction.

1.2.1 Mechanical Properties

As a replacement of cartilage, desired hydrogel should have similar level of mechanical properties including tensile strength, compressive strength, tensile modulus and compressive modulus in order to support various kinds of movements of our body. According to previous research, articular cartilage has a tensile strength range of 8.1-40 MPa, a compressive strength range of 14-59 MPa, a tensile modulus of 58-228 MPa and a compressive modulus of 8.1-20 MPa. [10-12] Mechanical properties of different kind of strong hydrogels are shown in Table 1.

Table 1: Mechanical properties of annealed BC-PVA, annealed BC-PVA-PAMPS, annealed PVA hydrogels, cartilage, and previously reported hydrogels.

Composition	Tensile Strength (MPa)	Tensile Modulus (MPa)	Compressive Strength (MPa)	Compressive Modulus (MPa)	Reference Number
Freeze-thawed BC-PVA	11.1	115.3	55.3	15.0	This work
Annealed BC-PVA	50.5	503.9	98.1	9.57	
Annealed BC-PVA-PAMPS	22.1	179.0	60.4	16.5	
Annealed PVA	15.6	24.5	56.7	12.1	
Freeze-thawed PVA	0.26	<0.14	14.8	2.41	
Human cartilage	8.1-40	58-228	14-59	8.1-20.1	11-13
BC-PVA-PAMPS	22.6	227	23.0	15.2	14
CNC-PA-PAAm	16.5	232.4	31.1	65.4	15
BC-PAAm	40	114	5.1	10	16
Polyaramid nanofiber-PVA	5	9.1	4	26.5	17
BC-gelatin	3.8	21	5.3	2.9	18
PVA-Agarose	14.6	6.38	3.66	0.09	19
PVA-HA/HAAC	3.05	0.7	40.15	0.88	20
3D printed PCL scaffold-PVA	4.41	9.53	3	1.2	21
PVA-CS	4.02	2.07	18	1.5	22

(a) Abbreviations used in this table: BC: bacterial cellulose; PVA: Poly(vinyl alcohol); PAMPS: poly(2-acrylamido-2-methyl-1-propanesulfonic acid sodium salt); PAAm: polyacrylamide; CNC: cellulose nanocrystal, PA: phenyl acrylate; HA: hydroxyapatite, HACC: 2-hydroxypropyltrimethyl ammonium chloride chitosan, PCL: polycaprolactone, CS: chitosan

(b) For the sake of clarity, the references in this table were limited to publications that report all four metrics, i.e., strength and modulus in tension and compression, and had a tensile and compressive strength higher than 3 MPa.

Different strategies were employed to increase the tensile strength and modulus of hydrogels to reach the cartilage equivalence range, including fiber reinforcement[23, 24], secondary bonding[25, 26], ionic crosslinking[27, 28], double network hydrogel[29], polymer chain alignment[30], etc.

Various secondary bandings can be used to increase the crosslinking density of a hydrogel and increase the strength. Cong et al[31] synthesized a hydrogel with cellulose nanocrystal and a network of poly(phenyl acrylate-co-acrylamide) and reported a tensile strength of 16.5 MPa. Hydrogen bonding is another promising secondary bonding to strengthen hydrogels. Zheng et al[32] created a supramolecular hydrogel with a poly(methacrylic acid-co-methacrylamide) and achieved a tensile strength of 8.3 MPa and a tensile modulus of 217.3 MPa. The hydrogel was also self-healing because of the reversible nature of the hydrogen bonding. The ionic bonding between metal ions and organic ligands in the polymer network creates an effective energy dissipation mechanism and can increase the toughness and strength of a hydrogel. Nie et al[25] introduced iron (III) ions into a poly(acrylamide-co-acrylic acid)-sodium alginate hydrogel and reported a tensile strength of 10.4 MPa and a tensile modulus of 24.6 MPa. The toughness of the hydrogel was ~4800 J m-2.

To increase the compression strength and modulus of hydrogels to reach that of cartilage, researchers have employed a number of different mechanisms including introducing hydrogen bonding[33], nanocomposite[34] or creating double network[35] or mineralize hydrogels[36].

Hydrogen bonds are commonly used for strengthening hydrogels. Qiu et al[37] utilized sodium phytate (with 6 hydrogen bonding sites per molecule) to crosslink a chitosan and gelatin hydrogel and achieved a compressive strength as high as 64 MPa. By adding nanoparticles, a hydrogel-nanoparticle composite can be created with high degree of physical crosslinking with a high strength[38, 39]. Silica based nanoparticles are a commonly used family of particles. For example, Yang et al added a silica nanoparticle (Laponite RDS) to the traditional PAMPS-PAAm double network hydrogel and increased the compressive strength to 61 MPa[40]. Double network hydrogel is a family of hydrogels that have two or more interpenetrating polymer networks[41]. Gong et al[41] reported the first tough double network hydrogel consisting of a stiff first network of poly(2-acrylamido-2- methyl-1-propanesulphonic acid) (PAMPS) and a ductile second network of polyacrylamide (PAAm), exhibiting a compressive strength of 17.2 MPa. The high strength of double network hydrogels is attributed to a local yielding effect, which means the first network fractures when exposed to stress, leading to energy dissipation without the failure of the whole hydrogel[41].

1.2.2 Crystallized PVA for Improving Mechanical Properties

Polyvinyl alcohol (PVA), as shown in Figure 1[49], is a semicrystalline, hydrophilic, linear synthetic polymer that is synthesized by hydrolyzing polyvinyl acetate. PVA is water

soluble above its glass transition, non-toxic, biodegradable, biocompatible, and its production does not rely on petroleum[42]. It also possesses favorable mechanical properties for various applications including attachment to biocompatible implants[43-48].

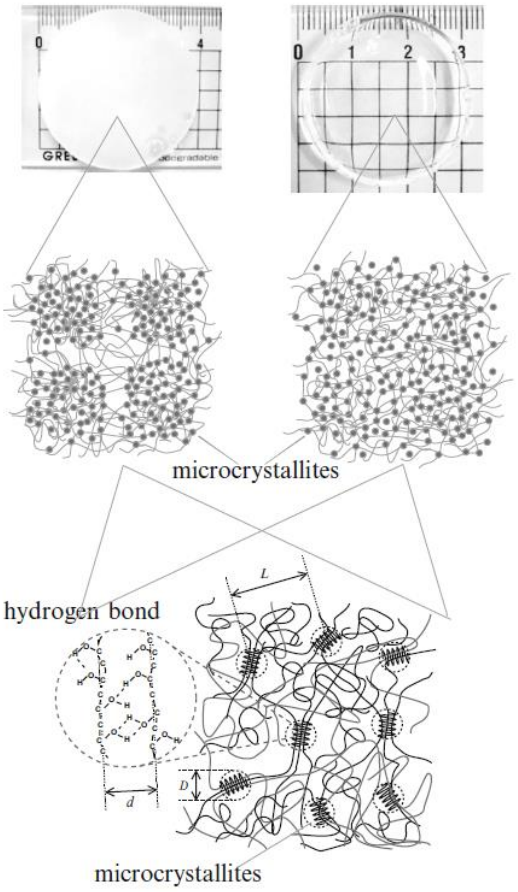

Figure 1: Schematic Illustration of the network structure of Physical PVA gel in multi-scale (milli-, micro, and nanoscales). Consist of a swollen amorphous network of PVA physically crosslinked by micro-crystallites.

Due to the abundance of hydrogen bonds, PVA can form crystallite alongside its amorphous zone. The molecular structure of PVA crystallite has been examined. Instead of a regular simple plane zigzag b-projection in which all of the hydroxyl groups lie on the

same side of the zigzag plane, PVA crystallite is more likely to have a random placement of hydroxyl group in the left-hand and right-hand position forming a c-projection[50].

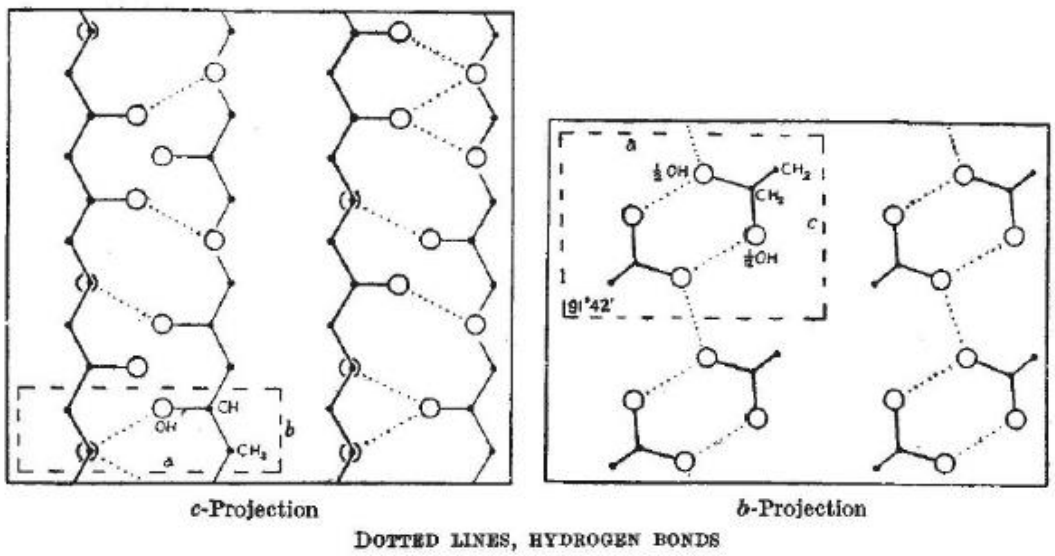

Figure 2: c-Projection and b-projection of PVA crystallite structure.

This arrangement, as shown in Figure 2, may be described as a layer structure with a double layer of molecules held together by hydrogen bonds and one double layer and the next layer held by weaker Van der Waals forces[50-52]. A folded chain structure of PVA chains leads to small, ordered regions or crystallites scattered in an unordered, amorphous polymer matrix[53]. In polymers, these crystallites can have different secondary and tertiary structure including lamelles, spherulite and platelets as shown in Figure 3[54]. These structures essentially served as additional crosslinks to redistribute external stresses among initial crosslinks and introduced crystallites[55, 56]. Under externally applied stress, the tertiary structure can approach a "shish kebab" arrangement, where there are planes of platelets separated by areas where there exist both crystalline and amorphous regions as illustrated in Figure 4[54]. These structures often organize into quaternary structures

consisting of bundles of “shish kebab” single-strand filament forming fibrils. The amorphous regions within these structures confer onto the material some flexibility while to crystalline platelets give the material strength. This combination of amorphous flexibility and crystalline strength and brittleness together provide the material with great overall mechanical strength[54]. So, it is pretty clear that a too high crystallinity is deleterious for the elasticity an makes the gels more fragile, whereas if crystallinity is too low, gels are poorly coherent and rather sticky. Therefore, it is very important to control the crystallinity of PVA hydrogels[57].

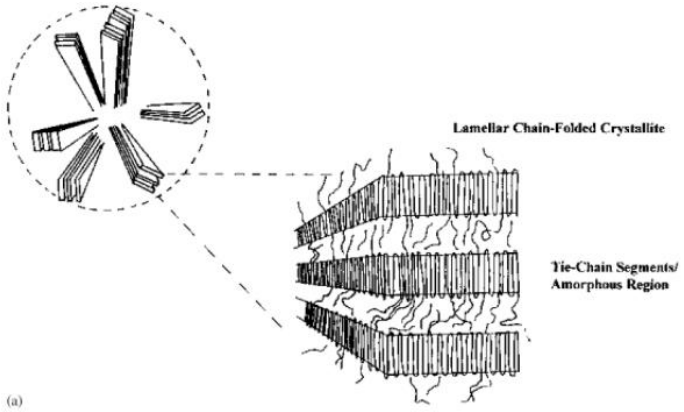

Figure 3: Spherulite structure showing the molecular-level lamellar chain-folded platelets and tie and frayed chain arrangements.

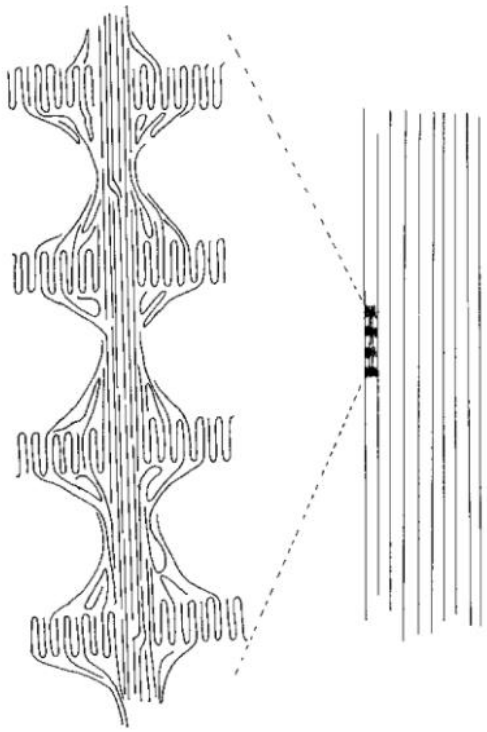

Figure 4: Crystalline polymer structures formed under applied. (Left) The tertiary mono-fibrilar structure including platelets and (right) these mono-fibrilar structures bundled together forming a quaternary structure fibril.

1.2.2 Coefficient of Friction (CoF) and Wear

Articular cartilage plays an important role in the lubrication of a joint such as the hip and the knee, due to its extremely low friction and minimum wear even under heavily load conditions[58]. This superior tribological performances is likely the result of not a single lubrication mode, but the synergistic combination of various lubrication modes depending on the severity of the operation condition[59]. Under different conditions, cartilage shows a combination of different lubrication modes like soft-elastohydrodynamic lubrication[60-63], biphasic lubrication[64-66], hydration lubrication[67-70], boundary lubrication[71-75].

These mechanisms can be divided into two general categories: fluid film and boundary lubrication[76]. In the fluid film category, a layer of viscous fluid with the thickness larger

than the surface roughness forms to partially or completely bear load and prevent contact of the articular surface. Under the conditions not suitable for fluid film lubrication like low sliding speeds, high load and low fluid viscosity, the articular surfaces are only separated by a boundary layer of a molecular film[77]. For articular cartilage, molecules in the synovial fluid like hyaluronic acid[78], proteoglycan[79, 80], and phospholipids[81] absorbs to the articular surface and contribute to the boundary lubrication. During the walking cycle, the articular cartilage bears a wide range of stress and sliding speeds[76]. Therefore, cartilage exhibit a mixed lubrication where both fluid film and boundary lubrication are both contributing.

For an effective cartilage repair, a hydrogel material ideally has a low coefficient of friction against a piece of articular cartilage under the physiological environment on top of the sufficient mechanical strength and modulus. Therefore, only those lubricative hydrogels that have cartilage equivalent strength will be discussed in this section. Generally, a strong hydrogel with a low COF should have good wear resistance[82, 83]. However, the long-term wear test was relatively under-studied among papers about cartilage-equivalent hydrogels.

1.2.3 Fatigue Properties

As a cartilage repair material, hydrogels would be exposed to cyclic stress in vivo. To prolong the lifetime of the implant (ideally >10 years), hydrogels must not fail after a very large number of stress cycles. When evaluating the Cartiva implant, 5 million cycles of fatigue tests were run to represent the equivalent of 5 years of continuous use.

Jenkins et al and Weightman et al characterized the fatigue behavior of articular cartilage by measuring the fatigue tensile strength after large numbers of cycles[84, 85]. They concluded a quantitative correlation between the tensile fatigue strength under a certain number of

cycles and the age of the cartilage. Generally, the tensile fatigue strength decreases linearly when the age of the cartilage increases. The ultimate goal of a hydrogel with cartilage equivalent strength is to also achieve a fatigue strength after a large number of cycles, e.g., 10 million cycles.

However, because directly measuring the fatigue strength of hydrogels is very time-consuming and needs specialized instruments, most of the researchers choose other methods to test and demonstrate the fatigue resistance for hydrogels.

One of the most commonly methods used is comparing the stress-strain curve over several cycles of loading and unloading. Shown in Figure 21A, Kotov et al[86] tested the fatigue resistance of an aramid fiber-PVA hydrogel that exhibited cartilage equivalent compressive strength with 5 cycles of tensile strain. They reported that the hydrogel samples retained >91% of the maximum stress after 5 cycles, and therefore demonstrate reconfigurability and fatigue resistance. Lu et al[87] applied 20,000 cycles of 30% compressive strain on a PAN/PMPC hydrogel with cartilage equivalent compressive strength.

Self-healing hydrogels generally have good fatigue resistance because of their ability to repair its mechanical strength over time. Researchers also test the self-recovery of hydrogels to demonstrate fatigue resistance. Luo et al synthesized a PVA-agar-ammonium sulfate hydrogel that exhibited a cartilage-equivalent tensile strength of 18 MPa[88]. Then, they conducted 10 tensile loading-unloading cycles on the samples, followed by healing at 90° C for 30 minutes. After 30 minutes, they reported a 56.8% recovery of energy dissipation capacity.

1.3 Hydrogel Attachment

Hydrogels can be created to have a similar stiffness and coefficient of friction as cartilage, thereby addressing concerns related to abnormal stress and wear[89]. However, there is currently no way to secure a hydrogel into a cartilage defect site with the same shear strength as the osteochondral junction (7.25±1.35 MPa)[90]. One of the strongest tissue adhesives is cyanoacrylate, which has been reported to achieve a lap shear strength of 0.7 MPa between two pieces of cartilage[91]. In contrast, cyanoacrylate bonds nylon to nylon and steel to steel with a shear strength of 2.8 and 7.3 MPa[92, 93], respectively. This comparison suggests that the presence of interfacial water in cartilage (cartilage is 60-85% water by weight)[94] hinders the creation of a stronger bond. Indeed, mussel and spider glues have mechanisms to displace interfacial water so as to create stronger bonds[95, 96]. This phenomenon has inspired the development of dry, tissue-bonding double-sided tape[97]. Thus, removal of water is an important strategy for forming strong bonds to hydrogels.

Another strategy to form strong bonds to hydrogels is to mimic the bonding of cartilage to bone[98]. The osteochondral junction is characterized by a layer of collagen nanofibers extending from the deep zone of cartilage into a mineralized region that is attached to subchondral bone through an interdigitated interface[99, 100]. In this way the collagen nanofibers that give cartilage its excellent tensile strength also anchors it to the surface of bone.

2. A Synthetic Hydrogel Composite with The Mechanical Behavior and Durability of Cartilage*

*This chapter adapted from F. Yang; J. Zhao; W. J. Koshut; J. Watt; J. C. Riboh; K. Gall; et al. A Synthetic Hydrogel Composite with the Mechanical Behavior and Durability of Cartilage. Adv. Funct. Mater. 2020 Vol. 30 Pages 2003451

2.1 Introduction

Every year, approximately 900,000 people in the United States suffer from damage to the articular cartilage that lines the ends of the bones, with the knee being most commonly affected.[101] Articular cartilage lesions have a limited intrinsic ability to heal and often lead to osteoarthritis.[102] Treatment of cartilage lesions can alleviate debilitating pain and delay the need for a total knee replacement.[103-106] Current strategies for cartilage restoration include bone marrow stimulation (microfracture), autologous cartilage cell implantation, and osteochondral transplantation.[107-110] These methods typically have high failure rates (25-50% at 10 years), prolonged rehabilitation times (> 12 months), and show decreasing efficacy in patients older than 40-50 years.[102, 106] Focal joint resurfacing with traditional orthopedic materials (e.g. cobalt-chromium alloy, ultra-high-molecular-weight polyethylene) is being explored as an alternative strategy, but due to their high stiffness, these implants may ultimately contribute to joint degeneration through abnormal stress and wear.[6, 7] The "holy grail" of cartilage restoration is a cost-effective procedure that can immediately and durably restore the mechanical function of cartilage.

Hydrogels have been extensively explored as a cartilage substitute because, like cartilage, they mostly consist of water and have a low permeability, giving them a very low coefficient of friction (COF). However, current hydrogels do not have sufficient

mechanical strength and durability under cyclic loading and wear conditions to serve as a load-bearing cartilage replacement. For example, Figure 5A shows that no previously reported gel achieved both the tensile and compressive strength of cartilage (see Table 1 for the data and references). If a synthetic hydrogel is to be used for replacement of cartilage, it should have at least the strength of cartilage so that it does not fail during a return to sporting activities. A hydrogel replacement for cartilage should also have the same time-dependent mechanical properties as cartilage to ensure a normal stress-distribution, as well as a fatigue strength and wear resistance the same as or better than cartilage to ensure durability.

This chapter describes a biomimetic approach to create the first hydrogel that has the strength and modulus of cartilage in both tension and compression (see Figure 5A&B). This hydrogel consists of BC, PVA, and poly(2-acrylamido-2-methyl-1-propanesulfonic acid sodium salt) (PAMPS), so we refer to it as the BC-PVA-PAMPS hydrogel. As demonstrated in Figure 5C&D, a cylindrical sample of BC-PVA-PAMPS hydrogel (59% water) with a diameter of 20 mm exhibited <5% strain under a 100 lb. weight (a compressive stress of 1.43 MPa). To put this into context, a 200 lb (890 N) human will have a peak force of 3000 N on the knee during walking, corresponding to a mean contact stress of 2.5 MPa.[111] In comparison, a double network hydrogel consisting of PAMPS and polydimethylacrylamide (PAMPS-PDMAAm) of the same diameter fractured under the 100 lb load even though it has been reported to exhibit a compressive strength of 3.1 MPa.[18] Although the PAMPS-PDMAAm hydrogel has been extensively studied for treatment of cartilage defects,[112, 113] it appears to be too weak to be used in the human knee. A

comparison with a polyvinyl alcohol (PVA) hydrogel was also made as it has received FDA approval to treat arthritis of the first metatarsophalangeal (MTP) joint.[114] A PVA hydrogel exhibited significant deformation (>20%) due to its low compressive modulus (0.31-0.8 MPa).[115] Such a large deformation means that PVA alone would transfer stress to the surrounding cartilage and bone if used as synthetic cartilage in the knee. In contrast, the BC-PVA-PAMPS hydrogel has the compressive strength and modulus necessary to potentially serve as a weight-bearing replacement for cartilage.

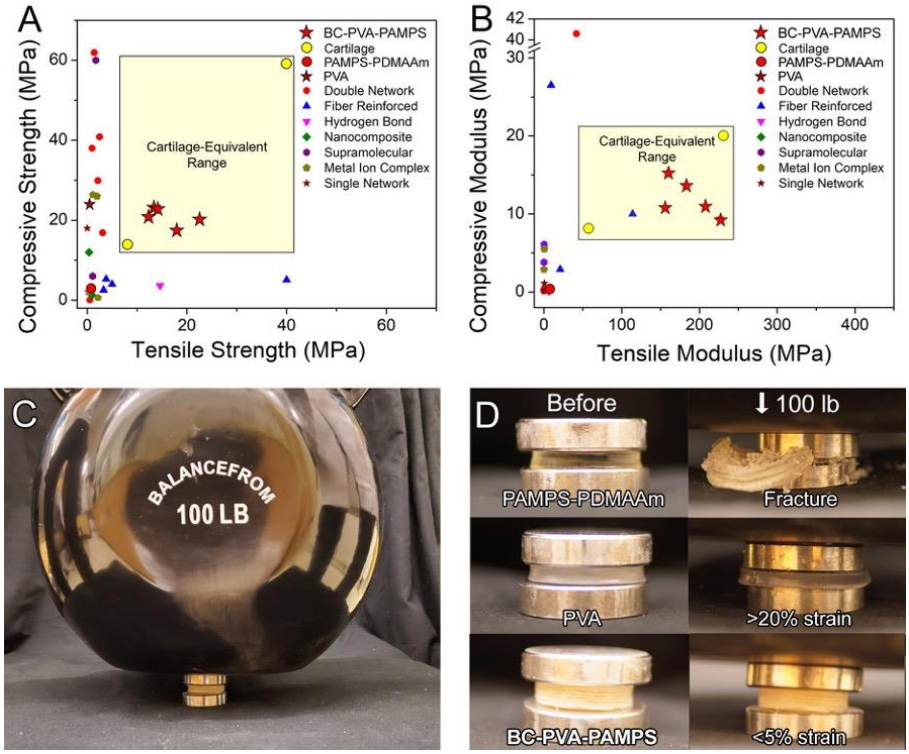

Figure 5: (A&B) A plot of the compressive vs. tensile strength and modulus for BC-PVA-PAMPS (this work) and other strong hydrogels (see Table 1 for data and references). The multiple data points for BC-PVA-PAMPS are for different compositions. (C) BC-PVA-PAMPS easily bears the weight of a 100 lb. kettlebell. (D) Cylinders of PAMPS-PDMAAm, PVA, and BC-PVA-PAMPS hydrogel before and after compression with 100 lbs.

2.2 Materials and Methods

2.2.1 Fabrication of BC-PVA-PAMPS Hydrogel

BC sheets were pressed to a controlled thickness between 2 aluminum plates (typically 0.5 mm, controlled by spacers between the aluminum plates) and placed into a hydrothermal reactor with a mixture of PVA (40 wt.%) and DI water (60 wt.%). The hydrothermal reactor was sealed and heated at 135°C for 24 hours to allow the PVA to diffuse into the voids of BC and form a BC-PVA hydrogel. The BC-PVA hydrogel was removed from the reactor when hot (>85°C). Note the hydrothermal reactor was pressurized with hot steam and created a burn hazard, so personal protective equipment including lab coat, heat resistant gloves and full-coverage face shields should be used when opening the reactor. The residual PVA solution was removed by scrapping the surface of the BC-PVA samples with a metal spatula. The samples were frozen in a -78°C fridge for 30 minutes and thawed at room temperature to physically crosslink the PVA network. The BC-PVA hydrogel was then soaked in a solution of AMPS (30 wt.%), MBAA (60 mM), I2959 (50 mM) and KPS (0.5 mg mL-1) for 24 hours. The hydrogel was cured with a UV transilluminator (VWR International) for 15 minutes on each side, and further cured in an oven at 60°C for 8 hours to ensure even and complete curing. The resulting BC-PVA-PAMPS hydrogel was stored in PBS for at least 24 hours before further characterization.

2.2.2 Fabrication of The PVA Hydrogel

To fabricate PVA hydrogel with a PVA concentration of 40 wt.%, a slurry of PVA (40 wt.%) and DI water (60 wt.%) were mixed in a glass petri dish (diameter: 90 mm) and heated at 121°C for 30 minutes in an autoclave sterilizer. The resulting hydrogel was frozen

in a -78°C fridge for 30 minutes and thawed to room temperature. The hydrogel was frozen and thawed for 4 additional cycles. The resulting PVA hydrogel was cut into the desired shape and stored in 0.15 M PBS for at least 24 hours before tests.

2.2.3 Fabrication of PAMPS-PDMAAm Hydrogel

The PAMPS hydrogel was synthesized following a modified procedure from previous work.[112] An aqueous solution of AMPS (1 M), MBAA (40 mM) and I2959 (50 mM) was made and cast in a silicone rubber mold and sandwiched between a pair of glass slides. The solution was cured with a UV transilluminator (VWR International) for 1 hour on each side. The PAMPS hydrogel was then removed from the mold and submerged in an aqueous solution of DMAAm (3 M), MBAA (3 mM) and I2959 (50 mM) for 24 hours. The hydrogel sample was then cured with a UV transilluminator for 30 minutes on each side to form a PAMPS-PDMAAm double network hydrogel. The resulting hydrogel was soaked in 0.15 M PBS for at least 24 hours before mechanical testing.

2.2.4 Fabrication of PVA-PAMPS Hydrogel

PVA hydrogel was made with the previously described procedure (see section 2.2.2). The PVA hydrogel was then soaked in a solution of AMPS (30 wt%), MBAA (60 mM), I2959 (50 mM) and KPS (0.5 mg mL^{-1}) solution for 24 hours. The hydrogel was cured with a UV transilluminator (VWR International) for 15 minutes on each side, and then heat cured in an oven of 60°C for 8 hours to ensure even and complete curing. The resulting PVA-PAMPS hydrogel was stored in 0.15 M PBS for at least 24 hours before tests.

2.2.5 Tension Tests

Monotonic tensile measurements were carried out on an Instron 1321 (Instron, Norwood, MA, USA) instrument as well as a TestResources 830 (TestResources, Shakopee, MN, USA) load frame at a rate of 0.25 mm s-1. Monotonic samples in an ASTM D638-14 Type V shape with a titanium hollow punch that was created through additive manufacturing. The dimensions of the samples were measured with a caliper before testing. The ultimate tensile strength (UTS) was the maximum stress measured before fracture. The tensile modulus was taken as the slope of the stress-strain curve at a stress of 1 MPa for comparison with previous studies of human cartilage.[12]

2.2.6 Compression Tests

The compressive properties of all samples were measured with an axial Torsion System (Test resources 830LE63). The cylindrical samples were cut out of films of hydrogel samples with a hollow steel punch (diameter: 4 mm). The dimensions of the samples were measured with a caliper before testing. The compressive properties were measured with a strain rate of 0.05 s^{-1}. The ultimate compressive strength was taken as the maximum stress measured before fracture. The compressive modulus was derived as the slope of the stress-strain curve at a stress of 0.4 MPa. The 0.4 MPa stress point was chosen for comparison with previous studies of human cartilage.[10]

2.2.7. Fatigue Resistance

Hydrogel samples for fatigue were prepared in an ASTM D638-14 Type V shape. Samples were initially analyzed for their ultimate tensile strength (UTS) in monotonic tension in a

37°C tap water bath. A minimum of four samples for each hydrogel was tested to obtain an average UTS value, which are listed in Table 2.

Table 2: Swelling ratios of hydrogel with different formulations

BC Weight Fraction (w.t.%)	PVA Concentration (w.t.%)	PVA Molecular Weight (g mol-1)	AMPS Concentration (w.t.%)	MBAA Concentration (mM)	Swelling ratio	Water Content (w.t. %)	Comment
22.1%	40%	146k	30%	60	2.46	59.4	BC-PVA-PAMPS
0	40%	146k	30%	60	2.69	62.8	PVA-PAMPS
22.1%	0%	146k	30%	60	3.79	73.6	BC-PAMPS
22.1%	40%	146k	0%	60	5.13	80.5	BC-PVA
22.1%	40%	146k	30%	0	2.2	55.2	
13.9%	40%	146k	30%	60	2.39	58.1	
49.8%	40%	146k	30%	60	5.29	81.1	
22.1%	20%	146k	30%	60	2.77	63.9	
22.1%	40%	77k	30%	60	3.57	72.0	
22.1%	40%	202k	30%	60	4.42	77.4	
22.1%	40%	146k	30%	20	2.30	56.5	
22.1%	40%	146k	30%	40	2.25	55.5	
22.1%	40%	146k	30%	80	2.07	51.8	
22.1%	40%	146k	30%	100	2.19	54.4	
22.1%	40%	146k	20%	60	1.99	49.7	
22.1%	40%	146k	40%	60	2.21	54.8	

Cyclic tensile tests were carried out with the hydrogel samples in a water bath at 37°C. Samples were cycled between 1 N of force to a specific load of interest at a frequency of 2.5 Hz. Target load values were based on the stress at 0.5, 1 and 2 standard deviations below the UTS. A maximum of 100,000 cycles were carried out. Every sample that did not fail after 100,000 cycles had no visible signs of damage accumulation or crack formation.

To ensure no changes in the hydrogel occurred over the course of the test, we performed tensile tests and dimensional measurements on the BC-PVA-PAMPS hydrogel after soaking in PBS for up to 12 days at room temperature. Figure S8 shows the hydrogel exhibited no changes in its tensile strength and dimensions over this period.

We have included the first 3 loading-unloading cycles in the tensile fatigue test in Figure

6. The hysteresis energy is defined here as the area inside the hysteresis loop of a loading-unloading cycle, as indicated in Figure 6. In the first cycle, the area in the hysteresis loop was 0.14 MJ m-3. The hysteresis dropped rapidly to 5 kJ m-3 and 1 kJ m-3 in the following cycles. This result is very similar to that of articular cartilage, where the hysteresis energy also decreased quickly over the first 3 cycles.[9, 116]

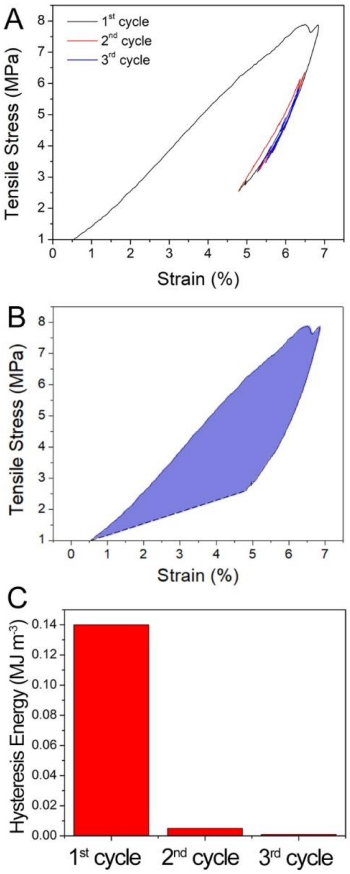

Figure 6: (A) The first 3 cycles of tensile cycles; (B) a representation of how the hysteresis area was calculated; (C) hysteresis energy of the first 3 cycles.

2.3. Results and Discussion

2.3.1 Design of The BC-PVA-PAMPS Hydrogel

Cartilage-equivalent properties were achieved in the BC-PVA-PAMPS hydrogel by mimicking the structure of cartilage. Articular cartilage principally consists of water (60-85% by weight), collagen fibers (15-22%) with diameters of ~100 nm, and negatively charged aggrecan (4-7%).[1, 94, 117, 118] The collagen fiber network gives cartilage its high tensile strength.[1] Aggrecan is a brush-like molecule with a negative charge that comes from sulfate groups on the glycosaminoglycan chains attached to a protein core.[117, 119] Aggrecan forms large aggregates with hyaluronan that are trapped within the collagen network, leading to an osmotic pressure that resists compressive loads.[94, 117, 118, 120-125]

Collagen cannot be used in a synthetic replacement for cartilage because it degrades in the human body, as is demonstrated by the high failure rate of decellularized allografts.[126] Bacterial cellulose (BC) was chosen as the nanofiber network to mimic collagen due to its biocompatibility, high tensile strength, and because the human body lacks the enzymes necessary to degrade cellulose.[127-130] The second network consisting of a PVA hydrogel was infiltrated into the BC network to provide an elastic restoring force and viscoelastic energy dissipation,[131-133] and to increase the tensile strength by allowing BC fibers to share load in the composite framework.[86, 134, 135] As shown in Figure 7A, a BC-PAMPS hydrogel had a tensile strength of 4.6 MPa, lower than the 8.1 MPa required to be in the cartilage-equivalent range. In contrast, a BC-PVA hydrogel has a cartilage-equivalent tensile strength of 12.3 MPa.

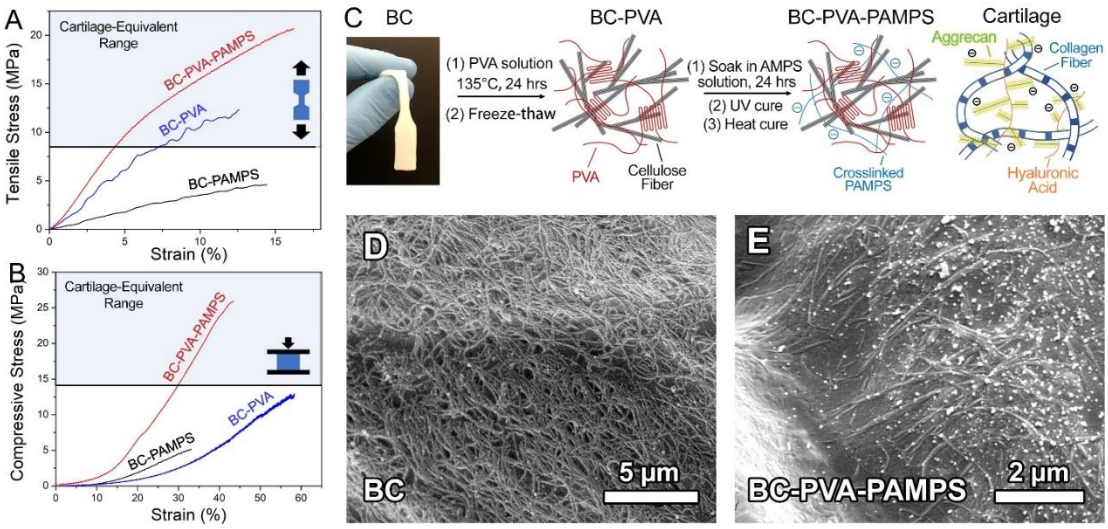

Figure 7: Mechanical properties of BC-PVA-PAMPS hydrogel and its illustration. (A&B) Tensile and compressive stress-strain curves for different hydrogels; (C) Illustration of the hydrogel fabrication process; (D&E) Cryo-SEM images of the BC and the BC-PVA-PAMPS hydrogel.

A PAMPS network was added to the hydrogel to provide it with a fixed negative charge from the sulfate groups on the PAMPS molecules, thereby mimicking the role of the chondroitin sulfate and keratan sulfate components that give aggrecan its negative charge.[120, 136] This negative charge results in an osmotic pressure that swells cartilage and contributes to its compressive strength. As shown in Figure 2B, neither the BC-PAMPS or the BC-PVA hydrogel had sufficient strength to be considered cartilage-equivalent. By adding the PAMPS network into the BC-PVA hydrogel, we increased both the compressive modulus (23 MPa) and strength (10.8 MPa) to within the cartilage-equivalent range.

We note that although the introduction of the BC into a PVA-PAMPS hydrogel increases the tensile strength from 1.06 to 20.6 MPa, it decreases the strain at failure from 66 to 17 % (see Figure 8). This is due to the fact that the BC films themselves have fracture strains

less than 25%, and the prestaining and alignment caused by compression of the films will decrease this further.[137] Cartilage has a tensile strain at failure in the range of 20-30%, only slightly greater than the strain at failure of the BC-PVA-PAMPS hydrogel.[138] For comparison, the strain at failure for human tendons is ~8%.[139]

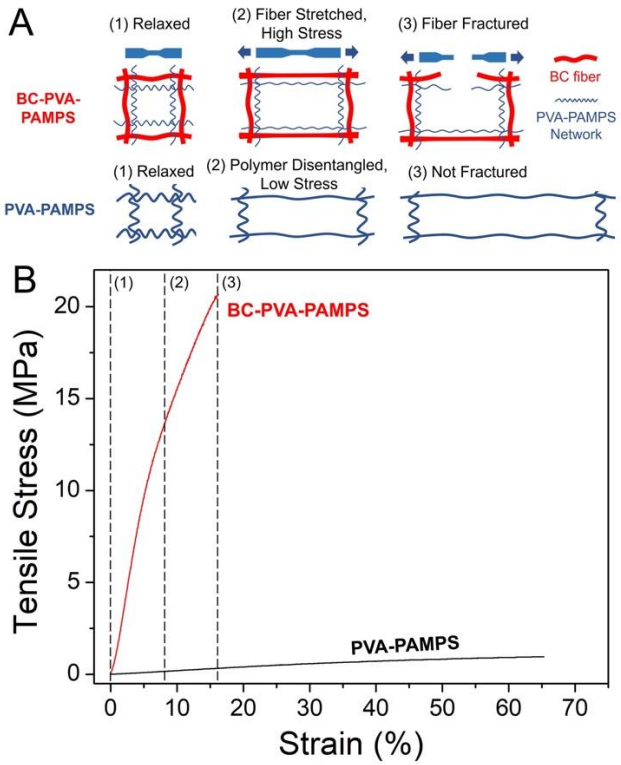

Figure 8: Schematics of the strength/modulus enhancement mechanism for a fiber-reinforced hydrogel.

2.3.2 Fabrication Process

Figure 7C provides an illustration of the fabrication process for the BC-PVA-PAMPS hydrogel. First, a piece of BC was pressed to a controlled thickness, typically 0.5 mm, by using spacers between 2 metal plates. A cryogenic scanning electron microscopy (cryo-SEM) image (Figure 7D) shows the nanofibrous nature of the BC. Next, the pressed BC

was soaked in an aqueous solution of 40 wt% PVA at 135°C for 24 hours to diffuse the PVA solution into the BC. The BC-PVA gel was then frozen at -78°C for 30 minutes and thawed to room temperature to physically crosslink the PVA network.[135] The BC-PVA hydrogel was then soaked in a solution of 30 wt. % AMPS, 60 mM MBAA, 50 mM I2959 and 0.5 mg mL^{-1} KPS solution for 24 hours. The hydrogel was cured with a UV transilluminator (VWR) for 15 minutes on each side, and then heat cured in an oven at 60°C for 8 hours to ensure even and complete curing. The resulting BC-PVA-PAMPS hydrogel was stored in 0.15 M phosphate buffered saline (PBS) solution for at least 24 hours before further characterization. Figure 2E shows a cryo-SEM image of the surface of the BC-PVA-PAMPS hydrogel.

2.3.3 Effect of Composition on Strength and Modulus

Thirty mechanical tests were performed on BC-PVA-PAMPS hydrogels with different molecular weights of PVA (fully hydrolyzed), and different concentrations of BC, PVA, AMPS, and MBAA cross-linker to determine the sensitivity of the hydrogel's mechanical properties to these parameters. The results are shown in Figure 9. Unless otherwise stated, the composition of the hydrogel selected for subsequent testing in the paper was 22.1 wt.% BC, 40 wt.% PVA (molecular weight: 144k g mol^{-1}, fully hydrolyzed), 30 wt.% PAMPS, and 60 mM MBAA. A list of the hydrogel compositions, including their water content and swelling ratio, is provided in Table 2.

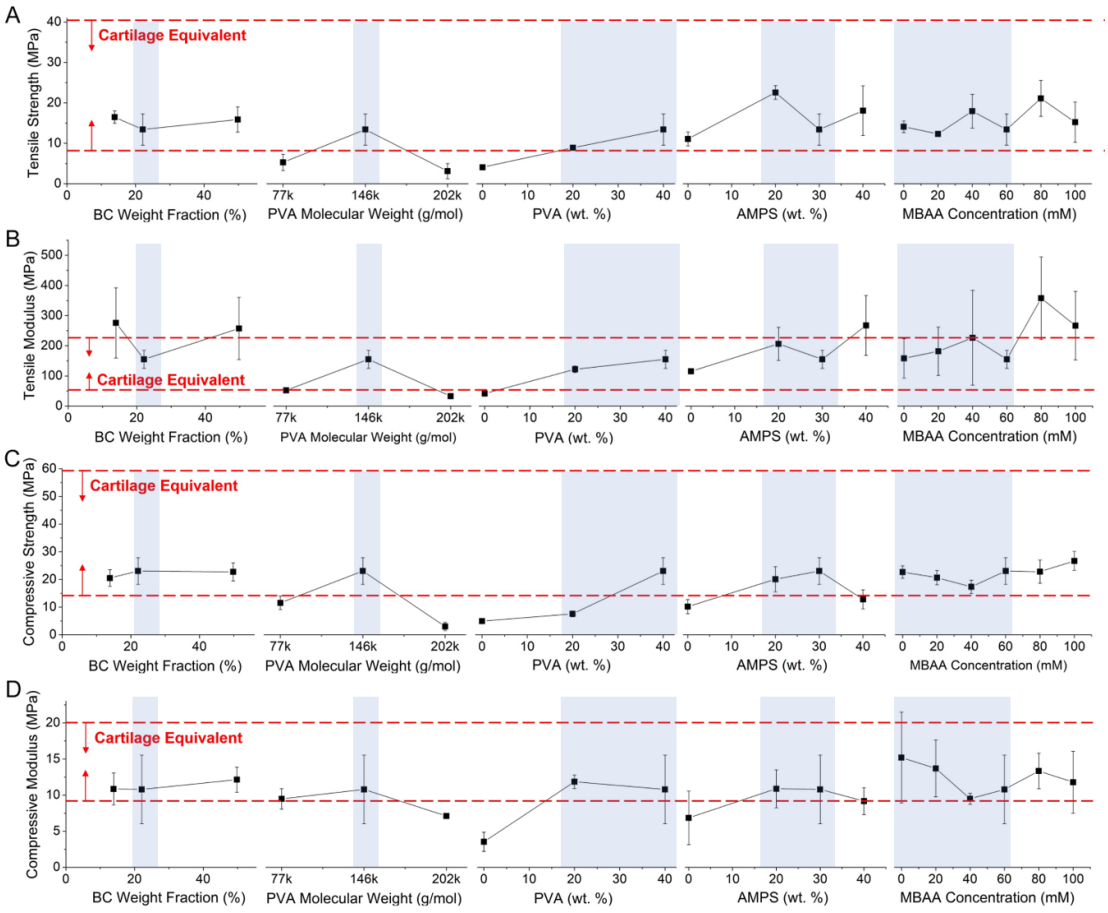

Figure 9: Detailed mechanical properties of BC-PVA-PAMPS hydrogel. Tensile strength (A), tensile modulus (B), compressive strength (C), and compressive modulus (D) of BC-PVA-PAMPS hydrogels with different formulations. The concentrations of BC, PVA, PAMPS, MBAA were 20 wt.%, 40 wt.%, 30 wt.% and 60 mM and the molecular we weight of PVA was 146k g mol-1 unless otherwise indicated. The range of compositions that corresponds to cartilage-equivalent hydrogels are denoted with blue shading.A BC wt.% of 13.9%, 22.1%, or 49.8% resulted in a cartilage-equivalent tensile and compressive strength, but only the intermediate value of 22.1% resulted in a hydrogel with a cartilage-equivalent tensile modulus. For the PVA network, molecular weights of 77k, 144k and 202k g mol^{-1} were tested. Increasing the PVA molecular weight from 77k to 144k g mol^{-1} increased the tensile and compressive strength of the hydrogel from below

to within the cartilage-equivalent range. This increased strength may be attributed to increased hydrogen bonding and entanglement between the polymer chains.[135, 140] However, increasing the molecular weight further to 202k g mol^{-1} lead to a decrease in strength outside of the cartilage-equivalent range because the higher molecular weight polymer did not fully dissolve during the infiltration processes. Compositions with PVA below 40 wt.% were not cartilage equivalent, while higher concentrations did not fully dissolve during infiltration.

PAMPS by itself forms a relatively stiff, brittle hydrogel. Thus, increasing the AMPS concentration increased the tensile and compressive moduli. The addition of an intermediate range of AMPS (20-30 wt.%) provided cartilage-equivalent mechanical properties. Further increasing the AMPS wt.% (e.g., 40 wt.%) made the hydrogel brittle under compression, decreasing its compressive strength below the cartilage-equivalent range.

MBAA crosslinks the PAMPS network. Interestingly, MBAA was not necessary to provide cartilage-equivalent mechanical properties. The MBAA concentration had a relatively minor effect on the mechanical properties of the hydrogel, but an MBAA concentration of 80 mM or higher increased the tensile modulus to outside the cartilage-equivalent range. Therefore, a range of 0-60 mM of MBAA provided cartilage-equivalent mechanical properties.

2.3.4 Fatigue Resistance

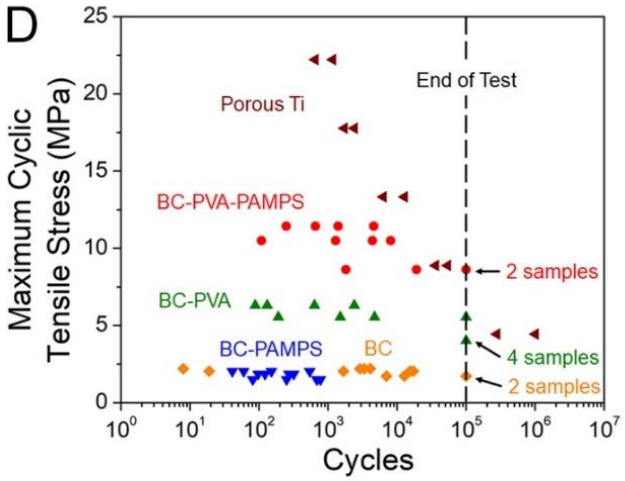

Figure 10: Maximum cyclic tensile stress applied vs. the number of cycles before fracture. Eight samples indicated by arrows did not fail after 100,000 cycles.

Cartilage experiences cyclic stress in vivo, so it is important to characterize the fatigue properties of materials that have the potential to be used for cartilage replacement.[85, 141, 142] Figure 10 shows the results from cyclic tensile testing for the BC-PVA-PAMPS hydrogel, its components in different combinations, as well as porous titanium for comparison.[143] We focused on tensile fatigue because tensile fatigue failure of collagen may play a role in the mechanical failure of cartilage,[142, 144-147] and failure in tension is more clearly defined than failure in compression for cartilage-like materials.[10] Cyclic tests were conducted at 2.5 Hz, so that a 100,000 cycle test took 11.1 hours, and samples with a higher strength experienced a higher stress rate (see Table 3 and supplemental information for testing conditions). The BC-PVA-PAMPS hydrogel exhibited a remarkably high fatigue strength of 8.62 MPa at 105 cycles, which is comparable to 85% porous 3d-printed titanium.[143] Addition of PAMPS to BC decreased its resistance to fatigue due to the brittle nature of PAMPS.[35] The

addition of PVA to BC increased fatigue resistance due to the toughness of PVA;[131-133] all four BC-PVA samples were free of damage at 105 cycles. BC-PVA-PAMPS exhibited superior fatigue strength than BC-PAMPS due to the ability of PVA to act as a toughening agent and cancel out the poor fatigue properties of PAMPS. The fatigue strength of BC-PVA-PAMPS is the same as the fatigue strength of cartilage in middle-aged adults.[85] We also showed the first 3 tensile loading-unloading in Figure 6.

Table 3: Average UTS and standard deviations for hydrogels in the fatigue tests.

Composition	UTS (MPa)	Standard Deviation (MPa)
BC-PVA-PAMPS	12.37	1.87
BC-PVA	7.06	1.52
BC-PAMPS	2.21	0.35
BC	2.36	0.32

2.4 Conclusion

In summary, a biomimetic approach was used to create the first hydrogel with the same strength and modulus as human articular cartilage in compression and tension. Bacterial cellulose nanofibers provided the hydrogel with a source of tensile strength in a manner analogous to collagen nanofibers in cartilage. PVA provided an elastic restoring force, viscoelastic energy dissipation, and prevented stress concentration on individual BC fibers. PAMPS provided the hydrogel with a source of fixed negative charge and osmotic restoring force similar to the role of aggrecan in cartilage. The BC-PVA-PAMPS hydrogel also exhibited cartilage-equivalent fatigue strength at 100,000 cycles. BC-PVA-PAMPS was not cytotoxic and is comprised of materials that have been previously demonstrated to be biocompatible. Taken together, these properties make the BC-PVA-

PAMPS hydrogel an excellent candidate material for use in the repair of cartilage lesions.

3. Hydrogel Attachment Through Nanofibrous Reinforcement*

* This chapter adapted from J. Zhao; A. Kirillova; C. N. Kelly; H. Xu; W. J. Koshut; F. Yang; et al. High-Strength Hydrogel Attachment through Nanofibrous Reinforcement. Adv. Healthc. Mater. 2021 Vol. 10 Issue 4 Pages 2001119

3.1 Introduction

Articular cartilage lesions, which most often occur in the knee, have a limited intrinsic ability to heal, and are associated with joint pain and disability.[3] Common strategies for cartilage restoration, such as microfracture, have high failure rates (~50% at 10 years) and prolonged rehabilitation times (12 to 18 months).[4, 148, 149] Implantation of fresh osteochondral allografts can allow immediate weight-bearing and, with a survivorship of 82% at 10 years, is the most successful strategy for treatment of cartilage defects.[150, 151] Unfortunately, the small supply of fresh allografts limits the number of these procedures to around 1% of all cartilage repair surgeries. Decellularized, shelf-stable allografts have very high failure rates (72% in 2 years) characterized by delamination of the articular cartilage in the graft due to collagen degradation.[152] There is a clear need for a cartilage repair method that is widely available, allows immediate weight bearing, has short recovery times, and has low long-term failure rates.

Based on the limitations of biological approaches to cartilage restoration, there are ongoing efforts to perform focal joint resurfacing with durable orthopedic materials (e.g. cobalt-chromium alloy) to fill chondral or osteochondral defects.[153, 154] A primary concern with these implants is that they do not match the tribology and mechanical response of native cartilage, resulting in abnormal stress and opposing surface wear causing joint

degeneration.[155, 156] Incorrect placement of these implants can lead to severe damage of the opposing cartilage surface.[157] A review of the results of focal metallic inlay resurfacing prosthesis indicates 20% of patients have to be converted to arthroplasty after 4 years.[158] Hydrogels can be created to have a similar stiffness and coefficient of friction as cartilage, thereby addressing concerns related to abnormal stress and wear.[89] However, there is currently no way to secure a hydrogel into a cartilage defect site with the same shear strength as the osteochondral junction (7.25±1.35 MPa).[90] One of the strongest tissue adhesives is cyanoacrylate, which has been reported to achieve a lap shear strength of 0.7 MPa between two pieces of cartilage.[91] In contrast, cyanoacrylate bonds nylon to nylon and steel to steel with a shear strength of 2.8 and 7.3 MPa,[92, 93] respectively. This comparison suggests that the presence of interfacial water in cartilage (cartilage is 60-85% water by weight)[94] hinders the creation of a stronger bond. Indeed, mussel and spider glues have mechanisms to displace interfacial water so as to create stronger bonds.[95, 96] This phenomenon has inspired the development of dry, tissue-bonding double-sided tape.[97] Thus, removal of water is an important strategy for forming strong bonds to hydrogels.

Another strategy to form strong bonds to hydrogels is to mimic the bonding of cartilage to bone.[98] The osteochondral junction is characterized by a layer of collagen nanofibers extending from the deep zone of cartilage into a mineralized region that is attached to subchondral bone through an interdigitated interface.[99, 100] In this way the collagen nanofibers that give cartilage its excellent tensile strength also anchor it to the surface of bone.

This chapter describes a new approach, Nanofiber-Enhanced STicking (NEST), that combines the strategies of water removal and nanofiber mineralization. The essence of this strategy, illustrated in Figure 11A&B, is to first attach a dry nanofibrous layer to a porous base of interest before infiltration of the hydrogel components. In this way, the adhesive or cement can penetrate into the porous nanofibrous network and create an interdigitating bond without the interference of water.

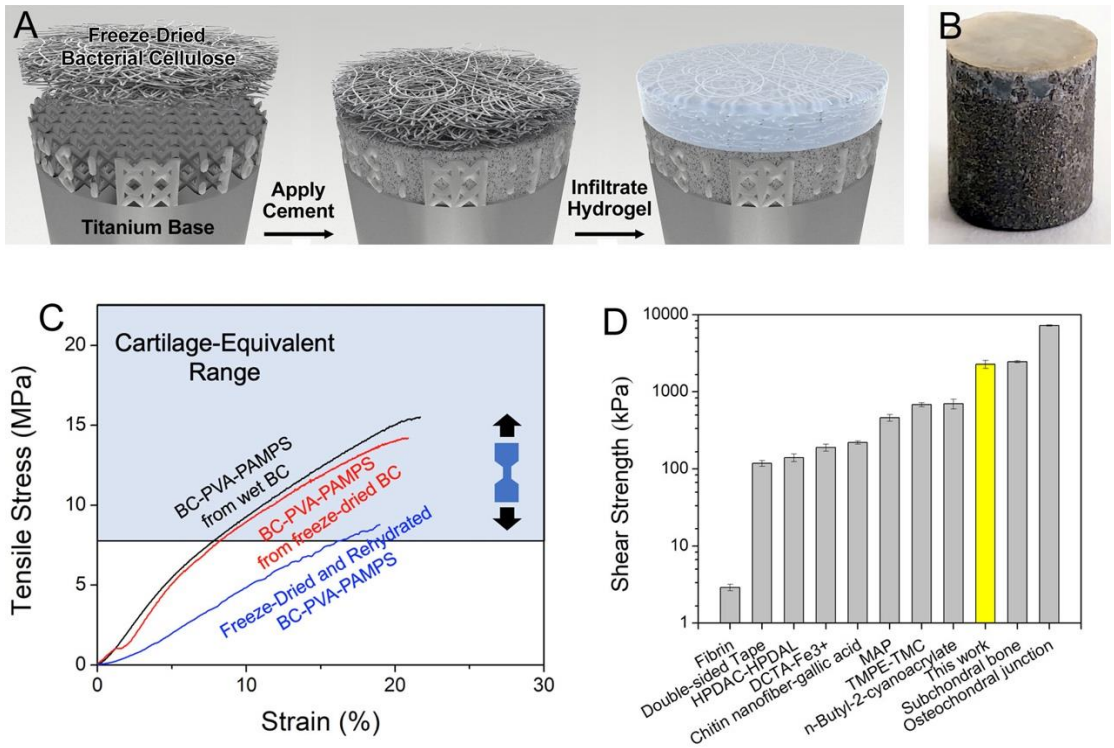

Figure 11: Illustration of NEST strategy and its performance. (A) Illustration of NEST. (B) Image of a hydrogel bonded to a titanium plug with the NEST method. (C) Tensile stress-strain curves of different hydrogels. (D) Sheer strength obtained for the NEST method compared to other hydrogel adhesives.

3.2 Experiments and Methods

3.2.1 Materials

Bacterial Cellulose (BC) was purchased from Gia Gia Nguyen Co. Ltd. Poly(vinyl alcohol) (PVA) (fully hydrolyzed, molecular weight: 145,000 g mol-1), N,N'-methylenediacrylamide (MBAA, 97.0%), 2-hydroxy-4'-(2-hydroxyethoxy)-2-methylpropiophenone (I2959), potassium persulfate (KPS) and 2-acrylamido-2-methylpropanesulfonic acid sodium salt (AMPS, 50 wt.% solution in water) were purchased from Sigma Aldrich. Phosphate buffered saline (PBS) was purchased from VWR International. Ti-6Al-4V ELI (Grade 23) powder was purchased from 3D Systems. The powder has a spherical morphology, with particle size distribution of 15 – 45 microns. An SEM image of the titanium powder is shown in Figure 12A. Figure 12B shows an SEM image of the printed titanium struts.

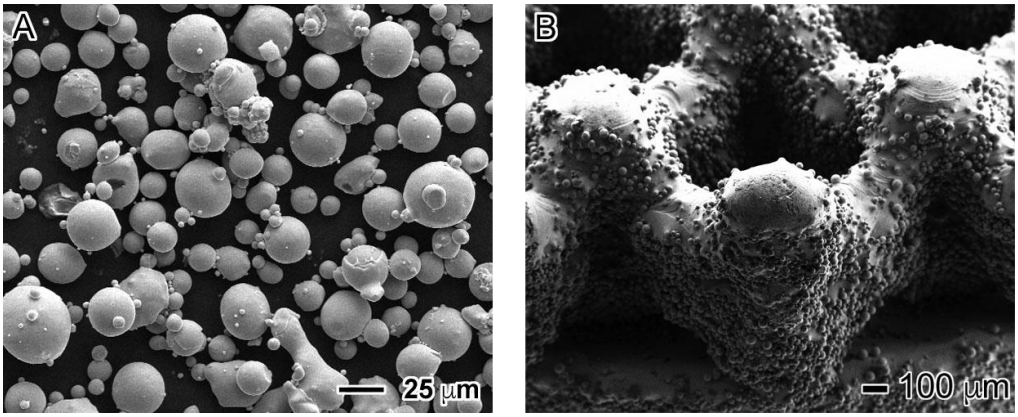

Figure 12: (A) SEM image of the Titanium powder used for 3D printing. (B) Image of the struts at the surface of the titanium plug.

3.2.2 Fabrication of BC-PVA-PAMPS Hydrogels for Tensile Testing.

BC sheets were pressed to a controlled thickness between 2 aluminum plates (typically 0.5 mm, controlled by spacers between the aluminum plates) and placed into a hydrothermal reactor with a mixture of PVA (40 wt.%) and DI water (60 wt.%). The hydrothermal reactor was sealed and heated at 110 °C for 24 hours to allow Poly(vinyl alcohol) (PVA) to diffuse into the voids of BC and form a BC-PVA hydrogel. The BC-PVA hydrogel was removed from the reactor when hot (>85°C). The residual PVA solution was removed by scrapping the surface of the BC-PVA samples with a metal spatula. The samples were frozen in a -78°C fridge for 30 minutes and thawed at room temperature to physically crosslink the PVA network. The BC-PVA hydrogel was then soaked in a solution of 2-acrylamido-2-methylpropanesulfonic acid sodium salt (AMPS, 30 wt.%), N,N'-methylenediacrylamide (MBAA, 60 mM), and potassium persulfate (KPS, 0.5 mg mL-1) for 24 hours. The hydrogel was cured with a UV transilluminator (VWR International) for 15 minutes on each side, and further cured in an oven at 60°C for 8 hours to ensure even and complete curing. The resulting BC-PVA-PAMPS hydrogel was stored in PBS for at least 24 hours before further characterization. Hydrogels using freeze-dried BC were made in the same manner except the starting bacterial cellulose sheet was freeze-dried at -78°C for 24h and put into DI water at 23°C for 4 hours to enable a complete rehydration before PVA infiltration.

3.2.3 Additive Manufacturing of Titanium.

Titanium plugs were fabricated via SLM (selective laser melting) of Ti-6Al-4V ELI powder on a titanium substrate in an inert argon atmosphere using a 3D Systems DMP

ProX 320. Plugs were designed to have a diameter of 6 mm and a height of 6.35 mm. The top 1 mm of the plug was composed of a porous strut structure with a porosity of 70% (see Figure 11A and Figure 12B), except where otherwise indicated. After printing, the samples were removed from the build plate via wire electrical discharge machining and cleaned by sonication for 15 min in DI water to remove excess unadhered powder.

3.2.4 Preparation of Samples for Cement Shear Testing.

To create samples for shear testing and study of the cement by itself, a dry cement mixture consisting of 0.040 g phosphoserine (PPS), 0.312 g of α-TCP and 0.048 g of stainless-steel powder (SSP) was placed into a small dish, 0.140 ml of water was added, and the powder was rapidly mixed with the water. Approximately 0.150 ml of the wet cement mixture was the added on top of a porous titanium plug in a metal die with an inner diameter of 6 mm. A second titanium plug was immediately placed into the die with the porous layer in contact with the wet cement, and the sandwich structure was pressed together for 1 hour at 250 MPa. The sample was placed into water at 85°C for at least 24 hours to facilitate the transformation of α-TCP into hydroxyapatite and was stored in water until just prior to shear testing.

3.3.5 Preparation of Samples for Hydrogel-Cement Shear Testing.

Testing of the hydrogel-cement adhesion was performed with a cement composed of 10 wt.% PPS, 78 wt.% α-TCP and 12 wt.% SSP. As with the cement testing, the titanium plug was placed into a die. The surface of the plug consisted of a 1-mm-thick 3D printed strut structure with a porosity of 70%. A cement mixture consisting of 0.080g PPS, 0.624 g of

α-TCP and 0.096 g of SSP was placed into a small dish, 0.280 ml of water was added, and the powder was rapidly mixed with the water. Then 0.150 ml of the wet cement mixture was then added on top of the porous titanium plug in the die. The BC sheet was then placed on top of the cement in the die, and an additional 0.150 ml of the wet cement mixture was added on top of the BC sheet. A second porous titanium plug was then placed on top of the BC sheet in the die to create a sandwich structure. The sandwich structure was pressed for 1 hour at 250 MPa. The sample was placed into water at 85°C for 24 hours to facilitate the transformation of α-TCP into hydroxyapatite. The sample was then placed into a hydrothermal reactor with a mixture of PVA (40 wt.%) and DI water (60 wt.%) to infiltrate PVA into the BC layer. The sample was frozen at -78°C and thawed to room temperature to further increase the strength of the hydrogel. The sample was then soaked in a solution containing AMPS, (30 wt.%) cross-linker (MBAA, 60 mM), and heat initiator (potassium persulfate, 0.5mg ml^{-1}) for 24 hours. The hydrogel was heat cured at 60 °C for 8 hours and the sample was soaked in DI water for at least 24 hours.

3.2.6 Monotonic Tensile Testing.

Monotonic tensile measurements were carried out on a TestResources 830 (TestResources, Shakopee, MN, USA) load frame at a rate of 0.25 mm s^{-1} using a 50 lb. load cell. Monotonic samples were prepared in an ASTM D638-14 Type V shape with a titanium punch that was created through additive manufacturing. The dimensions of the samples were measured with a caliper before testing. The ultimate tensile strength (UTS) was the maximum tensile stress recorded before fracture.

3.2.7 Shear Testing.

Adhesive shear testing was performed using 6 mm x 6.35 mm cylindrical samples on a Test Resources 830LE63 Axial Torsion Test Machine equipped with a 100 lb. load cell and a custom-made shear testing fixture (see Figure 13). A crosshead displacement rate of 2 mm min^{-1} was used for all the measurements. The plugs were placed in the fixture so that the interface between the plugs was centered in the gap between the L-shaped metal plates that make up the fixture. Three samples were measured for each formulation.

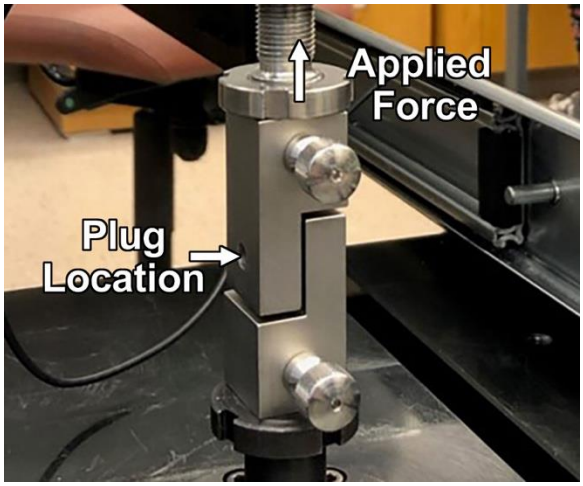

Figure 13: Image of the shear test fixture used for testing.

3.2.8 Scanning Electron Microscopy (SEM).

Samples from shear tests were dried in air for 24 hours to allow water to completely evaporate. To study the BC-cement interface, BC-cement disks were made by pressing a layer of freeze-dried BC into 150 mg of the cement mixture (10 wt.% PPS, 78 wt.% α-TCP and 12 wt.% SSP) in a 6 mm die at 250 MPa for 1 hour. These disks were then put into water at 85°C for 24 hours. The BC-cement disks were frozen with liquid nitrogen, broken apart, and freeze-dried for 24 hours. Samples were coated with gold with a current of 12

mA for 300 seconds with a sputter coater (Denton Desk V). The gold-samples were put into Apreo S Electron Microscope (ThermoFisher Scientific) and imaged with a current of 2.5 pA and a voltage of 2.00 kV.

3.2.9 X-ray Diffraction (XRD).

Approximately 50 mg of cement powder consisting of 10 wt.% PPS and 90 wt.% α-TCP were pressed inside a 6 mm diameter die for 15 minutes to form a disk. Multiple disks were made in this manner. XRD was subsequently performed on one of the disks. Other disks were placed into DI water at 85°C for 24 hours to facilitate the transformation from α-TCP to hydroxyapatite. The disk was taken out and dried at 60 °C for 1 hour to remove the remaining water. XRD testing was then performed on the disk to confirm the formation of hydroxyapatite from α-TCP. XRD tests were performed on the Panalytical X'Pert PRO MRD HR XRD System.

3.3 Results and Discussion

3.3.1 Design of NEST Method

A recently-reported cartilage-equivalent hydrogel composed of bacterial cellulose (BC), polyvinyl alcohol (PVA), and poly(2-acrylamido-2-methyl-1-propanesulfonic acid sodium salt) (PAMPS) proved to be an excellent candidate for this strategy.[89] The BC nanofibers in the hydrogel provide a source of tensile strength similar to collagen nanofibers in cartilage. Although this hydrogel was previously prepared from wet BC, we found that BC could be freeze-dried and infiltrated with PVA and PAMPS to create a hydrogel with nearly the same tensile strength (12.37±3.83 MPa) as one that is not freeze dried (13.42±3.86

MPa). As shown in Figure 11C, the tensile strength of hydrogels prepared by infiltration of wet or freeze-dried BC are well within the range of tensile strengths reported for human cartilage (8.1 - 40 MPa).[159] In contrast, if the full BC-PVA-PAMPS hydrogel is freeze-dried, the tensile strength is only 9.62±2.63 MPa. This result

suggests the nanofibrous BC can accommodate the formation of ice crystals by fiber displacement without fiber fracture, whereas the molecularly cross-linked hydrogel network is irreversibly damaged by ice crystal formation.

Figure 11D compares the maximum adhesive shear strength achieved for the NEST strategy compared to previous work (see also Table 4).[91, 160-175] Mimicking the osteochondral junction, we mineralized the BC nanofibers with a hydroxyapatite-forming cement to achieve an adhesive shear strength of 2.28±0.27 MPa, a three-fold increase over the state-of-the-art. This is lower than the shear strength reported for the human osteochondral junction (7.25±1.35 MPa),[90] but is similar to the shear strength reported for the bovine osteochondral junction (2.6±0.58 MPa)[176] and human subchondral bone (2.45± 0.85). The rest of this article describes the experiments performed to arrive at this shear strength.

Table 4: Comparison of the strength of bonds to hydrogels compared to the human osteochondral junction and subchondral bone.

Adhesive Types	Adherend	Shear Strength (MPa)	Reference
a-TCP with stainless steel powder and phosphoserine	**Porous titanium to BC-PVA-PAMPS hydrogel**	**2.28±0.27**	**This work**
Osteochondral junction	-	7.25±1.35	[90]
Subchondral bone	-	2.45±0.85	[90]
Double-sided tape	Skin	0.118±0.01	[97]
Fibrin	Sheep aorta	0.0029±0.00028	[161]
Fibrin tissue adhesive	Human dura	0.038	[162]
GRF	Sheep aorta	0.048±0.018	[177]
GRFG	Bovine pericardial strips	0.011±0.00067	[163]
n-Butyl-2-cyanoacrylate	Cartilage	0.70±	[91]
Acrylate-NHS hydrogel	Collagen sheet	0.074±0.005	[164]
ASA-AG hydrogel	Porcine skin	0.015±0.0013	[165]
Styrene-derivatized gelatin	Collagen film	0.016±0.0015	[166]
EGK glue	Chicken skin	0.016±0.001	[167]
HPDAC-HPDAL	Porcine skin	0.14±0.016	[168]
CSS-EPLM	Porcine skin	0.088±0.001	[169]
Chitin nanofiber-gallic acid	Aluminum to hydrogel	0.22±0.01	[170]
TMPE-TMC	Chamois leather	0.68±0.04	[171]
Xylose-PU-PEG	Muscle	0.094±0.003	[172]
PEG-polyester	Porcine skin	~0.039±0.005	[173]
PEG-polyester	Bovine pericardium	~0.058±0.007	[173]
MAP	Porcine intestine	0.46±0.046	[174]
DCTA-Fe^{3+}	Articular cartilage	0.19±0.02	[175]
DCTA-Fe^{3+}	Porcine skin	0.025±0.003	[175]

We focused on the use of α-tricalcium phosphate (α-TCP) as a hydroxyapatite-forming cement for attachment of the hydrogel due to its biocompatibility, osteoconductivity, and shear strength that exceeds that of cyanoacrylate.[178, 179] By itself, α-TCP does not act as an adhesive. Thus, we tested the addition of 10 wt.% phosphoserine (PPS), a component of sandcastle worm glue,[180] to promote adhesion. Hydroxyapatite is brittle and benefits from

reinforcement,[181] so we tested the addition of 12 wt.% Stainless-steel powder (SSP) with an average particle size of 150 μm to hinder crack propagation.

To create samples for adhesive shear testing and study of the cement by itself, a dry cement mixture consisting of 0.040 g PPS, 0.312 g of α-TCP and 0.048 g of SSP was placed into a small dish, 0.140 ml of water was added, and the powder was rapidly mixed with the water. Powders were also created without PPS or SSP to examine the effects of these additives. Approximately 0.150 ml of the wet cement mixture was added on top of a porous titanium plug in a metal die with an inner diameter of 6 mm. The plug consisted of a titanium alloy (Ti6Al4V) topped with a 1-mm-thick layer of 3D printed struts with a porosity of 70%. Figure 11A includes a rendering of the strut structure in the computer aided design (CAD) file used for 3D printing. Scanning electron microscopy (SEM) images of the powder used for 3D printing and the printed strut structure are shown in Figure 12. The titanium plug is 6 mm in diameter and 6.35 mm in height. A second titanium plug was immediately placed into the die with the porous layer in contact with the wet cement, and the sandwich structure was pressed together for 1 hour at 250 MPa. Samples were also made without the application of pressure to test the effect of this step on shear strength. The application of pressure has previously been demonstrated to reduce the porosity of calcium phosphate cements, thereby improving their compression and flexural strength,[182-184] but the effect of pressure on the adhesive shear strength of an α-TCP cement has not been reported. The sample was placed into water at 85°C for at least 24 hours to facilitate the transformation of α-TCP into hydroxyapatite and was stored in water until just prior to shear testing. Figure 14 shows the x-ray diffraction (XRD) pattern of the α-TCP cement

before and after hydration, confirming the conversion to hydroxyapatite.[185] Figure 15A shows an image of the sandwich structure in which the α-TCP cement bonds two titanium plugs.

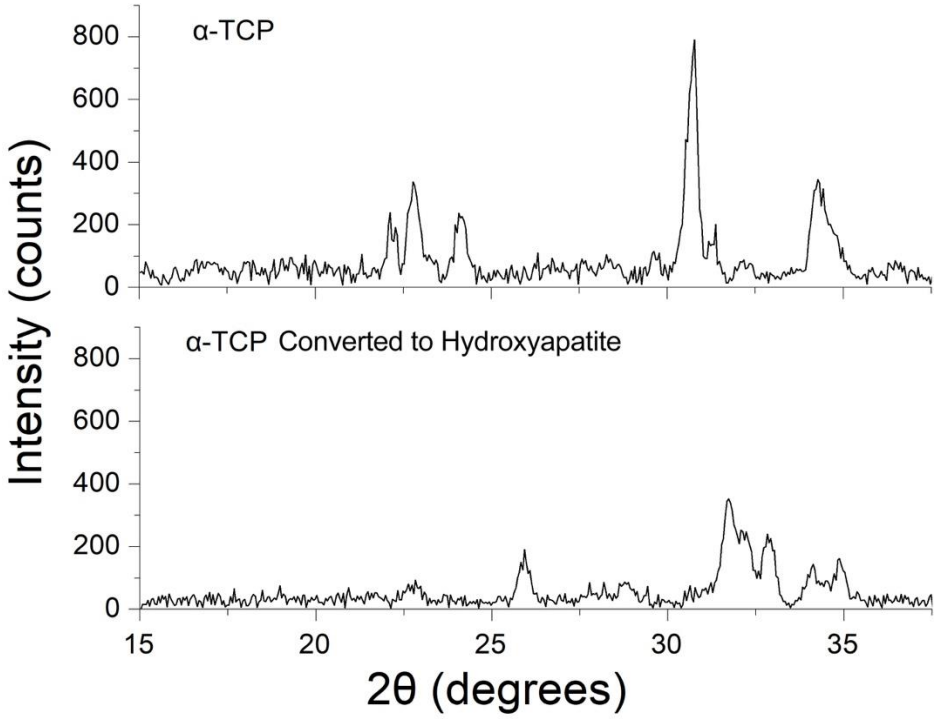

Figure 14: XRD of α-TCP disks before and after hydration in into DI water at 85°C for 24 hours.

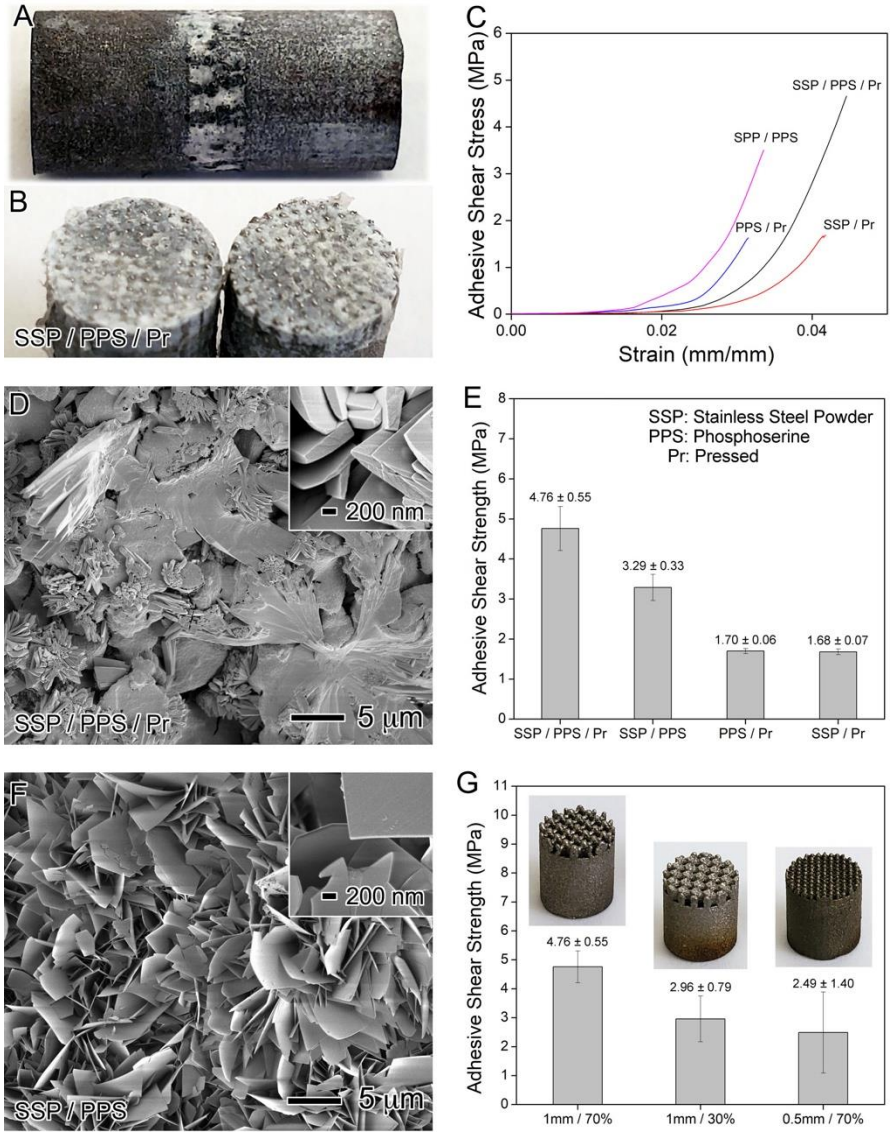

Figure 15: Shear tests Results of different cement compositions. Image of an α-TCP cement sample (A) before and (B) after shear testing. (C) Stress-strain curves for different cement compositions. (D) SEM image of the fracture surface for the sample containing SSP and PPS that was pressed at 250 MPa. (E) Effect of composition and pressing on adhesive shear strength (n=3). (F) SEM image of the fracture surface for the sample made with SSP and PPS without pressing. (G) Effect of the strut structure on adhesive shear strength (n=3).

3.3.2 Shear Strength of Different Cement and Implant Geometry

Shear testing was performed on a Test Resources 830LE63 Axial Torsion Test Machine equipped with a 100 lb. load cell and a custom-made shear testing fixture (see Figure 13). A crosshead displacement rate of 2 mm min^{-1} was used for all the measurements.

Figure 15B is an optical image of the cement fracture surface after shear testing, indicating cohesive failure. This particular sample contained SSP, PPS, and was pressed, but all cement samples exhibited a similar cohesive fracture surface. A previous study of a PPS-containing α-TCP cement demonstrated that failure can be partially adhesive for bonding smooth titanium plugs but becomes cohesive when the cementitious bond is made between porous titanium surfaces.[89]

Figure 15C shows typical stress strain curves for shear testing of cements with different compositions, and Figure 15D shows the average and standard deviation of the strength for three samples of each composition. The cement composition with the highest adhesive shear strength (4.76±0.55 MPa) was pressed at 250 MPa and contained both SSP and PPS, in addition to the α-TCP cement. Without the pressing step, the adhesive shear strength decreased to 3.29±0.33 MPa. The scanning electron microscopy

(SEM) image of the fracture surface for the pressed sample in Figure 15C shows the hydroxyapatite crystals at the fracture surface were thicker than the flake-like hydroxyapatite crystals that grew in samples that were not pressed (Figure 15E). Both surfaces differ substantially in morphology from the spheroidal α-TCP cement particles (Figure 16). Thus, the application of pressure not only changes the porosity but also the

crystal morphology of the hydroxyapatite in the cement, with the stronger sample consisting of a thicker hydroxyapatite crystal morphology.

Without PPS, the adhesive shear strength decreased to 1.68±0.07 MPa. Without the SSP, the adhesive shear strength decreased to 1.70±0.06 MPa. Thus, SSP, PPS, and mechanical pressing were all necessary to maximize the adhesive shear strength of the cement.

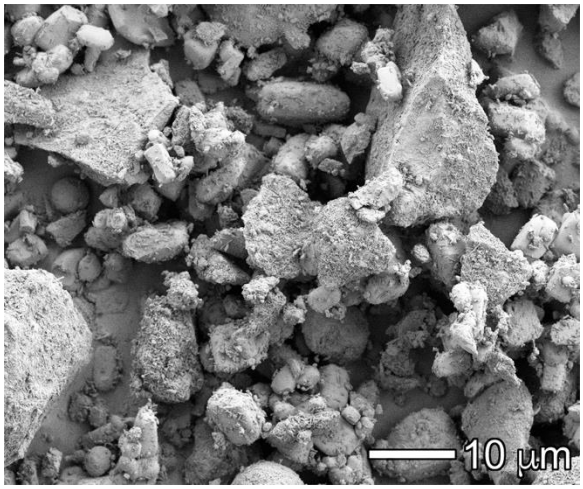

Figure 16: SEM image of α-TCP powder.

3.3.3 Shear Strength of Implant Made with NEST Method

Next, we studied how the structure of the 3D printed titanium layer affected the shear strength between two titanium plugs. Two changes were made: (1) decreasing the porosity from 70% to 30% and (2) decreasing the thickness of the strut layer from 1 mm to 0.5 mm. As shown in Figure 15F, both changes led to a decrease in the adhesive shear strength, so the 1-mm-thick layer with a porosity of 70% was used for the rest of the experiments.

After optimizing the adhesive shear strength of the cement and the structure of the porous titanium layer, we turned to studying the attachment of the titanium plugs to the hydrogel in a sandwich structure. Testing was performed with a cement composed of 10 wt.% PPS,

78 wt.% α-TCP and 12 wt.% SSP. The cement mixture consisting of 0.080 g PPS, 0.624 g of α-TCP and 0.096 g of SSP was placed into a small dish, 0.280 ml of water was added, and the powder was rapidly mixed with the power. Then 0.150 ml of the wet cement mixture was added on top of the porous titanium plug in the die. The BC sheet was placed on top of the cement in the die, and an additional 0.150 ml of the wet cement mixture was added on top of the BC sheet. A second porous titanium plug was then placed on top of the BC sheet in the die to create a sandwich structure. The sandwich structure was pressed for 1 hour at 250 MPa. The sample was placed into water at 85°C for 24 hours to facilitate the transformation of α-TCP into hydroxyapatite. The sample was then placed into a hydrothermal reactor with a mixture of PVA (40 wt.%) and DI water (60 wt.%) to infiltrate PVA into the BC layer. The sample was frozen at -78°C and thawed to room temperature to further increase the strength of the PVA hydrogel. The sample was then soaked in a solution containing AMPS, (30 wt.%) cross-linker (N,N'-Methylenebisacrylamide, 60 mM), and heat initiator (I2959, 50 mM) for 24 hours. The hydrogel was heat cured at 60 °C for 8 hours and the sample was soaked in DI water for at least 24 hours. An image of the finished sample is shown in Figure 17A.

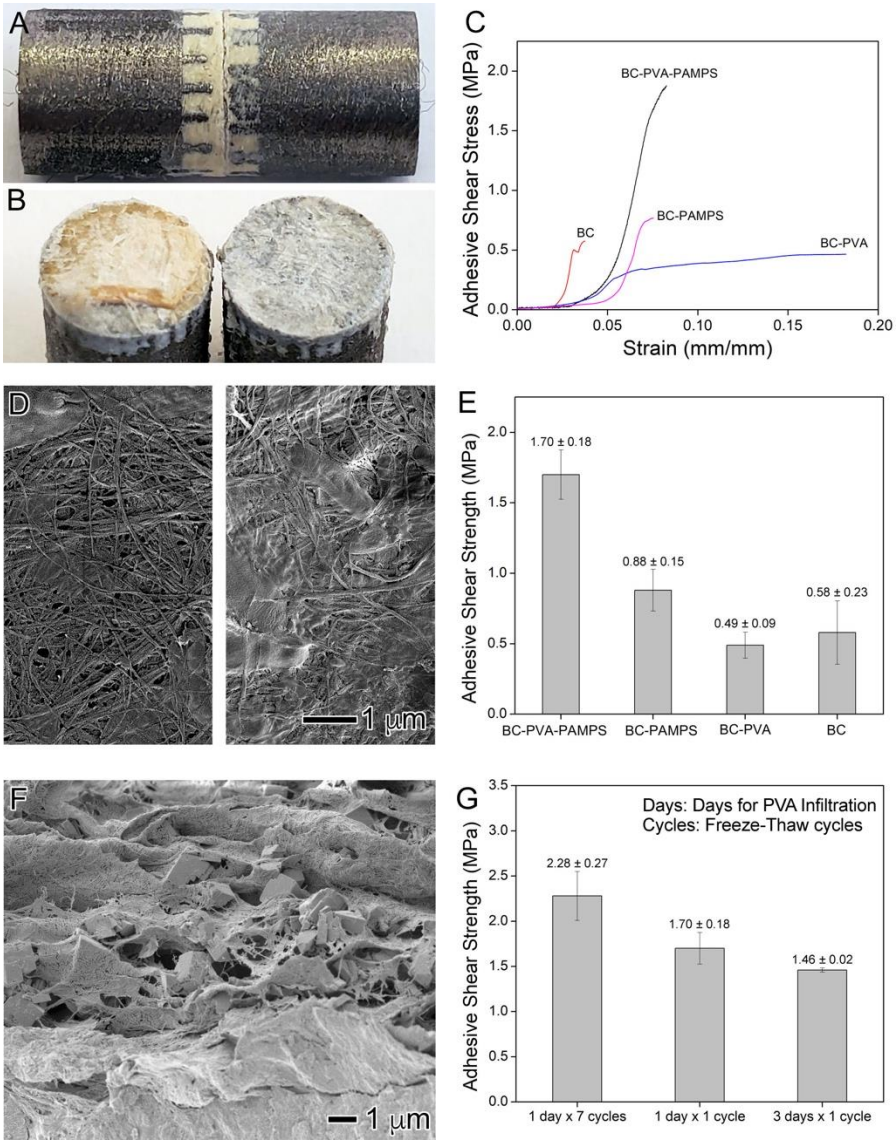

Figure 17: Shear tests results under different experimental conditions. Image of sample for testing hydrogel-cement adhesive shear strength (A) before and (B) after shear testing. (C) Typical stress strain curves for hydrogels with different compositions. (D) SEM images of the fracture surfaces in B. (E) Adhesive shear strength and standard deviation of different hydrogel compositions (n = 3). (F) Cross-section SEM image of hydroxyapatite mineralizing the BC nanofibers. (G) Effect of the hydrogel processing on adhesive shear strength (n = 3).

An image of the fracture surface after adhesive shear testing is shown in Figure 17B. For the fracture surface between the two titanium plugs in Figure 17B, the titanium prongs are

visible through the cement, suggesting that the metal prongs were in contact prior to fracture. In contrast, for the fracture surface with the BC-PVA-PAMPS hydrogel between the titanium plugs in Figure 17B, the titanium prongs are not visible. Instead, the white, fibrous BC layer is covering the prongs on the right plug, and the hydrogel infiltrated into the remaining BC is covering the prongs on the left. This shows that the hydrogel completely penetrated through the BC layer in between the plugs. This fracture surface, as well as other similar fracture surfaces not shown, also suggests that fracture took place close to the interface between the hydrogel and cement in the BC layer. This may be due to stress concentration at the interface between the relatively soft hydrogel and hard cement. Previous studies of shear fracture of the osteochondral junction similarly show that fracture of the osteochondral junction occurs at the tidemark, i.e., the border between cartilage and mineralized cartilage, presumably due to stress concentration at this interface.[176] Figure 17D shows SEM images of the left and right fracture surfaces in Figure 17B, showing the presence of BC and hydrogel on both surfaces. We could not observe hydroxyapatite at the fracture surface after hydrogel infiltration.

Figure 17C shows typical stress-strain curves for different hydrogel compositions, and Figure 17E shows the adhesive shear strength and standard deviation of three samples for each condition. With BC only in between the two titanium plugs the adhesive shear strength was 0.58±0.23 MPa, eight times lower than the shear strength of the cement without the BC. This again indicates the cement is attached to the BC layer rather than forming a continuous bond through the BC layer. We note that, as shown by the SEM image in Figure 16, the size of the α-TCP cement particles is 6.6 ± 4.9 μm, which is much larger than the

pores in the BC layer. Therefore, even though a large pressure is applied to the sandwich structure, the α-TCP particles did not completely penetrate through the BC layer. To confirm this, we created disks consisting of BC pressed into the cement at 250 MPa, put them into water at 85°C for 24 hours to form hydroxyapatite, and broke the disks in half to image the BC-cement interface. Figure 17F shows hydroxyapatite crystals can be found up to about 10 microns from the cement-BC interface, with their frequency decreasing with increasing distance from the interface. This interface shows that the BC is indeed mineralized by the hydroxyapatite. The hydroxyapatite did not extend into the BC beyond about 10 microns. Figure 18 shows the BC 40 microns from the interface with cement is completely devoid of hydroxyapatite.

Infiltration of PVA into the BC layer increased the strain at failure, but not the adhesive shear strength. Infiltration of PAMPS into the BC layer also did not significantly increase the strength and led to a smaller increase in the strain at failure than PVA due to the more brittle nature of the PAMPS hydrogel.[89] However, infiltration of both PVA and PAMPS into the BC layer leads to an increase in the adhesive shear strength to 1.70±0.18 MPa, an increase of almost 300%. These results indicate the hydrogel components are penetrating into the BC layer and that both components are necessary to achieve a larger adhesive shear strength than BC alone.

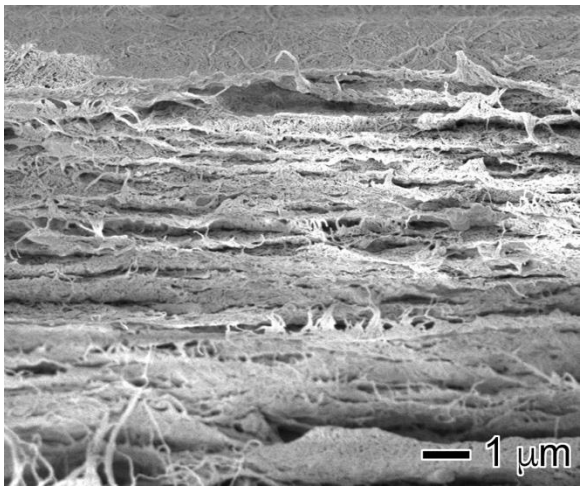

Figure 18: SEM image of BC about 40 ~ 10 microns from the cement-BC interface.

The adhesive shear strength can be further improved by performing multiple freeze-thaw cycles on the PVA hydrogel. It has previously been shown that multiple freeze-thaw cycles increase the tensile strength of PVA film.[186] Therefore, we applied seven cycles of freezing and thawing to the PVA after infiltration into the BC, and before infiltration of the PAMPS. Multiple cycles of freezing and thawing increase the adhesive shear strength to 2.28±0.27 MPa (see Figure 17G). This is within the range of the shear strength between cartilage and subchondral bone (2.45±0.85 MPa), indicating the strength of this interface may be sufficient for attachment of the hydrogel to a porous titanium implant that allows for bone ingrowth. We also tested extending the time for diffusing the PVA into the BC layer by heating in the hydrothermal reactor for three days instead of one day at 110 °C. This processing change did not improve performance, indicating that the PVA is fully diffused into the BC layer within 24 hours.

3.4 Conclusion

In summary, we have described a new strategy, NEST, for forming bonds to hydrogels three times stronger than the state-of-the-art. NEST involves the formation of an adhesive bond to a nanofibrous sheet in the dry state, followed by the formation of a hydrogel within the nanofibrous sheet. An example of NEST was illustrated using an α-TCP cement containing phosphoserine for adhesion and stainless steel micropowder for reinforcement. The cement undergoes hydrolysis to form hydroxyapatite flakes that mineralize a ~10-micron-thick layer of the nanofibrous sheet of BC. This bond is strengthened further after infiltration of PVA and PAMPS into the BC sheet, resulting in nanofiber-mediated attachment between the hydrogel and the cement. These results show strong bonds to hydrogels can be achieved by mimicking the nanoscale structure of the osteochondral junction, namely the mineralization of the collagen nanofibers that give cartilage its tensile strength. Although we have focused on the use of α-TCP cement, other adhesives and cements may be employed with the NEST strategy. NEST may prove useful for creating hydrogel-capped titanium implants for cartilage resurfacing, in which the porous titanium base facilitates osseointegration and long-term fixation.

4. A Synthetic Hydrogel Composite with a Strength and Wear Resistance Greater than Cartilage

4.1 Introduction

Osteoarthritis (OA) is a degenerative joint disease that is a common cause of disability.[187, 188] OA leads to the formation of lesions in the articular cartilage that lines the ends of bones. Articular cartilage lesions most commonly occur in the knee and cause debilitating pain. Cartilage has a limited capacity for healing because it is avascular.[189] One approach to treating cartilage lesions is to attempt to regrow cartilage with a technique such as microfracture or autologous chondrocyte implantation.[102, 190, 191] Unfortunately, these methods have high failure rates (25-50% at 10 years), prolonged rehabilitation times (>12 months), and show decreasing efficacy in patients older than 40–50 years.[102, 106] Implantation of fresh osteochondral allografts can speed recovery as grafts eliminate the need to regrow cartilage and, with a survivorship of 82% at 10 years, this approach is the most successful strategy for treatment of cartilage defects in the knee.[192, 193] Unfortunately, the small supply of fresh allografts limits the number of these procedures to around 1% of all cartilage repair surgeries.[102] Failure of these treatment strategies usually leads to more invasive total knee replacement. While total knee replacement is successful in older patients, it is not suitable for younger patients for whom the implant is likely to fail within their lifetime, thus requiring a second invasive surgery. For example, risk of revision surgery for total knee replacement is 5% for men in their 70's, but rises to 35% for men in their early 50's.[194] Thus there is a clear need for minimally invasive treatment options that

treat cartilage lesions with a low failure rate, enable rapid recovery, and are widely available.

Given the need for a less invasive alternative to total knee replacement for treatment of OA, there are ongoing efforts to replace damaged cartilage with a device made of traditional orthopedic materials, such as a cobalt-chrome alloy or ultra-high-molecular-weight polyethylene. [195-197] However, these materials have a much higher coefficient of friction (COF) than cartilage which leads to an unacceptable level of wear on the opposing cartilage surface. In addition, these materials are much stiffer than cartilage and will therefore cause an abnormal, non-physiological stress distribution in the joint, potentially contributing to the damage of surrounding cartilage. The failure rate for such implants is approximately 20% after 4 years.[198]

Hydrogels, polymer networks swollen with water, are the most promising synthetic material for replacement of cartilage because hydrogels can be made to have identical mechanical and tribological properties as articular cartilage.[14, 199, 200] We have previously reported an approach to create the first hydrogel that is equivalent to cartilage in its tensile and compressive strength. This hydrogel was made by infiltrating a bacterial cellulose (BC) nanofiber network with polyvinyl alcohol (PVA) and poly(2-acrylamido-2-methyl-1-propanesulfonic acid sodium salt) (PAMPS).[14] This hydrogel exhibited a tensile strength of 22.6 MPa and a compression strength of 20 MPa. In comparison, the range of tensile and compression strengths reported for human cartilage are 8.1-40 MPa and 14-59 MPa, respectively.[10-12] Thus, there is still room to improve the strength of hydrogels to be at the higher end of the range of strengths reported for cartilage, or to even exceed cartilage in

strength, while having a similar modulus, coefficient of friction, and resistance to wear. Achieving higher strengths would reduce the risk of failure for a weight-bearing hydrogel-based implant.

In preparing the BC-PVA-PAMPS hydrogel, we used the freeze-thaw method to gel the PVA-water mixture after infiltration into the BC. This gelation step is necessary to increase the strength of the PVA hydrogel, and to prevent dissolution of the PVA in the following PAMPS infiltration step. The freeze-thaw method is commonly used to create PVA hydrogels with tensile strengths up to 1 MPa.[201-204] The increase in strength upon freezing and thawing the PVA is attributed to crystallization of the PVA chains and phase segregation.[201, 202] The tensile strength of PVA hydrogel can be further increased to 18-20 MPa by drying and annealing the PVA, followed by rehydration.[56, 205, 206] We will hereafter often refer to the process of drying, annealing, and rehydration as simply "annealing" to be concise, i.e., an "annealed" hydrogel is one that has gone through the process of drying, annealing, and rehydration. The reason for the higher strength of annealed hydrogels is that the annealing process greatly increases the crystallinity and decreases the water content of PVA relative to the freeze-thaw process. A disadvantage of the annealing process is that it can result in more bubbles and cracks in the PVA, especially as the sample thickness or water content increases.

Given the higher tensile strength of annealed PVA relative to freeze-thawed PVA, we decided to test whether changing from a freeze-thaw to annealing process can improve the mechanical strength of a BC-PVA-PAMPS hydrogel while retaining adequate control over the hydrogel shape and defect content. Given the tensile strength of a BC-PVA-PAMPS

hydrogel (22.6 MPa), is already similar to the tensile strength of a PVA hydrogel made by annealing (20 MPa), it was not obvious that switching to the annealing process for a BC-reinforced hydrogel would yield further improvements in the mechanical strength. In addition, the presence of BC or PAMPS could potentially interfere with the crystallization of PVA that occurs during the annealing process, thereby hindering the improvement in mechanical strength that occurs as a result of crystallization. It was also not clear whether we could obtain high-quality, bubble-free, crack-free samples after annealing PVA reinforced with BC. Minimizing defects is necessary to maximize the mechanical strength of the hydrogel. Finally, it was unclear whether the lower water content of the annealed hydrogel increase the COF and wear of an opposing cartilage surface.

This work shows that reinforcement of annealed PVA with BC leads to a 3.2-fold improvement in the tensile strength and a 1.7-fold increase in the compressive strength (see Figure 19 and Table 1). The highly crystallized BC-PVA hydrogel that results from annealing is the first hydrogel with a tensile and compressive strength that exceeds that of cartilage. Reinforcement of the PVA with BC essentially eliminated the deformation and bubbles that would otherwise occur during annealing. When tested against cartilage for 1 million cycles, annealed BC-PVA wore an opposing cartilage surface to the same extent as cartilage and was three times more resistant to wear than cartilage. Annealed BC-PVA was 4.3 times more wear resistant than annealed PVA. The COF of BC-PVA against cartilage was equivalent to that of cartilage against cartilage, whereas the COF of annealed PVA increased over the course of the test to be 6.75 times greater than cartilage. In contrast to results with freeze-thawed BC-PVA, addition of PAMPS to the annealed BC-PVA

decreased the tensile strength of the hydrogel due to a loss of crystallized PVA and an increase in water content. The improved tensile strength of annealed BC-PVA enabled it to attach to a metal base with a shear strength 68% greater than the shear strength of cartilage on bone. The high strength, high wear resistance, and low COF of annealed BC-PVA make it an excellent material for replacing damaged cartilage.

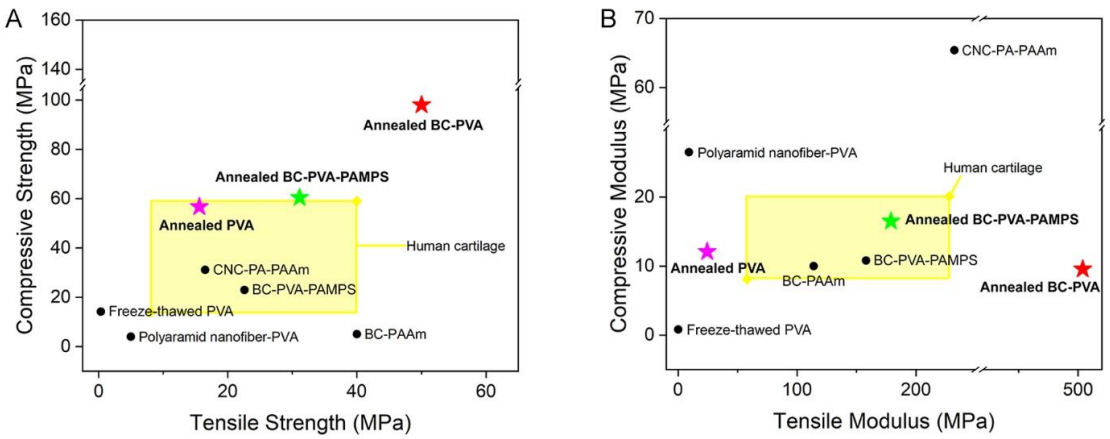

Figure 19: Mechanical properties of annealed BC-PVA and BC-PVA-PAMPS hydrogels. (A) Compressive vs. tensile strength and (B) compressive vs. tensile modulus for annealed BC-PVA and annealed BC-PVA-PAMPS compared with other strong hydrogels.

4.2 Experiments and Methods

4.2.1 Materials

Bacterial Cellulose (BC) was purchased from Gia Gia Nguyen Co. Ltd. Poly(vinyl alcohol) (PVA) (fully hydrolyzed, molecular weight: 145,000 g mol^{-1}), N,N'-methylenediacrylamide (MBAA, 97.0%), 2-hydroxy-4'-(2-hydroxyethoxy)-2-methylpropiophenone (I2959), potassium persulfate (KPS) and 2-acrylamido-2-methylpropanesulfonic acid sodium salt (AMPS, 50 wt.% solution in water) were

purchased from Sigma Aldrich. Phosphate buffered saline (PBS) was purchased from VWR International. Fetal bovine serum (FBS, Canada origin, collected from cattle typically 12-24 months old) was purchased from Corning. Shape memory alloy ring clamps were purchased from Intrinsic Devices.

4.2.2 Fabrication of BC-PVA-PAMPS Hydrogel

BC sheets were pressed to be 0.5 mm thick and placed into a hydrothermal reactor with a mixture of PVA (40 wt.%) and DI water (60 wt.%). The hydrothermal reactor was sealed and heated at 135°C for 24 hours to allow the PVA to diffuse into the voids of BC and form a BC-PVA hydrogel. The BC-PVA hydrogel was removed from the reactor when hot (>85°C). Note the hydrothermal reactor was pressurized with hot steam and is a burn hazard, so personal protective equipment including lab coat, heat resistant gloves and full-coverage face shields should be used when opening the reactor. The residual PVA solution was removed by scrapping the surface of the BC-PVA samples with a metal spatula. The samples were frozen at -78°C for 30 minutes and thawed at room temperature to physically crosslink the PVA network. The BC-PVA hydrogel was then soaked in a solution of AMPS (30 wt.%), MBAA (60 mM), I2959 (50 mM) and KPS (0.5 mg mL-1) for 24 hours. The hydrogel was cured with a UV transilluminator (VWR International) for 15 minutes on each side, and further cured in an oven at 60°C for 8 hours to ensure even and complete curing. The resulting BC-PVA-PAMPS hydrogel was stored in PBS for at least 24 hours before further characterization.

4.2.3 Fabrication of Annealed BC

BC sheets were pressed to be 0.5 mm thick. The BC sheets were then placed into a 90°C oven for 24 hours before being annealed at 90°C for an additional hour. The resulting annealed BC was cut into the desired shape and stored in PBS (0.15 M) for at least 24 hours.

4.2.4 Fabrication of PVA Hydrogel

To fabricate the PVA hydrogel, a slurry of PVA (40 wt.%) and DI water (60 wt.%) were mixed in a metal baking pan (diameter: 203.2 mm) and heated at 120°C for 20 minutes in an autoclave sterilizer. To make annealed PVA hydrogel, the resulting hydrogel was dried in an oven at 90°C for 24 hours before being annealed at 90°C, 120°C or 140°C for an additional hour. To make freeze thawed PVA hydrogel, the autoclaved hydrogel was frozen at -80 °C for 30 minutes and thawed at 23°C for 30 minutes. The resulting PVA hydrogel was cut into the desired shape and stored in PBS (0.15 M) for at least 24 hours before testing.

4.2.5 Fabrication of Annealed BC-40 wt.% PVA Hydrogel

BC sheets were pressed to be 0.5 mm thick and placed into a hydrothermal reactor with a mixture of PVA (40 wt.%) and DI water (60 wt.%). The hydrothermal reactor was sealed and heated at 135°C for 24 hours to allow the PVA to diffuse into the voids of BC and form a BC-PVA hydrogel. The BC-PVA hydrogel was removed from the reactor when hot (>85°C). The residual PVA solution was removed by scrapping the surface of the BC-PVA samples with a metal spatula. The samples were dried in an oven at 90°C for 24 hours before annealing at 90°C, 120°C or 140°C for an additional hour. The resulting annealed

BC-PVA hydrogel was cut into a desired shape and stored in PBS (0.15 M) for at least 24 hours before tests.

4.2.6 Fabrication of Annealed BC-10 wt.% PVA Hydrogel

BC sheets were pressed to be 0.5 mm thick and placed into a baking pan (15.6 cm × 8.6 cm × 4.2 cm). Approximately 30 mL of 10 wt.% PVA solution was added to the baking pan. The baking pan was placed in an oven at 90°C for 24 hours and annealed at 90°C for an additional hour. The resulting annealed BC-PVA hydrogel was cut into the desired shape and stored in PBS (0.15 M) for at least 24 hours.

4.2.7 Fabrication of Annealed BC-PVA-PAMPS Hydrogel

BC sheets were pressed to be 0.5 mm thick and placed into a hydrothermal reactor with a mixture of PVA (40 wt.%) and DI water (60 wt.%). The hydrothermal reactor was sealed and heated at 120°C for 24 hours to allow the PVA to diffuse into the voids of BC and form a BC-PVA hydrogel. The BC-PVA hydrogel was removed from the reactor when hot (>85°C). Note the hydrothermal reactor was pressurized with hot steam and created a burn hazard, so personal protective equipment including a lab coat, heat resistant gloves and full-coverage face shields should be used when opening the reactor. The residual PVA solution was removed by scrapping the surface of the BC-PVA samples with a metal spatula. The samples were dried in an oven at 90°C for 24 hours before being annealing at 90°C, 120°C or 140°C for an additional hour. The annealed BC-PVA hydrogel was then soaked in a solution of AMPS (30 wt.%), MBAA (60 mM), I2959 (50 mM) and KPS (0.5 mg mL-1) for 24 hours. The hydrogel was cured with a UV transilluminator (VWR

International) for 15 minutes on each side, and further cured in an oven at 60°C for 8 hours to ensure even and complete curing. The resulting annealed BC-PVA-PAMPS hydrogel was stored in PBS (0.15 M) for at least 24 hours before further characterization.

4.2.8 Fabrication of Hydrogel on A Stainless-Steel Pin

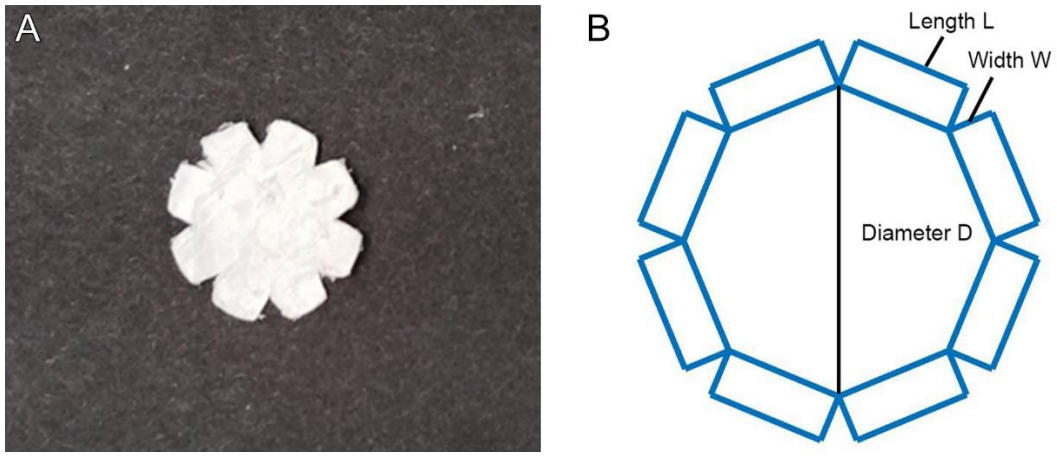

Figure 20: (A) Example of a BC sheet cut to have legs that wrap over the edge of a metal rod. (B) Diagram denoting the diameter, length, and width dimensions of the sheet.

Preparation of hydrogel samples on a stainless-steel pin started with cutting the freeze-dried BC. The BC was cut in the shape of an octagon with diameter D, 8 legs of length of L, and widths of W=0.383D (See Figure 20 for example). The sample was labeled as BC-D-L after cutting. The 8-piece star shape (BC-D-L) was generated by MATLAB and loaded into Adobe Illustrator. In Adobe Illustrator the stroke of the shape was changed to 0.0001 pt to ensure accurate cutting. The file was sent to the laser cutter (Epilog Fusion M2) using the print function and the laser cutter was selected as the printer. The vector process was used, with 100% speed, 20% power and 100% Frequency. For cutting the BC, a clean metal plate was placed on the bed of the laser cutter, and the freeze-dried BC was placed onto the metal plate. Another metal plate was placed onto the edge of the BC to ensure the BC did

not move. The focus was adjusted, and the shape was cut by the machine. After cutting, the BC was collected and stored in a petri dish for future use.

Figure 21: Overview of the method for attaching a hydrogel to a metallic pin with a shape memory alloy clamp.

For preparing the shear test samples, six pieces of BC were adhered to the stainless-steel rod with one layer of cement and a clamp. An overview of the assembly method is shown in Figure 21. A stainless-steel test rod was machined to have a top section with a diameter of 5.2 mm and a height of 2 mm, and a bottom section with a diameter of 6.75 mm and a height of 13 mm. Three pieces of BC-6.5-2.25 and 3 pieces of BC-6.5-2 were placed in an alignment fixture. Scotchbond Universal Adhesive was applied to the layer of the BC in contact with the rod and the top surface of the rod. The adhesive was allowed to set for 20 seconds before being blown by air for another 5 seconds. About 0.15 g of RelyX Ultimate Cement was then applied to the same surfaces coated with the Scotchbond Universal Adhesive. The rod was pressed into the BC layers and then into a shape memory alloy ring clamp. The cement was cured for 1 h. The sample was heated in an oven at 175℃ for 10 min to shrink the clamp. The sample was then soaked in DI water for 1 hour in a centrifuge

tube before future use. The sample with BC on top then went through the specific hydrogel fabrication process.

Compression test samples were fabricated using the stainless-steel rod and a clamp, but without cement. Wear test samples were fabricated with a stainless-steel rod 5.7 mm in diameter and 38 mm in height, 3 pieces of BC-6.5-2, and the shape memory alloy ring, but without cement.

4.2.9 Monotonic Tensile and Compression Tests

Monotonic tensile tests were carried out on an Instron 1321 load frame (Instron, Norwood, MA, USA) and a Test Resources 830LE63 Axial Torsion Test Machine (TestResources, Shakopee, MN, USA) at a rate of 0.25 mm s^{-1}. The finished hydrogel was cut into an ASTM D638-14 Type V shape with a titanium hollow punch for testing (see Figure 22 for examples). The dimensions of the samples were measured with a caliper before testing. The ultimate tensile strength (UTS) was the maximum stress measured before fracture in the case of the BC-PVA samples, or the maximum compressive stress at 80% strain for the PVA samples. The tensile modulus was taken as the slope of the stress-strain curve at a stress of 1 MPa for comparison with previous studies of human cartilage.[12]

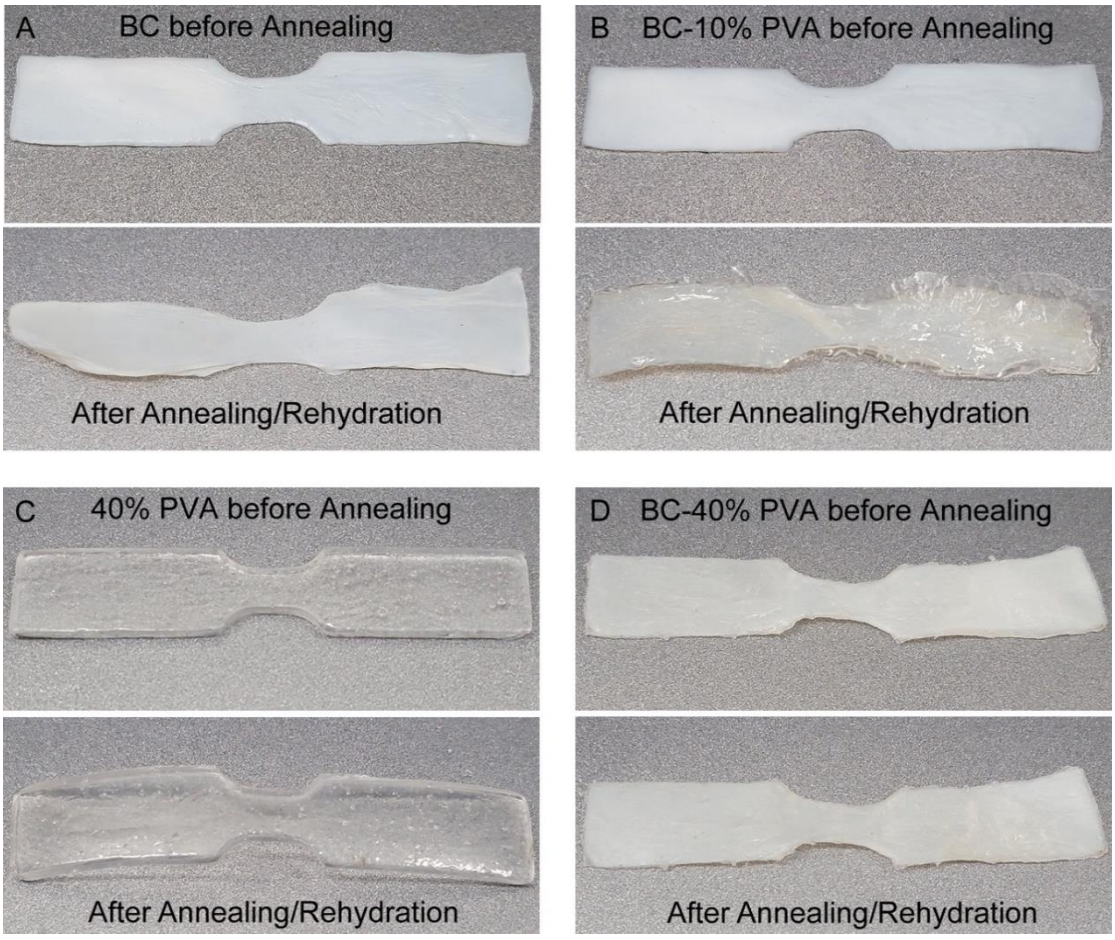

Figure 22: Hydrogel samples before and after annealing and rehydration. All samples were annealed at 90°C for 25 hours and rehydrated in PBS solution for 24 hours at 23°C. (A) A sample of BC without PVA. (B) A sample of BC that was annealed in a solution of 10 wt.% PVA. (C) A sample of 40 wt.% PVA. (D) A BC sample that was infiltrated with 40 wt.% PVA in a hydrothermal bomb for 24 hours at 120°C before annealing and rehydration.

The compressive properties of all samples were measured with a Test Resources 830LE63 Axial Torsion Test Machine. Cylindrical samples of PVA were cut out of films of hydrogel samples with a hollow steel punch with a diameter of 4 mm. BC-PVA samples were attached to a metal pin for compression testing in order to have a sample that was sufficiently thick. The dimensions of the samples were measured with a caliper before

testing. The compressive properties were measured with a strain rate of 0.05 s^{-1}. The compressive strength was taken stress at a strain of 0.8, or the stress at fracture if the material failed before a strain of 0.8. The compressive modulus was derived as the slope of the stress-strain curve at a stress of 0.4 MPa for comparison with previous studies of human cartilage.[10]

4.2.10 Differential Scanning Calorimetry

Differential scanning calorimetry (DSC) was performed on hydrogel samples to determine the crystallinity of the PVA. The tests were completed on a TA Instruments TGA550. In a typical test, a hydrogel sample of approximately 5 mg was placed in an aluminum pan and heated at a scanning rate of 10 °C/min under a nitrogen gas flow from 25°C to 300°C. Typical thermograms for PVA, BC-PVA and BC-PVA-PAMPS hydrogels are shown in Figure 23.

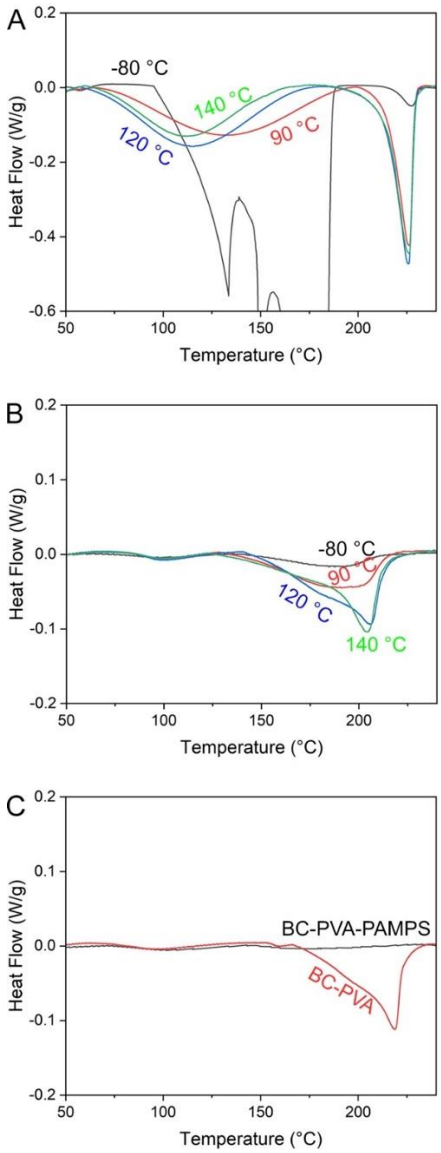

Figure 23: DSC thermograms for (A) freeze-thawed and annealed PVA hydrogels, (B) freeze-thawed and annealed BC-PVA hydrogels, and (C) annealed BC-PVA and annealed BC-PVA-PAMPS. The concentration of the AMPS solution used to make the BC-PVA-PAMPS was 10 wt.%.

The calculation for how much of the PVA was crystallized, i.e., the degree of crystallinity, was adopted from Hassan et al.[207] After the DSC thermogram was acquired, the area under the melting peak over the range 140-220°C (as shown in Figure 24) was integrated to obtain

a value with units of $J \cdot °C \cdot S^{-1} \cdot g^{-1}$. This number was then divided by the heating rate (0.17 $°C \cdot S^{-1}$) to obtain ΔH ($J \cdot g^{-1}$). The crystallinity of PVA, χ_{PVA} was then calculated by dividing ΔH for the sample by the heat required for melting a 100% crystalline PVA sample, $\Delta H_c = 138.6\ J/g$, and the weight fraction of PVA in the sample, w_{PVA}:

$$\chi_{PVA} = \frac{\Delta H}{w_{PVA} \times \Delta H_c}$$

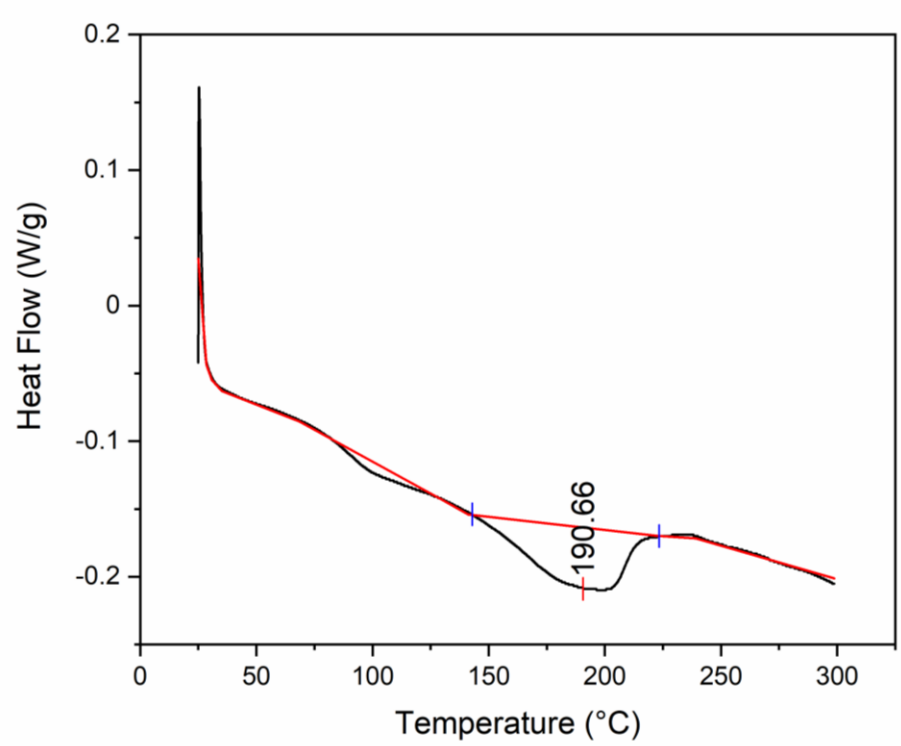

Figure 24: DSC thermogram for an annealed BC-PVA hydrogel sample demonstrating how the peak was integrated.

4.2.11 Measurement of Solid Weight Fraction

The weight of approximately 1 g of hydrated hydrogel was measured before drying at 90°C for 24 hours. The weight of the dehydrated sample was then measured. The weight after

dehydration was divided by the weight before dehydration to determine the solid weight fraction of the hydrogel sample.

4.2.12 Fourier Transform Infrared Spectroscopy

Fourier Transform Infrared (FTIR) spectroscopy was performed on hydrogel samples to analyze changes in bonding after annealing. Hydrogel samples were cut into a 1 cm by 1 cm square before testing. The tests were completed on a Thermo Scientific Nicolet iS50 FT-IR. In a typical test, the sample was held under the detector with the number of scans set to 32, resolution set to 4 (0.482 cm^{-1}) and format set to % transmittance. Typical FTIR spectra are shown in Figure 25.

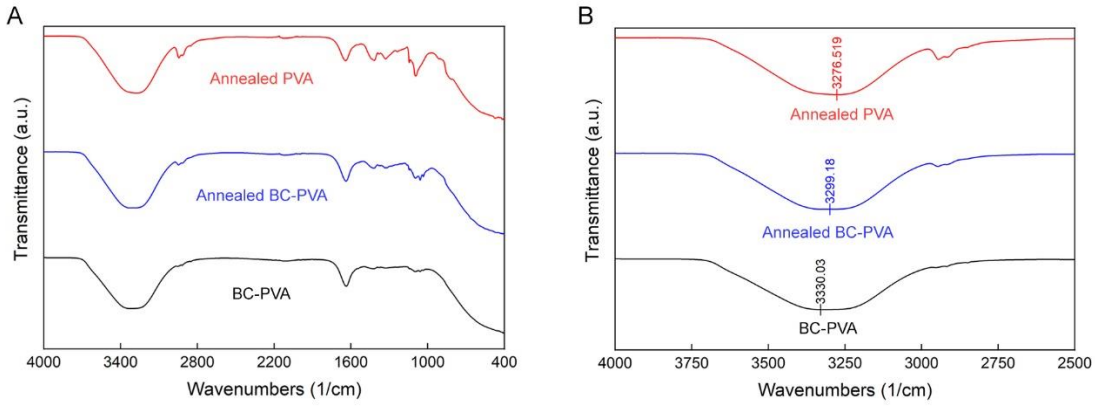

Figure 25: (A) FTIR spectra of BC-PVA, annealed BC-PVA and annealed PVA hydrogels. (B) Zoomed in region highlighting the shift of the hydroxyl peak.

4.2.13 Wear Testing

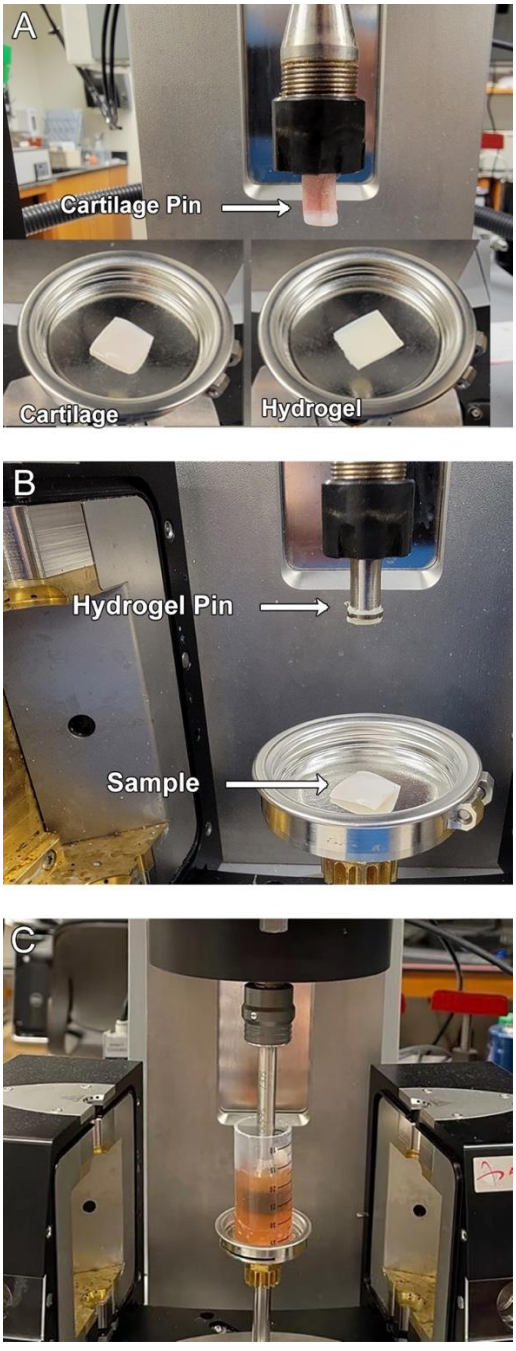

Figure 26: Images of the test setup using (A) a cartilage pin and (B) a hydrogel pin for the measurement of the wear and COF. (C) Image during the wear test.

The wear resistance of the hydrogels and porcine cartilage samples were determined with the pin-on-disk setup shown in Figure 26. The pin-on-disk method was used with an Anton Paar Rheometer (MR302) and a tribology accessory (SCF7). Cartilage samples were harvested from pig femurs with an osteochondral autograft transfer system (Arthrex). The femurs were purchased from a local grocery store and frozen at -78°C before harvesting the samples. Hydrogel samples were polished with #600, #800, #1000, #1200, #1500, #2000, #2500 and #3000 sandpapers to make them smooth prior to testing. A hydrogel pin was fabricated by using the method described in section 4.2.8. A disk of hydrogel or porcine cartilage with a diameter of 12.7 mm was adhered with cyanoacrylate glue (Gorilla Glue Company) to the sample holder. The testing parameters were as follows: 1,000,000 rotations; angular speed: 319 rounds per minute (maximum linear velocity: 100 mm s-1); normal force: 28.26 N (pressure: 1 MPa). A pressure of 1 MPa was applied to each sample for 5 minutes before starting the test. The tests were performed in FBS. FBS is often used during wear tests to mimic the lubrication provided by synovial fluid[208-210].

After the wear test, the samples were rehydrated in FBS for 24 hours to allow the gels to recover from the applied pressure before the wear depth was measured with a High-Resolution X-ray Computed Tomography (Micro-CT) Scanner (Nikon XTH 225 ST). A 3D model of the reconstructed Micro-CT images was rendered with Avizo 9 Lite. To measure the wear depth, a slice of the 3D model was taken in the middle of the wear mark. The wear depths were measured from the images of the middle slices with ImageJ.

For calculating the COF, we determined the total friction force (F) from the torque (T) and the radius of the pin in the pin-on-disk setup (R):[211]

$$F = \frac{3T}{2R}$$

The *COF* can then be calculated by:

$$COF = \frac{F}{F_N}$$

Here F_N is the normal force (28.26 N). The linear velocity (v) was calculated by:

$$v = \omega R$$

where ω was the angular speed of the pin.

4.2.14 Shear Testing

Shear testing was performed on a Test Resources 830LE63 Axial Torsion Test Machine equipped with a 100 lb. load cell. Each test was performed in a customized shear test fixture (see Figure 27). For shearing of cartilage off bone or hydrogel off metal samples, the sample was secured in a cylindrical hole in the left side of the fixture. Spacers were added underneath the samples to precisely align the shear plane to the cartilage-bone or hydrogel-metal interface. The right side of the fixture was machined to have a complementary half-cylinder that was used to push the hydrogel or cartilage off of their substrates. A rubber spacer was placed between the sample and the right shear fixture to apply pressure during the shear test in order to minimize cleavage and peeling. A crosshead displacement rate of 2 mm min-1 was used for all the measurements.

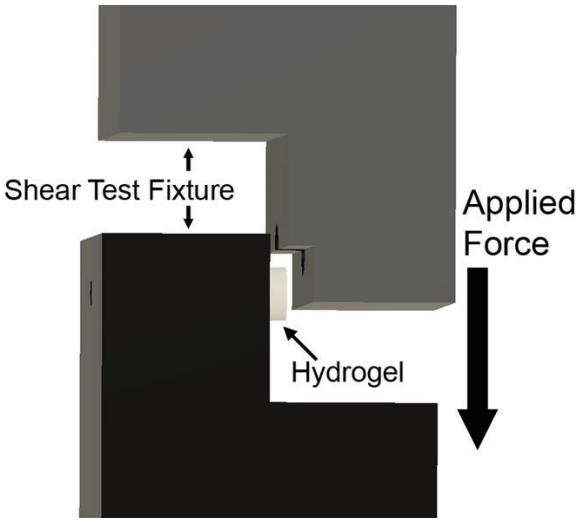

Figure 27: Image of the shear test fixture used for shearing cartilage off bone and the hydrogel off metal rods.

4.2.15 Fabrication of Human-Size Implant

A human-sized osteochondral implant 20 mm in diameter was fabricated. The top surface of the implant had a radius of curvature of 20 mm to match the native curvature of the femoral condyle. This implant was fabricated with 5 BC layers. A 0.25-mm-thick coating of commercially pure titanium was applied to the stem of the implant and underneath the base with a plasma spray process in order to improve integration with bone.[212]

4.3 Results

4.3.1 Effect of Annealing on Morphology

We first examine the effect of the hydrogel composition on the shape of the sample after drying, annealing and rehydration (or simply "annealing" to be concise). Figure 22A shows a sample of BC became wrinkled and folded at the edges after annealing. BC samples that were annealed in a 10 wt.% solution of PVA were also deformed (Figure 22B). The PVA layer that forms on top of the BC after annealing contains a large number of bubbles and

easily delaminates from the BC film. Figure 22C shows a sample of 40 wt.% PVA also formed a large number of bubbles and deformed during the annealing process. However, reinforcement of 40 wt.% PVA with BC allowed the hydrogel to retain its shape without deformation after annealing. We attribute this lack of deformation to the higher solid content and tensile modulus of the BC-reinforced PVA. The nanoscale network of the BC layer appears to suppress the formation of the large bubbles that are visible in the 40 wt.% PVA sample. Comparing Figure 22B&D indicates that the approach of infiltrating a high concentration of PVA into BC in a hydrothermal bomb, followed by removal of excess PVA from the BC surface, results in a more uniform hydrogel than if a BC sample is placed in a more dilute PVA solution that is concentrated via drying. These results demonstrate that, unlike BC alone, PVA alone, or the combination of BC with a 10 wt.% of PVA, the BC infiltrated with 40 wt.% PVA could retain its shape and remain relatively free of bubbles and other defects after annealing.

4.3.2 Effect of Annealing on The Mechanical Properties of PVA Hydrogel.

To determine the effects of annealing on the mechanical properties of various hydrogel compositions, we first analyzed the effects of annealing on a PVA hydrogel as a reference point. The PVA was fully hydrolyzed with a molecular weight of 145,000 g mol^{-1}. A 40 wt.% PVA solution was dried at 90°C for 24 hours, annealed at 90°C, 120°C or 140°C for 1 hour, and then placed in a 0.15 M PBS solution for 24 hours for rehydration. PVA samples that underwent a freeze-thaw cycle were tested for comparison. Figure 28A and 28B show that annealing the hydrogel dramatically increased the tensile and compressive

strength relative to samples that had undergone a freeze-thaw cycle. Figure 28D and Table 1 show that, relative to the freeze-thaw process, annealing increased the tensile strength by 60 times (from 0.26 to 15.6 MPa) and the compressive strength by 9 times (from 14.8 to 140.8 MPa). Increasing the annealing temperature from 90°C to 140°C led to an increase in the tensile strength and modulus, similar to previous work.[56, 205] The increase in strength and modulus has been ascribed to the increase in the crystallinity and solid content of the hydrogel after annealing. Figure 28E confirms that the crystallinity and solid content of the annealed PVA hydrogels are much greater than that of a freeze thawed PVA hydrogel. For example, a PVA hydrogel made via the freeze-thaw process has an overall solid content of 0.09 wt.% and a PVA crystallinity of 0.21 wt.%, whereas a PVA hydrogel made via annealing at 90°C has an overall solid content of 0.42 wt.% and a PVA crystallinity of 0.58 wt.%. The crystallites formed during annealing strengthen the otherwise amorphous PVA by acting as tough cross-links that redistribute applied stresses and hinder crack propagation.[53, 56] The crystallites also increase the solid content and strength of the hydrogel by reducing the amount of water taken up by the PVA when it is soaked in PBS (0.15M) after annealing.

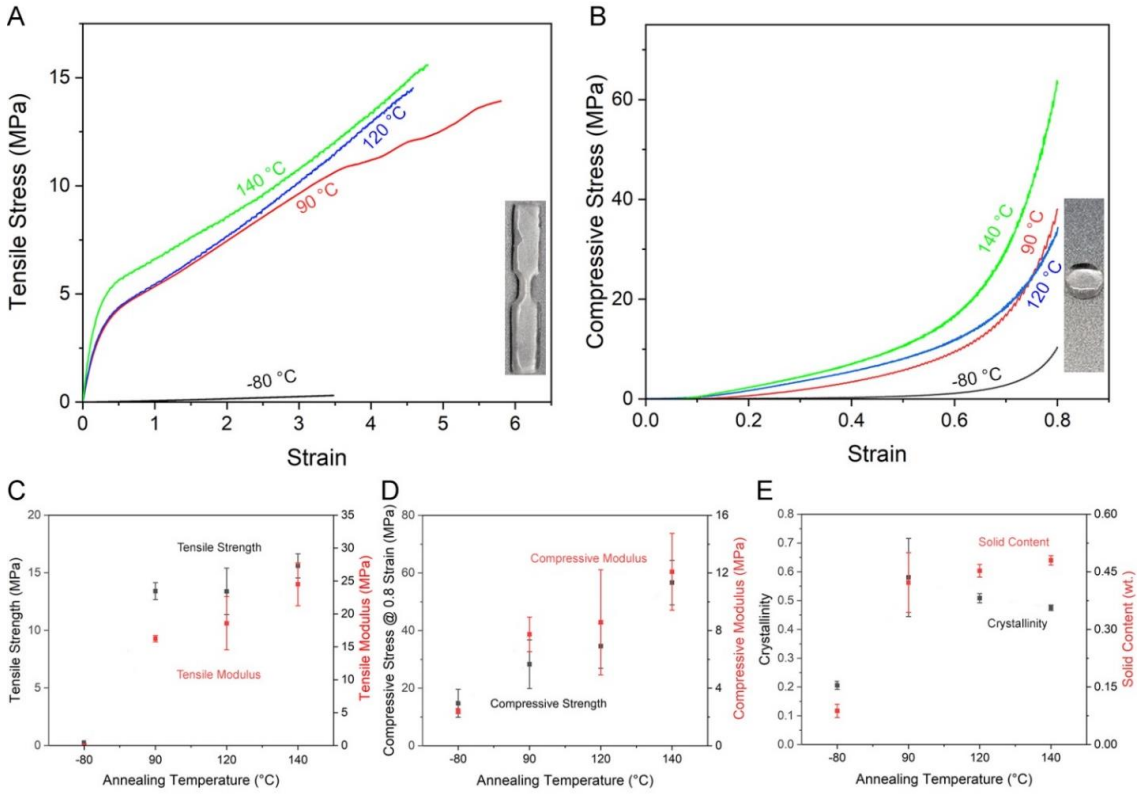

Figure 28: Mechanical tests results for PVA hydrogels. (A&B) Representative tensile and compressive stress-strain curves for PVA hydrogels annealed at different temperatures. (C) Tensile strength and moduli of PVA annealed at different temperatures. (D) Compressive stress at 0.8 strain and moduli of PVA annealed at different temperatures. (E) Crystallinity and solid content weight fraction of PVA annealed at different temperatures.

4.3.3 Effect of Annealing on A BC-PVA Hydrogel.

Next, we applied the same annealing process to BC-PVA hydrogels. As with the PVA hydrogels, the BC-PVA hydrogels were dried at 90°C for 24 hours, annealed at 90°C, 120°C or 140°C for 1 hour and then placed in a PBS (0.15 M) solution for 24 hours for rehydration. Figure 29A and 29C show the tensile strength of the annealed BC-PVA hydrogels reached 50.4 MPa, an increase of 4.6 times relative to the BC-PVA that went through a freeze-thaw cycle, and an increase of 3.2 times relative to annealed PVA that

was not reinforced with BC. Figure 29B and 29D show the compressive strength increased from 55.3 MPa to 95.4 MPa after annealing. Note the compression strength was measured for a BC-PVA hydrogel attached to a metal pin (see Supporting Information). Similar to the PVA hydrogel, this dramatic increase in strength can be attributed to the increase in crystallinity and solid content after annealing. Figure 29E shows the crystallinity of the BC-PVA hydrogel increased from 0.07 wt.% after a freeze-thaw cycle to 0.4 wt.% after annealing. The solid weight fraction of the BC-PVA hydrogel increased from 0.11 wt.% after a freeze-thaw cycle to 0.53 wt.% after annealing.

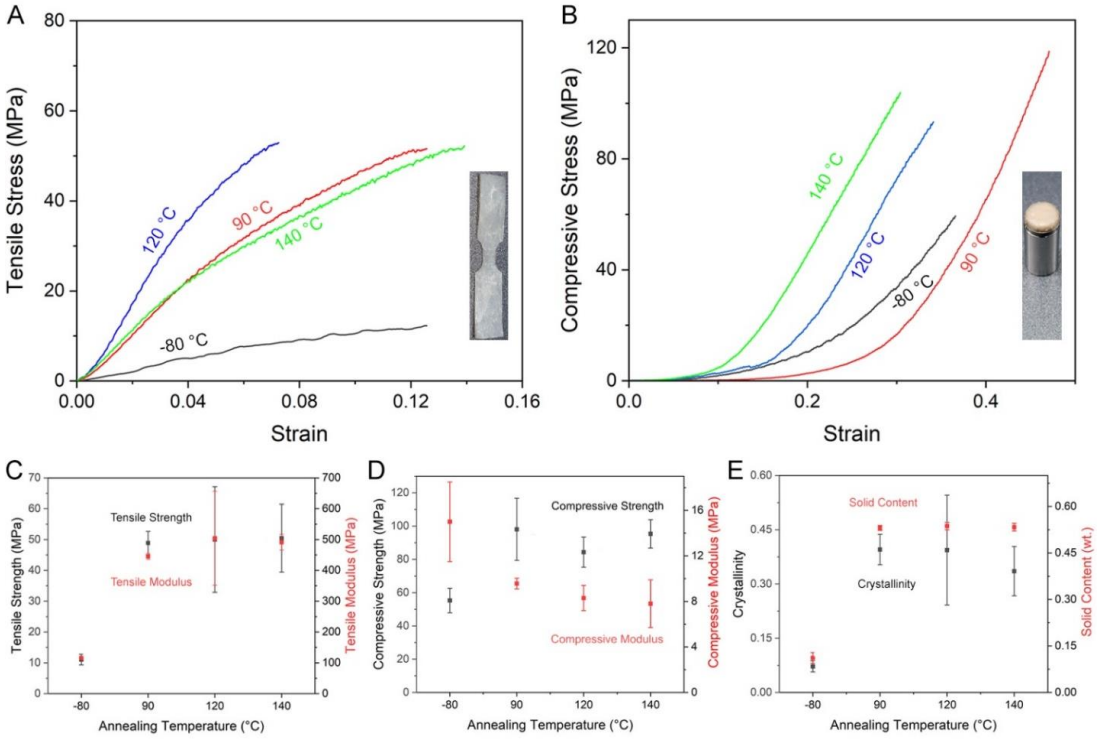

Figure 29: Mechanical tests results for BC-PVA hydrogels. (A&B) Representative tensile and compressive stress-strain curves for BC-PVA hydrogels annealed at different temperatures. (C) Tensile strength and moduli of BC-PVA annealed at different temperatures. (D) Compressive strength and moduli of BC-PVA annealed at different temperatures. Crystallinity and solid content weight fraction (E) of BC-PVA

annealed at different temperatures. Crystallinity here stands for the weight fraction of crystalline PVA in the entire hydrogel sample, including the PVA and water.

FTIR spectra (see Figure 25) show there was a decrease in the frequency of the hydroxyl stretching peak (from 3330 cm^{-1} to 3299 cm^{-1}) after annealing, indicating an increase in hydrogen bond formation[213, 214]. This peak shift and increase in hydrogen bond formation corroborates the increase in crystallinity measured with DSC. These results show that PVA can crystalize within the nanofibrous BC network, and that these crystallites increase the solid content and strength of the hydrogel.

4.3.4 Effect of PAMPS on An Annealed BC-PVA Hydrogel.

We previously reported that the incorporation of PAMPS into a BC-PVA hydrogel made with a freeze-thaw cycle resulted in an increase in the tensile and compressive strength of the hydrogel.[14] Thus, we next sought to determine the effect of incorporating PAMPS into an annealed BC-PVA hydrogel. As shown in Figure 30A, the addition of PAMPS into the annealed BC-PVA hydrogel led to a decrease in the solid content relative to BC-PVA alone, from 0.53 to 0.37. DSC thermograms (see Figure 23C) show that after the addition of 10 wt% PAMPS, the peak from melting crystalline PVA disappeared, indicating the addition of PAMPS destroys the PVA crystallites that form during the annealing process. The decrease in solid content and loss of crystallinity upon addition of PAMPS led to a decrease in the tensile strength (from 48.9 MPa to 20.8 MPa), tensile modulus (from 444.8 MPa to 150.5 MPa) and compressive strength (from 98.1 MPa to 56.0 MPa in Figure 30B) of the hydrogel. The increase in water content of the hydrogel and loss of strength was

likely due to the fact that PAMPS is a negatively charged polymer, and this negative charge results in an osmotic pressure that swells the hydrogel with water.[14]

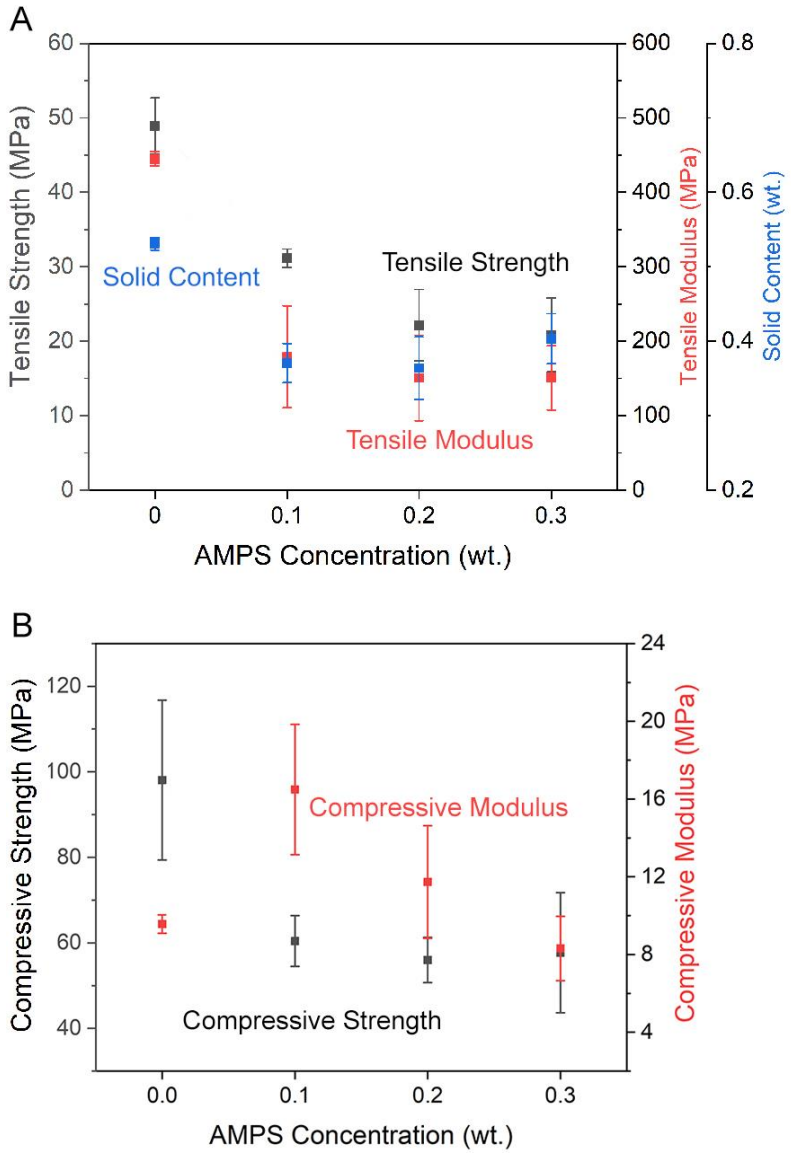

Figure 30: Mechanical tests results for BC-PVA-PAMPS hydrogels. (A) Tensile strength, tensile moduli and solid content weight fraction of BC-PVA-PAMPS hydrogels that were made with solutions containing different concentrations of the AMPS monomer. BC-PVA samples were annealed before infiltration of AMPS. (B) Compressive strength and moduli of BC-PVA-PAMPS hydrogels.

4.3.5 Wear and COF of Hydrogels Against Cartilage

The wear resistance of a potential replacement for cartilage should exceed that of cartilage to ensure durability and minimize the generation of wear debris that could potentially cause an adverse biological reaction. We have previously shown that the wear resistance of a BC-PVA-PAMPS hydrogel is equivalent to that of cartilage and is superior to that of PVA or PVA-PAMPS when tested against a stainless-steel pin.[14] These hydrogels were made by applying a freeze-thaw cycle to crystallize the PVA. Here we compare the wear resistance of PVA-based hydrogels (PVA, BC-PVA, and BC-PVA-PAMPS) that have been dried and annealed at 90ºC to that of porcine cartilage when tested against a porcine cartilage plug in FBS. Figure 26 shows our pin-on-disc configuration for testing the wear of hydrogels in fetal bovine serum (FBS). The porcine cartilage plug was rotated against the hydrogel surface 10^6 times under 1 MPa of pressure and at a speed of 319 rotations per minute (maximum linear velocity was 100 mm s^{-1}). Figure 31A is a schematic illustration of how the wear test was performed.

Figure 31B shows cross-sectional Micro-CT images of the hydrogels that were acquired in the center of the wear mark to measure the maximum wear depth. Figure 31C compares the wear depth of the hydrogels and cartilage. The wear depth of the BC-PVA hydrogel with 0% AMPS was 70.1 μm. The addition of 20% AMPS decreased the mean wear depth to 65.9 μm, but the difference between the 0% and 20% AMPS samples was not statistically significant. This comparison illustrates that the negative charge and higher water content caused by incorporating PAMPS into an annealed BC-PVA hydrogel does not significantly

improve the wear resistance. Both of these values were 3 times lower than the wear depth on the cartilage sample, which was 227.8 μm. The wear depth for annealed and rehydrated PVA was 301.0 μm, four times greater than either BC-PVA sample. These results indicate the presence of BC in the hydrogel can dramatically improve the wear resistance of an annealed PVA hydrogel to be superior to that of cartilage

We also recorded the COF during the wear test. Cartilage maintained a constant COF of 0.020 during the test. The COF of BC-PVA decreased during the test from 0.040 to 0.021. The BC-PVA hydrogel with 20% AMPS had a similar COF as that without AMPS. In contrast, the COF of PVA increased dramatically during the test, from 0.033 to 0.135. Previous work has similarly demonstrated the COF of PVA against cartilage increases over time while the COF of cartilage against cartilage is constant.[215, 216] The increase in the COF for a PVA-Cartilage interface has been ascribed to transfer of damaged PVA to the cartilage surface, which in turn decreases the ability of the cartilage surface to maintain a lubricating water layer.[216] The incorporation of BC into PVA clearly inhibits damage of the hydrogel, allowing it to maintain a low coefficient of friction similar to that cartilage during the wear test. The presence of PAMPS in the hydrogel is not necessary for maintaining a low COF and high resistance to wear.

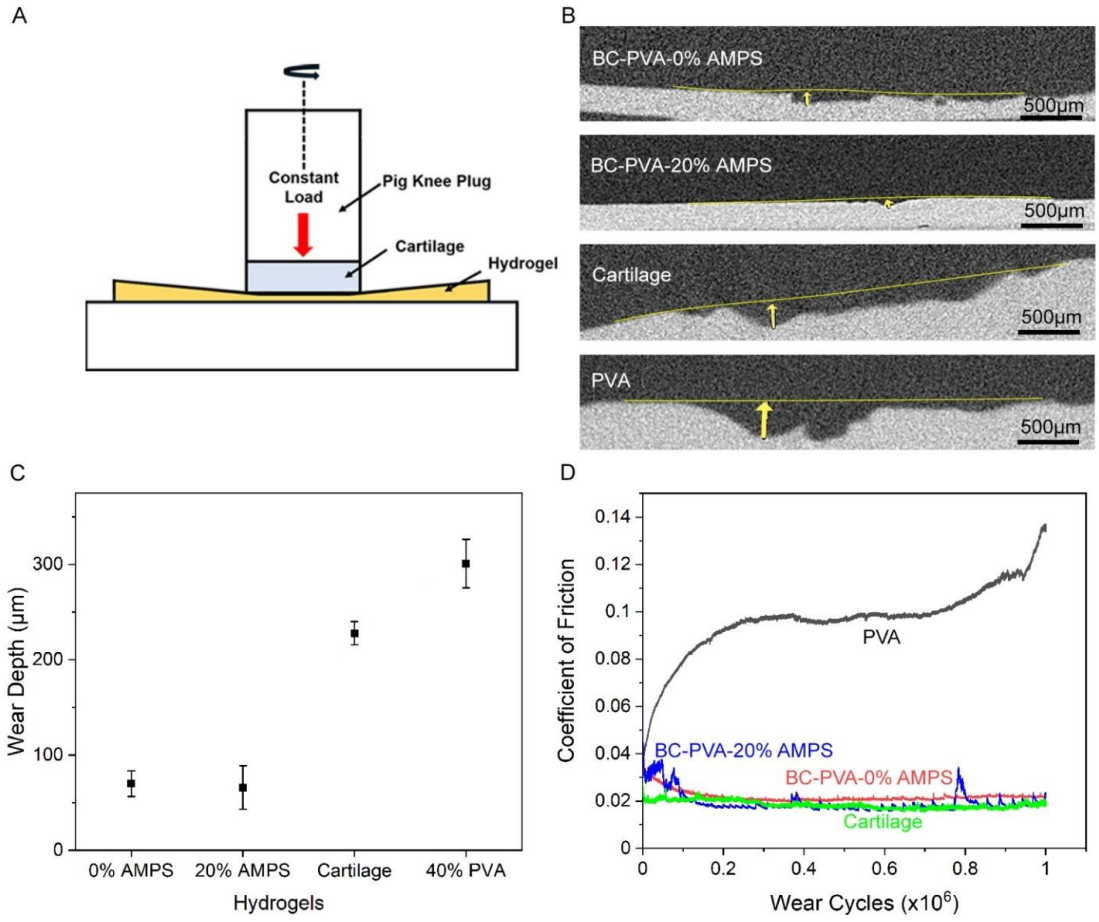

Figure 31: Cartilage-on-gel wear test results. (A) A schematic for how the wear of hydrogels vs. cartilage was measured. (B) Micro-CT cross-section images and (C) the wear depth of cartilage and hydrogel samples after 106 cycles under 1 MPa of pressure, a spin rate of 100 mm/s, and with FBS as the lubricant. (D) The coefficient of friction between cartilage and the hydrogels during the tests.

It is critical that materials used for cartilage replacement on one side of the joint, i.e., on the femoral condyle, do not cause wear of cartilage on the opposing surface, i.e., the tibial plateau. Traditional orthopedic materials like cobalt-chrome and ultra-high molecular-weight polyethylene are known to damage an opposing cartilage surface to a greater extent than hydrogels due to the higher COF and hardness of traditional orthopedic materials.[217-219] To assess the wear caused by BC-PVA and BC-PVA-PAMPS hydrogels on cartilage,

we created hydrogel plugs for wear testing (as described in Supplemental Information). Hydrogel plugs were pressed against cartilage samples (see Figure 32A and Figure 26B) with 1 MPa of pressure and rotated 10^6 times at a speed of 319 rotations per minute (the maximum linear velocity at the circumference of the pin was 100 mm s^{-1}).

Figure 32B shows cross-sectional μ-CT images of the cartilage samples that were acquired in the center of the wear mark to measure the maximum wear depth. Figure 32C compares the wear depth on cartilage caused by the hydrogels or cartilage. The wear caused by the BC-PVA on cartilage (247 ± 16 μm) was not significantly different from the wear caused by cartilage on cartilage (228 ± 12 μm). The addition of PAMPS into the BC-PVA reduced the wear on the opposing cartilage surface to 81 ± 27 μm, significantly below the wear of cartilage on cartilage.

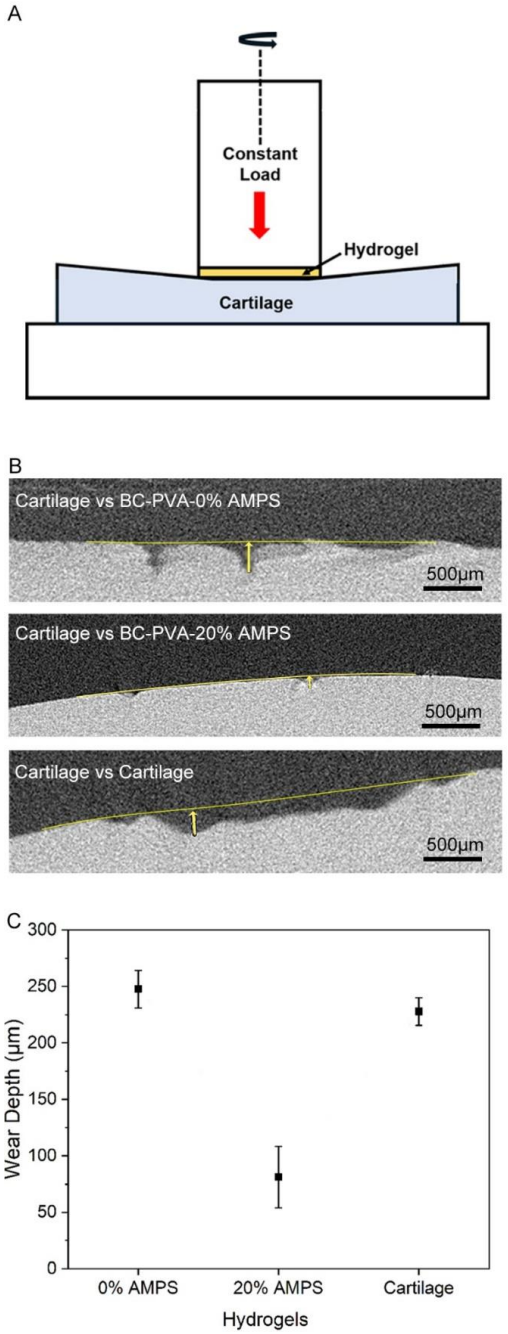

Figure 32: Gel-on-cartilage wear test results. (A) A schematic for how the wear of cartilage vs. hydrogels was measured. (B) Micro-CT cross-section images and (C) the wear depth of cartilage and hydrogel samples after 106 cycles under 1 MPa of pressure, a spin rate of 100 mm/s, and with FBS as the lubricant (N=3).

4.3.6 Shear Strength

We hypothesized that increasing the tensile strength of the hydrogel should also increase the shear strength. In order to be used for a cartilage replacement material, a synthetic hydrogel must be secured into a defect site with the same shear strength as the junction between cartilage and bone. One way to accomplish this goal is to have hydrogels that directly attach to bone or cartilage with sufficient strength, but this has not been achieved. Alternatively, the hydrogel can be attached to a metallic base, such as titanium, which has the ability to integrate with bone. As illustrated in Figure 21, we did this by first attaching freeze-dried BC to a metal rod with a combination of an adhesive and a shape memory alloy clamp, followed by infiltration of the hydrogel into the BC.

The setup used for shear testing is illustrated in Figure 27. Figure 33 shows the results for the shear testing of a plug of porcine cartilage on bone extracted from a pig knee, a BC-PVA-PAMPS hydrogel made with the previous freeze-thaw process, and a BC-PVA hydrogel annealed at 90 °C and then rehydrated. Both of the hydrogels are attached to stainless-steel rods with a combination of RelyX Ultimate cement and a shape memory alloy ring. The BC-PVA shear strength of 1.98 MPA (Figure 33A) is significantly greater than that of porcine cartilage (p-value from one-way ANOVA is <0.05). The average value of the shear strength for BC-PVA is also 40% greater than that of BC-PVA-PAMPS, but the error in the measurements is such that the difference in these values is not statistically significant. Comparison of the samples after failure shows that while pig cartilage was sheared completely off of the underlying bone (Figure 33B), both freeze-thawed BC-PVA-PAMPS and annealed BC-PVA were fractured on one side of the cylindrical sample but

remained attached (Figure 33C&D). These results show that the shear strength of attachment for the annealed BC-PVA is greater than that of pig cartilage.

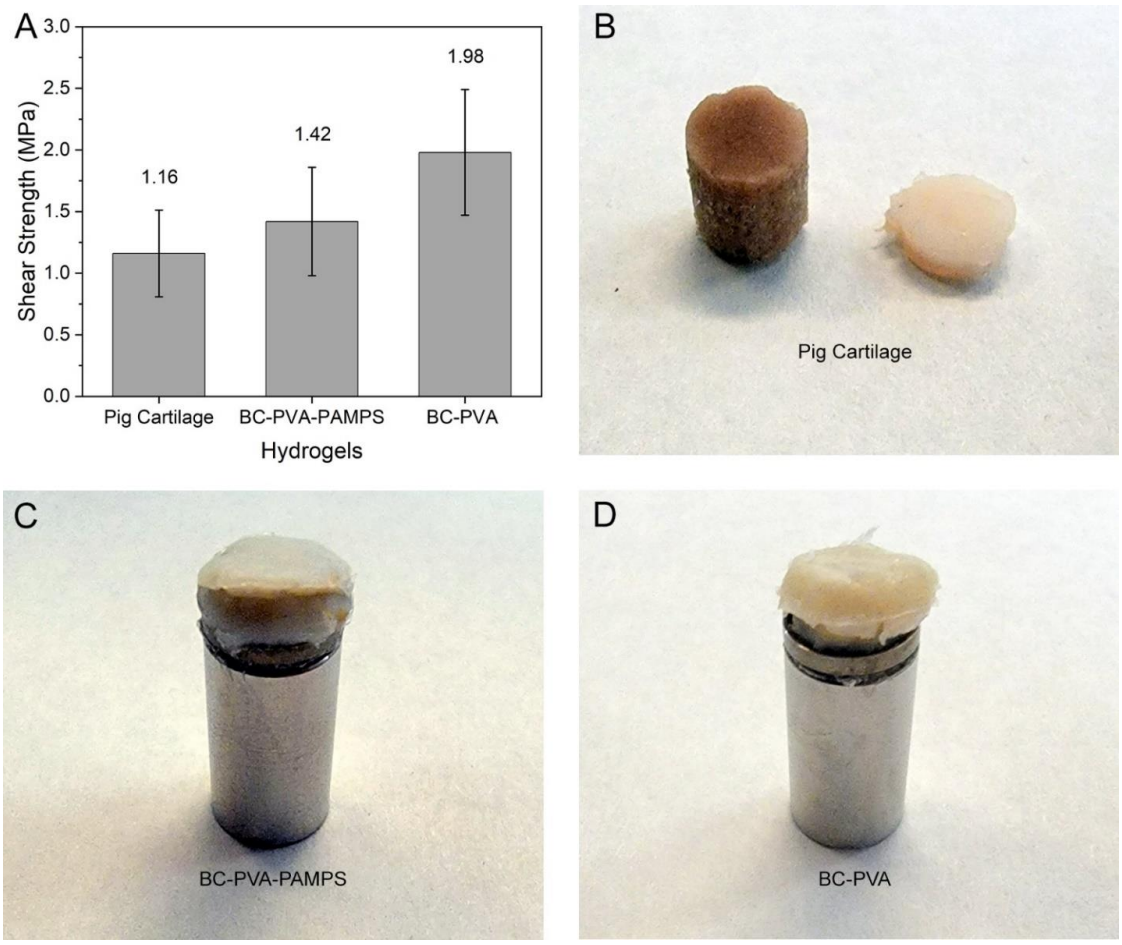

Figure 33: Shear tests results. (A) Results for shear testing of pig cartilage and hydrogels secured to metal pins with adhesive and a shape memory alloy clamp (N=3). (B-D) Images of samples after testing to failure. The osteochondral plug was extracted from a pig knee. The BC-PVA-PAMPS hydrogel was fabricated with the freeze-thaw process. The BC-PVA hydrogel was annealed at 90 ℃ and rehydrated.

4.3.7 Application to An Implant for Partial Knee Resurfacing

Thus far we have described the compression strength and shear strength of BC-reinforced hydrogels attached to a metal pin with a diameter of 5.2 mm. While this size is convenient

for testing, such a diameter is too small to serve as an implant for partial knee resurfacing. In addition, the samples lacked the curvature necessary to mimic the natural curvature of the femoral condyle. Thus, we sought to demonstrate the ability of the hydrogel to attach to a metal base with a size and shape representative of an implant for partial knee resurfacing.

Figure 34A show images of an implant 20 mm in diameter with a radius of curvature of 20 mm. An implant diameter of 20 mm is a typical size used for an osteochondral allograft, and a 20 mm radius of curvature is within the range of typical curvatures for the femoral condyle.[220] In this case, five pieces of BC were cut into shapes with 8 octagonal legs to enable the BC to fold over the edge of the implant. A 0.25-mm-thick coating of commercially pure titanium was applied to the stem of the implant and underneath the base with a plasma spray process in order to improve integration with bone.[212] Figure 34B&C show an example of how such an implant would be used to resurface the knee. Figure 34B shows an example of a cartilage defect. The surgeon would drill out a hole over the defect site that is complementary to the shape of the hydrogel-capped implant. The hydrogel-capped implant would then be pressed into the hole to replace the damaged cartilage.

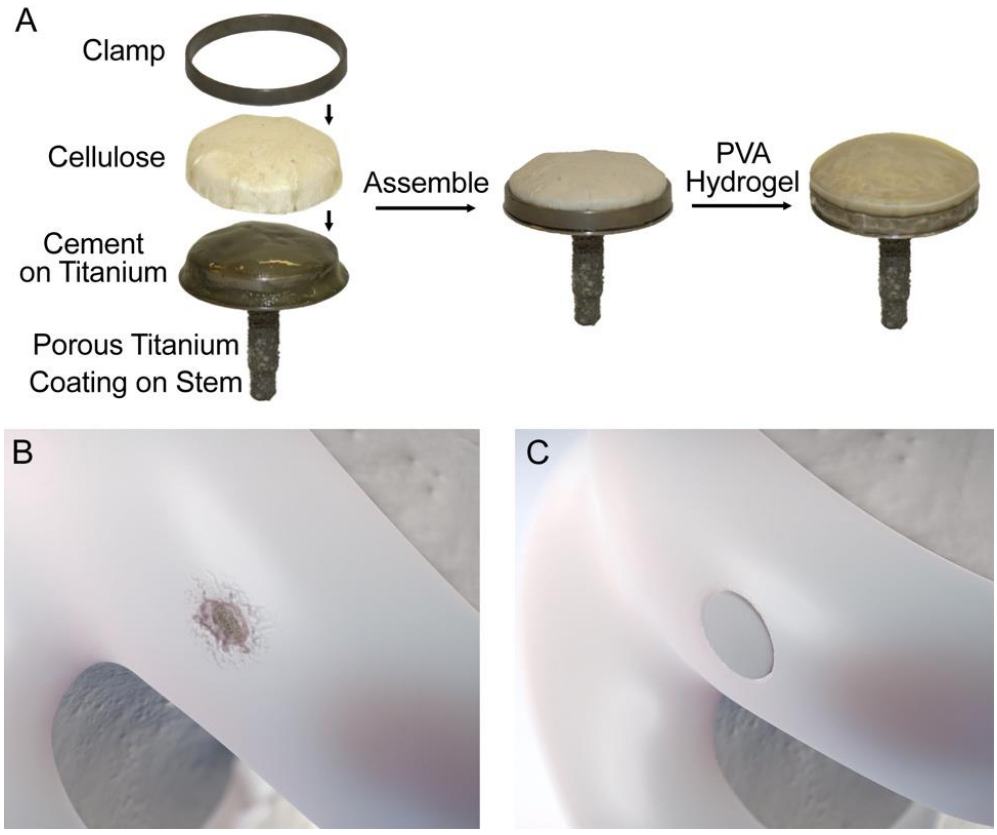

Figure 34: (A) Process for attaching the BC-PVA-PAMPS hydrogel to a titanium implant for (B&C) treatment of osteochondral defects.

4.4 Conclusion

This work shows that reinforcement of an annealed PVA hydrogel with BC enables the production of the first hydrogel with a compression and tensile strength greater than cartilage. Annealing increased the tensile strength of BC-PVA by 5 times and the compressive strength by 1.8 times relative to a freeze-thaw process due to the greater crystallization and lower water content that was achieved by annealing. Reinforcement of PVA with BC lowered the wear of the hydrogel by 4 times relative to PVA alone, and 3 times relative to cartilage. The annealed BC-PVA hydrogel caused a minimal amount of opposing surface wear, similar to what was caused by cartilage on itself. Attachment of the

BC to a metal plug via an adhesive and clamp, followed by infiltration and annealing of the PVA, enabled attachment of the BC-PVA hydrogel to a metal backing with a shear strength greater than the attachment of cartilage to bone. These advances in hydrogel strength and attachment enable the creation of an implant with a hydrogel surface and titanium backing that can enable durable resurfacing of damaged cartilage in an articulating joint.

5. Conclusion

Patients suffer from damage to the cartilage of their joints and are desperate for a less invasive alternative to total knee replacement. Resurfacing of their joints with a hydrogel would provide a more natural, less invasive alternative to the metal-on-plastic joints available today. A hydrogel-based implant could be used to resurface cartilage in joints without the concern of causing opposing surface wear that exists with traditional orthopedic materials. Currently no such implant is available in the US. Most cartilage lesions go untreated due to the lack of effective treatment strategies, leading to further cartilage deterioration and the need for a total knee replacement. Key hurdles to development of a hydrogel device for cartilage resurfacing are (1) the development of a hydrogel with properties better or at least similar to those of cartilage and (2) fixation of this hydrogel onto the surface of an articulating joint.

This dissertation described the clearing of these hurdles through the development of the first hydrogel with the strength that exceeds that of cartilage, and the first attachment of a hydrogel to a metal backing (which can integrate with bone) with a shear strength that exceeds that of cartilage on bone.

First, we combined the advantages of all its components, the high strength of BC, the high elasticity of PVA and the osmotic pressure brought by PAMPS to create a BC-PVA-PAMPS hydrogel that for the first time, had possessed cartilage-equivalent mechanical properties. Then, we developed the NEST strategy, using the in-network mineralization of calcium phosphate cement, to attach the hydrogel to a porous titanium base. This new

strategy achieved a shear strength of 3 times as high as the previous best result and was already comparable to the subchondral bone.

To further improve the incredible mechanical properties of our hydrogel, we introduced a heat-annealing step of PVA into the fabrication process of the hydrogel. This updated process saw a significant increase in all aspects of the mechanical properties including a 3.6-time increase in tensile strength and a 0.7-time increase in compressive strength. This new hydrogel also did not need PAMPS as a third network to maintain a similar level of CoF and cause similar level of wear on opposing cartilage while showed much better wear resistance compared to cartilage itself. With this new hydrogel in hand, we then developed a brand-new method to attach the hydrogel to a metal base, the ring-clamp attachment method. This method was designed to overcome the delamination of BC we noticed during the previous shear tests. With an updated and more representative shear test setup, we achieved a shear strength of 1.7 times as high as the pig cartilage.

Taken all of the progress together, we successfully developed a cartilage-replacing medical device that outperforms all currently available treatments to cartilage damage. With preclinical tests ongoing and clinical trials already planned next year, we hope our work would be able to help people in need and bring happiness back to their lives in the near future.

Reference

1. Sophia Fox, A. J.; Bedi, A.; Rodeo, S. A., The basic science of articular cartilage: structure, composition, and function. *Sports health* **2009,** *1* (6), 461-468.

2. Lattermann, C.; Kang, R. W.; Cole, B. J., What's new in the treatment of focal chondral defects of the knee? *Orthopedics* **2006,** *29* (10), 898-903.

3. Makris, E. A.; Gomoll, A. H.; Malizos, K. N.; Hu, J. C.; Athanasiou, K. A., Repair and tissue engineering techniques for articular cartilage. *Nat Rev Rheumatol* **2015,** *11* (1), 21-34.

4. Devitt, B. M.; Bell, S. W.; Webster, K. E.; Feller, J. A.; Whitehead, T. S., Surgical treatments of cartilage defects of the knee: Systematic review of randomised controlled trials. *Knee* **2017,** *24* (3), 508-517.

5. Knutsen, G.; Drogset, J. O.; Engebretsen, L.; Grontvedt, T.; Ludvigsen, T. C.; Loken, S.; Solheim, E.; Strand, T.; Johansen, O., A Randomized Multicenter Trial Comparing Autologous Chondrocyte Implantation with Microfracture: Long-Term Follow-up at 14 to 15 Years. *J Bone Joint Surg Am* **2016,** *98* (16), 1332-9.

6. Bollars, P.; Bosquet, M.; Vandekerckhove, B.; Hardeman, F.; Bellemans, J., Prosthetic inlay resurfacing for the treatment of focal, full thickness cartilage defects of the femoral condyle: a bridge between biologics and conventional arthroplasty. *Knee Surgery, Sports Traumatology, Arthroscopy* **2012,** *20* (9), 1753-1759.

7. Bowland, P.; Ingham, E.; Jennings, L.; Fisher, J., Review of the biomechanics and biotribology of osteochondral grafts used for surgical interventions in the knee. *Proceedings of the Institution of Mechanical Engineers, Part H: Journal of Engineering in Medicine* **2015,** *229* (12), 879-888.

8. Barbour, K. E.; Helmick, C. G.; Boring, M.; Zhang, X.; Lu, H.; Holt, J. B., Prevalence of doctor-diagnosed arthritis at state and county levels—United States, 2014. *Morbidity and mortality weekly report* **2016,** *65* (19), 489-494.

9. Kempson, G., Relationship between the tensile properties of articular cartilage from the human knee and age. *Annals of the rheumatic diseases* **1982,** *41* (5), 508-511.

10. Kerin, A. J.; Wisnom, M. R.; Adams, M. A., The compressive strength of articular cartilage. *Proc. Inst. Mech. Eng. H* **1998,** *212*, 273-80.

11. Kempson, G. E., Relationship between the tensile properties of articular cartilage from the human knee and age. *Ann. Rheum. Dis.* **1982,** *41*, 508-511.

12. Kempson, G. E., Age-related changes in the tensile properties of human articular cartilage: a comparative study between the femoral head of the hip joint and the talus of the ankle joint. *Biochim. Biophys. Acta. Gen. Subj.* **1991,** *1075*, 223-230.

13. Adams, M. A.; Kerin, A. J.; Wisnom, M. R., Sustained loading increases the compressive strength of articular cartilage. *Connect. Tissue. Res.* **1998,** *39*, 245-56.

14. Yang, F.; Zhao, J.; Koshut, W. J.; Watt, J.; Riboh, J. C.; Gall, K.; Wiley, B. J., A Synthetic Hydrogel Composite with the Mechanical Behavior and Durability of Cartilage. *Adv. Funct. Mater.* **2020,** *30*, 2003451.

15. Zhang, Z.; Liu, R.; Zepeda, H.; Zeng, L.; Qiu, J.; Wang, S., 3D Printing Super Strong Hydrogel for Artificial Meniscus. *ACS Appl. Polym.* **2019,** *1*, 2023-2032.

16. Hagiwara, Y.; Putra, A.; Kakugo, A.; Furukawa, H.; Gong, J. P., Ligament-like tough double-network hydrogel based on bacterial cellulose. *Cellulose* **2010,** *17*, 93-101.

17. Xu, L.; Zhao, X.; Xu, C.; Kotov, N. A. J. A. M., Water‐rich biomimetic composites with abiotic self‐organizing nanofiber network. **2018,** *30* (1), 1703343.

18. Yasuda, K.; Gong, J. P.; Katsuyama, Y.; Nakayama, A.; Tanabe, Y.; Kondo, E.; Ueno, M.; Osada, Y. J. B., Biomechanical properties of high-toughness double network hydrogels. **2005,** *26* (21), 4468-4475.

19. Shao, J.; Zhang, Z.; Zhao, S.; Wang, S.; Guo, Z.; Xie, H.; Hu, Y. J. S. S., Self‐Healing Hydrogel of Poly (Vinyl Alcohol)/Agarose with Robust Mechanical Property. **2019,** *71* (5-6), 1800281.

20. Gan, S.; Lin, W.; Zou, Y.; Xu, B.; Zhang, X.; Zhao, J.; Rong, J. J. C. P., Nano-hydroxyapatite enhanced double network hydrogels with excellent mechanical properties for potential application in cartilage repair. **2020,** *229*, 115523.

21. Jiang, Y.; Yang, Y.; Zheng, X.; Yi, Y.; Chen, X.; Li, Y.; Sun, D.; Zhang, L. J. N. A. M., Multifunctional load-bearing hybrid hydrogel with combined drug release and photothermal conversion functions. **2020,** *12* (1), 1-11.

22. Xiang, X.; Chen, G.; Chen, K.; Jiang, X.; Hou, L. J. I. J. o. B. M., Facile preparation and characterization of super tough chitosan/poly (vinyl alcohol) hydrogel with low temperature resistance and anti-swelling property. **2020,** *142*, 574-582.

23. Bakarich, S. E.; Gorkin III, R.; in het Panhuis, M.; Spinks, G. M., Three-dimensional printing fiber reinforced hydrogel composites. *ACS applied materials & interfaces* **2014,** *6* (18), 15998-16006.

24. Agrawal, A.; Rahbar, N.; Calvert, P. D., Strong fiber-reinforced hydrogel. *Acta biomaterialia* **2013,** *9* (2), 5313-5318.

25. Liang, Y.; Xue, J.; Du, B.; Nie, J., Ultrastiff, tough, and healable ionic–hydrogen bond cross-linked hydrogels and their uses as building blocks to construct complex hydrogel structures. *ACS applied materials & interfaces* **2019,** *11* (5), 5441-5454.

26. Gong, Z.; Zhang, G.; Zeng, X.; Li, J.; Li, G.; Huang, W.; Sun, R.; Wong, C., High-strength, tough, fatigue resistant, and self-healing hydrogel based on dual physically cross-linked network. *ACS applied materials & interfaces* **2016,** *8* (36), 24030-24037.

27. Hong, S.; Sycks, D.; Chan, H. F.; Lin, S.; Lopez, G. P.; Guilak, F.; Leong, K. W.; Zhao, X., 3D printing of highly stretchable and tough hydrogels into complex, cellularized structures. *Advanced materials* **2015,** *27* (27), 4035-4040.

28. Narayanan, R. P.; Melman, G.; Letourneau, N. J.; Mendelson, N. L.; Melman, A., Photodegradable iron (III) cross-linked alginate gels. *Biomacromolecules* **2012,** *13* (8), 2465-2471.

29. Haque, M. A.; Kurokawa, T.; Gong, J. P., Super tough double network hydrogels and their application as biomaterials. *Polymer* **2012,** *53* (9), 1805-1822.

30. Mredha, M. T. I.; Guo, Y. Z.; Nonoyama, T.; Nakajima, T.; Kurokawa, T.; Gong, J. P., A facile method to fabricate anisotropic hydrogels with perfectly aligned hierarchical fibrous structures. *Advanced Materials* **2018,** *30* (9), 1704937.

31. Wei, J.; Wang, J.; Su, S.; Wang, S.; Qiu, J.; Zhang, Z.; Christopher, G.; Ning, F.; Cong, W., 3D printing of an extremely tough hydrogel. *Rsc Advances* **2015,** *5* (99), 81324-81329.

32. Wang, Y. J.; Zhang, X. N.; Song, Y.; Zhao, Y.; Chen, L.; Su, F.; Li, L.; Wu, Z. L.; Zheng, Q., Ultrastiff and tough supramolecular hydrogels with a dense and robust hydrogen bond network. *Chemistry of Materials* **2019,** *31* (4), 1430-1440.

33. Hoffman, A. S., Hydrogels for biomedical applications. *Advanced drug delivery reviews* **2012,** *64*, 18-23.

34. Haraguchi, K., Nanocomposite hydrogels. *Current Opinion in Solid State and Materials Science* **2007,** *11* (3-4), 47-54.

35. Gong, J. P.; Katsuyama, Y.; Kurokawa, T.; Osada, Y., Double - network hydrogels with extremely high mechanical strength. *Advanced materials* **2003,** *15* (14), 1155-1158.

36. Fukao, K.; Nonoyama, T.; Kiyama, R.; Furusawa, K.; Kurokawa, T.; Nakajima, T.; Gong, J. P., Anisotropic growth of hydroxyapatite in stretched double network hydrogel. *ACS nano* **2017,** *11* (12), 12103-12110.

37. Xu, L.; Wang, C.; Cui, Y.; Li, A.; Qiao, Y.; Qiu, D., Conjoined-network rendered stiff and tough hydrogels from biogenic molecules. *Science advances* **2019,** *5* (2), eaau3442.

38. Xu, H.; Tan, Y.; Rao, W.; Wang, D.; Xu, S.; Liao, W.; Wang, Y.-Z., Ultra-strong mechanical property and force-driven malleability of water-poor hydrogels. *Journal of colloid and interface science* **2019,** *542*, 281-288.

39. Shin, M. K.; Spinks, G. M.; Shin, S. R.; Kim, S. I.; Kim, S. J., Nanocomposite hydrogel with high toughness for bioactuators. *Advanced Materials* **2009,** *21* (17), 1712-1715.

40. Yang, F.; Tadepalli, V.; Wiley, B. J., 3D printing of a double network hydrogel with a compression strength and elastic modulus greater than those of cartilage. *ACS Biomaterials Science & Engineering* **2017,** *3* (5), 863-869.

41. Gong, J. P., Why are double network hydrogels so tough? *Soft Matter* **2010,** *6* (12), 2583-2590.

42. Thomas, D.; Cebe, P., Self-nucleation and crystallization of polyvinyl alcohol. *Journal of Thermal Analysis and Calorimetry* **2017,** *127* (1), 885-894.

43. Ushio, K.; Oka, M.; Hyon, S. H.; Hayami, T.; Yura, S.; Matsumura, K.; Toguchida, J.; Nakamura, T., Attachment of artificial cartilage to underlying bone. *Journal of Biomedical Materials Research Part B: Applied Biomaterials: An Official Journal of The Society for Biomaterials, The Japanese Society for Biomaterials, and The Australian Society for Biomaterials and the Korean Society for Biomaterials* **2004,** *68* (1), 59-68.

44. Yarimitsu, S.; Nakashima, K.; Sawae, Y.; Murakami, T., Study on the mechanisms of wear reduction of artificial cartilage through in situ observation on forming protein boundary film. *Tribology Online* **2007,** *2* (4), 114-119.

45. Bodugoz-Senturk, H.; Choi, J.; Oral, E.; Kung, J. H.; Macias, C. E.; Braithwaite, G.; Muratoglu, O. K., The effect of polyethylene glycol on the stability of pores in polyvinyl alcohol hydrogels during annealing. *Biomaterials* **2008,** *29* (2), 141-149.

46. Bodugoz-Senturk, H.; Macias, C. E.; Kung, J. H.; Muratoglu, O. K., Poly (vinyl alcohol)–acrylamide hydrogels as load-bearing cartilage substitute. *Biomaterials* **2009,** *30* (4), 589-596.

47. Kobayashi, M.; Hyu, H. S., Development and evaluation of polyvinyl alcohol-hydrogels as an artificial atrticular cartilage for orthopedic implants. *Materials* **2010,** *3* (4), 2753-2771.

48. Cha, W. I.; Hyon, S. H.; Oka, M.; Ikada, Y. In *Mechanical and wear properties of poly (vinyl alcohol) hydrogels*, Macromolecular symposia, Wiley Online Library: 1996; pp 115-126.

49. Suzuki, A.; Sasaki, S.; Murakami, T., Development of PVA Hydrogels with Superior Lubricity for Artificial Cartilage. In *Rheology of Biological Soft Matter*, Springer: 2017; p 343.

50. Bunn, C., Crystal structure of polyvinyl alcohol. *Nature* **1948,** *161* (4102), 929-930.

51. Keller, A., A note on single crystals in polymers: Evidence for a folded chain configuration. *Philosophical Magazine* **1957,** *2* (21), 1171-1175.

52. Ravve, A., *Principles of polymer chemistry*. Springer Science & Business Media: 2013.

53. Hassan, C. M.; Peppas, N. A., Structure and Applications of Poly(vinyl alcohol) Hydrogels Produced by Conventional Crosslinking or by Freezing/Thawing Methods. In *Biopolymers · PVA Hydrogels, Anionic Polymerisation Nanocomposites*, Springer Berlin Heidelberg: Berlin, Heidelberg, 2000; pp 37-65.

54. Seymour, R. B.; Carraher, C. E., Polymer chemistry. Marcel Dekker New York: 2000; Vol. 181.

55. Peppas, N. A.; Merrill, E. W., Differential scanning calorimetry of crystallized PVA hydrogels. *Journal of Applied Polymer Science* **1976,** *20* (6), 1457-1465.

56. Peppas, N. A.; Merrill, E. W., Poly(vinyl alcohol) hydrogels: Reinforcement of radiation-crosslinked networks by crystallization. *J. Polym. Sci., Polym. Chem. Ed.* **1976,** *14*, 441-457.

57. Ricciardi, R.; Auriemma, F.; Gaillet, C.; De Rosa, C.; Lauprêtre, F., Investigation of the crystallinity of freeze/thaw poly (vinyl alcohol) hydrogels by different techniques. *Macromolecules* **2004,** *37* (25), 9510-9516.

58. Ateshian, G. A., The role of interstitial fluid pressurization in articular cartilage lubrication. *Journal of biomechanics* **2009,** *42* (9), 1163-1176.

59. Murakami, T.; Yarimitsu, S.; Nakashima, K.; Sakai, N.; Yamaguchi, T.; Sawae, Y.; Suzuki, A., Biphasic and boundary lubrication mechanisms in artificial hydrogel cartilage: A review. *Proceedings of the Institution of Mechanical Engineers, Part H: Journal of Engineering in Medicine* **2015,** *229* (12), 864-878.

60. Mow, V.; Hou, J.; Owens, J.; Ratcliffe, A., Biphasic and quasilinear viscoelastic theories for hydrated soft tissues. In *Biomechanics of diarthrodial joints*, Springer: 1990; pp 215-260.

61. Dowson, D. In *Paper 12: modes of lubrication in human joints*, Proceedings of the institution of mechanical engineers, conference proceedings, SAGE Publications Sage UK: London, England: 1966; pp 45-54.

62. Medley, J.; Dowson, D.; Wright, V., Transient elastohydrodynamic lubrication models for the human ankle joint. *Engineering in medicine* **1984,** *13* (3), 137-151.

63. Unsworth, A., Soft layer lubrication of artificial hip joints. *Proc. Inst. Mech. Eng., 1987* **1987,** *219*, 715-724.

64. Mansour, J. M.; Mow, V. C., On the natural lubrication of synovial joints: Normal and degenerate. **1977**.

65. Forster, H.; Fisher, J., The influence of loading time and lubricant on the friction of articular cartilage. *Proceedings of the Institution of Mechanical Engineers, Part H: Journal of Engineering in Medicine* **1996,** *210* (2), 109-119.

66. Ateshian, G., A theoretical formulation for boundary friction in articular cartilage. **1997**.

67. Sasada, T., Lubrication of Human Joints-Nature of Joint Friction and" Surface Gel Hydration Lubrication". *J. Japanese Soc. for Clinical Biomechanics* **2000,** *21*, 17-22.

68. Klein, J., Molecular mechanisms of synovial joint lubrication. *Proceedings of the Institution of Mechanical Engineers, Part J: Journal of Engineering Tribology* **2006,** *220* (8), 691-710.

69. Ikeuchi, K., Origin and future of hydration lubrication. *Proceedings of the Institution of Mechanical Engineers, Part J: Journal of Engineering Tribology* **2007,** *221* (3), 301-305.

70. Klein, J., Hydration lubrication. *Friction* **2013,** *1* (1), 1-23.

71. Swann, D. A.; Hendren, R. B.; Radin, E. L.; Sotman, S. L., The lubricating activity of synovial fluid glycoproteins. *Arthritis & Rheumatism: Official Journal of the American College of Rheumatology* **1981,** *24* (1), 22-30.

72. Hills, B. A., Oligolamellar lubrication of joints by surface active phospholipid. *The Journal of rheumatology* **1989,** *16* (1), 82-91.

73. Higaki, H., Role of Constituents in Synovial Fluid and Surface Layer of Articular Cartilage in Joint Lubrication (Part 2)-The Boundary Lubrication Ability. *Japanese J. Tribology* **1995,** *40* (7), 691-700.

74. Higaki, H.; Murakami, T.; Nakanishi, Y.; Miura, H.; Mawatari, T.; Iwamoto, Y., The lubricating ability of biomembrane models with dipalmitoyl phosphatidylcholine and γ-globulin. *Proceedings of the Institution of Mechanical Engineers, Part H: Journal of Engineering in Medicine* **1998,** *212* (5), 337-346.

75. Zappone, B.; Ruths, M.; Greene, G. W.; Jay, G. D.; Israelachvili, J. N., Adsorption, lubrication, and wear of lubricin on model surfaces: polymer brush-like behavior of a glycoprotein. *Biophysical journal* **2007,** *92* (5), 1693-1708.

76. McNary, S. M.; Athanasiou, K. A.; Reddi, A. H., Engineering lubrication in articular cartilage. *Tissue Engineering Part B: Reviews* **2012,** *18* (2), 88-100.

77. Schmidt, T. A.; Gastelum, N. S.; Nguyen, Q. T.; Schumacher, B. L.; Sah, R. L., Boundary lubrication of articular cartilage: role of synovial fluid constituents. *Arthritis & Rheumatism* **2007,** *56* (3), 882-891.

78. Noyori, K.; Takagi, T.; Jasin, H., Characterization of the macromolecular components of the articular cartilage surface. *Rheumatology international* **1998,** *18* (2), 71-77.

79. Schumacher, B. L.; Block, J. A.; Schmid, T. M.; Aydelotte, M. B.; Kuettner, K. E., A novel proteoglycan synthesized and secreted by chondrocytes of the superficial zone of articular cartilage. *Archives of biochemistry and biophysics* **1994,** *311* (1), 144-152.

80. Jay, G. D., Lubricin and surfacing of articular joints. *Current Opinion in Orthopaedics* **2004,** *15* (5), 355-359.

81. Sarma, A.; Powell, G.; LaBerge, M., Phospholipid composition of articular cartilage boundary lubricant. *Journal of orthopaedic research* **2001,** *19* (4), 671-676.

82. Sahoo, P.; Das, S. K.; Davim, J. P., Tribology of materials for biomedical applications. In *Mechanical Behaviour of Biomaterials*, Elsevier: 2019; pp 1-45.

83. Jin, Z.; Fisher, J., Tribology in joint replacement. In *Joint replacement technology*, Elsevier: 2014; pp 31-61.

84. Weightman, B., Tensile fatigue of human articular cartilage. *Journal of biomechanics* **1976,** *9* (4), 193-200.

85. Weightman, B.; Chappell, D.; Jenkins, E., A second study of tensile fatigue properties of human articular cartilage. *Annals of the rheumatic diseases* **1978,** *37* (1), 58-63.

86. Xu, L.; Zhao, X.; Xu, C.; Kotov, N. A., Water‐rich biomimetic composites with abiotic self‐organizing nanofiber network. *Advanced Materials* **2018,** *30* (1), 1703343.

87. Bai, T.; Zhang, P.; Han, Y.; Liu, Y.; Liu, W.; Zhao, X.; Lu, W., Construction of an ultrahigh strength hydrogel with excellent fatigue resistance based on strong dipole–dipole interaction. *Soft Matter* **2011,** *7* (6), 2825-2831.

88. Sun, X.; Luo, C.; Luo, F., Preparation and properties of self-healable and conductive PVA-agar hydrogel with ultra-high mechanical strength. *European Polymer Journal* **2020,** *124*, 109465.

89. Yang, F.; Zhao, J.; Koshut, W. J.; Watt, J.; Riboh, J.; Gall, K.; Wiley, B. J., A Synthetic Hydrogel Composite with the Mechanical Behavior and Durability of Cartilage. *Advanced Functional Materials* **2020**, DOI:10.1002/adfm.202003451.

90. Kumar, P.; Oka, M.; Nakamura, T.; Yamamuro, T.; Delecrin, J., Mechanical strength of osteochondral junction. *Nihon Seikeigeka Gakkai Zasshi* **1991,** *65* (11), 1070-1077.

91. Chivers, R.; Wolowacz, R., The strength of adhesive-bonded tissue joints. *International journal of adhesion and adhesives* **1997,** *17* (2), 127-132.

92. Petrov, C.; Serafimov, B.; Kotzev, D. L., Strength, deformation and relaxation of joints bonded with modified cyanoacrylate adhesives. *International Journal of Adhesion and Adhesives* **1988,** *8* (4), 207-210.

93. Shantha, K. L.; Thennarasu, S.; Krishnamurti, N., Developments and applications of cyanoacrylate adhesives. *Journal of Adhesion Science and Technology* **1989,** *3* (1), 237-260.

94. Mow, V. C.; Huiskes, R., *Basic Orthopaedic Biomechanics & Mechano-biology*. Lippincott Williams & Wilkins: Philadelphia, 2005.

95. Maier, G. P.; Rapp, M. V.; Waite, J. H.; Israelachvili, J. N.; Butler, A., Adaptive synergy between catechol and lysine promotes wet adhesion by surface salt displacement. *Science* **2015,** *349* (6248), 628.

96. Singla, S.; Amarpuri, G.; Dhopatkar, N.; Blackledge, T. A.; Dhinojwala, A., Hygroscopic compounds in spider aggregate glue remove interfacial water to maintain adhesion in humid conditions. *Nature Communications* **2018,** *9* (1), 1890.

97. Yuk, H.; Varela, C. E.; Nabzdyk, C. S.; Mao, X.; Padera, R. F.; Roche, E. T.; Zhao, X., Dry double-sided tape for adhesion of wet tissues and devices. *Nature* **2019,** *575* (7781), 169-174.

98. Liu, J.; Lin, S.; Liu, X.; Qin, Z.; Yang, Y.; Zang, J.; Zhao, X., Fatigue-resistant adhesion of hydrogels. *Nature Communications* **2020,** *11* (1), 1071.

99. Madry, H.; van Dijk, C. N.; Mueller-Gerbl, M., The basic science of the subchondral bone. *Knee Surgery, Sports Traumatology, Arthroscopy* **2010,** *18* (4), 419-433.

100. Keeney, M.; Pandit, A., The Osteochondral Junction and Its Repair via Bi-Phasic Tissue Engineering Scaffolds. *Tissue Engineering Part B: Reviews* **2009,** *15* (1), 55-73.

101. Lattermann, C.; Kang, R. W.; Cole, B. J., What's new in the treatment of focal chondral defects of the knee? *ORTHOPEDICS-NEW JERSEY-* **2006,** *29* (10), 898.

102. Devitt, B. M.; Bell, S. W.; Webster, K. E.; Feller, J. A.; Whitehead, T. S., Surgical treatments of cartilage defects of the knee: Systematic review of randomised controlled trials. *Knee* **2017,** *24*, 508-517.

103. Heir, S.; Nerhus, T. K.; Røtterud, J. H.; Løken, S.; Ekeland, A.; Engebretsen, L.; Årøen, A., Focal cartilage defects in the knee impair quality of life as much as severe osteoarthritis: a comparison of knee injury and osteoarthritis outcome score in 4 patient

categories scheduled for knee surgery. *The American journal of sports medicine* **2010,** *38* (2), 231-237.

104. Wang, C.-J., Treatment of focal articular cartilage lesions of the knee with autogenous osteochondral grafts. *Archives of orthopaedic and trauma surgery* **2002,** *122* (3), 169-172.

105. Bekkers, J.; de Windt, T. S.; Raijmakers, N.; Dhert, W.; Saris, D., Validation of the Knee Injury and Osteoarthritis Outcome Score (KOOS) for the treatment of focal cartilage lesions. *Osteoarthritis and cartilage* **2009,** *17* (11), 1434-1439.

106. Knutsen, G.; Drogset, J. O.; Engebretsen, L.; Grontvedt, T.; Ludvigsen, T. C.; Loken, S.; Solheim, E.; Strand, T.; Johansen, O., A Randomized Multicenter Trial Comparing Autologous Chondrocyte Implantation with Microfracture: Long-Term Follow-up at 14 to 15 Years. *J. Bone Joint. Surg. Am.* **2016,** *98*, 1332-9.

107. Mithoefer, K.; Williams III, R. J.; Warren, R. F.; Potter, H. G.; Spock, C. R.; Jones, E. C.; Wickiewicz, T. L.; Marx, R. G., The microfracture technique for the treatment of articular cartilage lesions in the knee: a prospective cohort study. *JBJS* **2005,** *87* (9), 1911-1920.

108. Marlovits, S.; Zeller, P.; Singer, P.; Resinger, C.; Vécsei, V., Cartilage repair: generations of autologous chondrocyte transplantation. *European journal of radiology* **2006,** *57* (1), 24-31.

109. Barber, F. A.; Chow, J. C., Arthroscopic osteochondral transplantation: histologic results. *Arthroscopy: The Journal of Arthroscopic & Related Surgery* **2001,** *17* (8), 832-835.

110. Imhoff, A.; Ottl, G.; Burkart, A.; Traub, S., Autologous osteochondral transplantation on various joints. *Der Orthopade* **1999,** *28* (1), 33-44.

111. Brown, T. D.; Shaw, D. T., In vitro contact stress distribution on the femoral condyles. *J. Orthop. Res.* **1984,** *2*, 190-199.

112. Yasuda, K.; Kitamura, N.; Gong, J. P.; Arakaki, K.; Kwon, H. J.; Onodera, S.; Chen, Y. M.; Kurokawa, T.; Kanaya, F.; Ohmiya, Y., A novel double‐network hydrogel induces spontaneous articular cartilage regeneration in vivo in a large osteochondral defect. *Macromolecular bioscience* **2009,** *9* (4), 307-316.

113. Nonoyama, T.; Wada, S.; Kiyama, R.; Kitamura, N.; Mredha, M. T. I.; Zhang, X.; Kurokawa, T.; Nakajima, T.; Takagi, Y.; Yasuda, K., Double‐network hydrogels

strongly bondable to bones by spontaneous osteogenesis penetration. *Advanced Materials* **2016,** *28* (31), 6740-6745.

114. FDA, U. CARTIVA SYNTHETIC CARTILAGE IMPLANT. https://www.accessdata.fda.gov/scripts/cdrh/cfdocs/cfpma/pma.cfm?id=P150017 (accessed 06-02-2022).

115. Cartiva Summary of Safety and Effectiveness Data. https://www.accessdata.fda.gov/cdrh_docs/pdf15/P150017B.pdf (accessed 06-02-2022).

116. Kelm, L. N., *Hysteretic response of articular cartilage to cyclic loading*. Rice University: 2002.

117. Chandran, P. L.; Horkay, F., Aggrecan, an unusual polyelectrolyte: review of solution behavior and physiological implications. *Acta biomaterialia* **2012,** *8* (1), 3-12.

118. Lu, X.; Mow, V., Biomechanics of articular cartilage and determination of material properties. *Medicine+ Science in Sports+ Exercise* **2008,** *40* (2), 193.

119. Kiani, C.; Chen, L.; Wu, Y. J.; Yee, A. J.; Yang, B. B., Structure and function of aggrecan. *Cell research* **2002,** *12* (1), 19-32.

120. Lu, X. L.; Miller, C.; Chen, F. H.; Guo, X. E.; Mow, V. C., The generalized triphasic correspondence principle for simultaneous determination of the mechanical properties and proteoglycan content of articular cartilage by indentation. *Journal of biomechanics* **2007,** *40* (11), 2434-2441.

121. Basser, P. J.; Schneiderman, R.; Bank, R. A.; Wachtel, E.; Maroudas, A., Mechanical properties of the collagen network in human articular cartilage as measured by osmotic stress technique. *Archives of biochemistry and biophysics* **1998,** *351* (2), 207-219.

122. Huster, D.; Naji, L.; Schiller, J.; Arnold, K., Dynamics of the biopolymers in articular cartilage studied by magic angle spinning NMR. *Applied Magnetic Resonance* **2004,** *27* (3), 471-487.

123. Maroudas, A. In *Physico-chemical properties of human articular cartilage*, Orthopaedic Proceedings, The British Editorial Society of Bone & Joint Surgery: 2002; pp 309-310.

124. Maroudas, A.; Bannon, C., Measurement of swelling pressure in cartilage and comparison with the osmotic pressure of constituent proteoglycans. *Biorheology* **1981,** *18* (3-6), 619-632.

125. Maroudas, A.; Wachtel, E.; Grushko, G.; Katz, E.; Weinberg, P., The effect of osmotic and mechanical pressures on water partitioning in articular cartilage. *Biochimica et Biophysica Acta (BBA)-General Subjects* **1991,** *1073* (2), 285-294.

126. Farr, J.; Gracitelli, G. C.; Shah, N.; Chang, E. Y.; Gomoll, A. H., High failure rate of a decellularized osteochondral allograft for the treatment of cartilage lesions. *The American journal of sports medicine* **2016,** *44* (8), 2015-2022.

127. Helenius, G.; Bäckdahl, H.; Bodin, A.; Nannmark, U.; Gatenholm, P.; Risberg, B., In vivo biocompatibility of bacterial cellulose. *Journal of Biomedical Materials Research Part A: An Official Journal of The Society for Biomaterials, The Japanese Society for Biomaterials, and The Australian Society for Biomaterials and the Korean Society for Biomaterials* **2006,** *76* (2), 431-438.

128. Guhados, G.; Wan, W.; Hutter, J. L., Measurement of the elastic modulus of single bacterial cellulose fibers using atomic force microscopy. *Langmuir* **2005,** *21* (14), 6642-6646.

129. Nakagaito, A.; Iwamoto, S.; Yano, H., Bacterial cellulose: the ultimate nano-scalar cellulose morphology for the production of high-strength composites. *Applied Physics A* **2005,** *80* (1), 93-97.

130. Czaja, W. K.; Young, D. J.; Kawecki, M.; Brown, R. M., The future prospects of microbial cellulose in biomedical applications. *biomacromolecules* **2007,** *8* (1), 1-12.

131. Grant, C.; Twigg, P.; Egan, A.; Moody, A.; Smith, A.; Eagland, D.; Crowther, N.; Britland, S., Poly (vinyl alcohol) hydrogel as a biocompatible viscoelastic mimetic for articular cartilage. *Biotechnology progress* **2006,** *22* (5), 1400-1406.

132. Kosukegawa, H.; Mamada, K.; Kuroki, K.; Liu, L.; Inoue, K.; Hayase, T.; Ohta, M., Measurements of dynamic viscoelasticity of poly (vinyl alcohol) hydrogel for the development of blood vessel biomodeling. *Journal of Fluid Science and Technology* **2008,** *3* (4), 533-543.

133. Fumio, U.; Hiroshi, Y.; Kumiko, N.; Sachihiko, N.; Kenji, S.; Yasunori, M., Swelling and mechanical properties of poly (vinyl alcohol) hydrogels. *International journal of pharmaceutics* **1990,** *58* (2), 135-142.

134. Stammen, J. A.; Williams, S.; Ku, D. N.; Guldberg, R. E., Mechanical properties of a novel PVA hydrogel in shear and unconfined compression. *Biomaterials* **2001,** *22* (8), 799-806.

135. Ku, D. N.; Braddon, L. G.; Wootton, D. M., Poly (vinyl alcohol) cryogel. Google Patents: 1999.

136. Mow, V. C.; Kuei, S.; Lai, W. M.; Armstrong, C. G., Biphasic creep and stress relaxation of articular cartilage in compression: theory and experiments. *Journal of biomechanical engineering* **1980,** *102* (1), 73-84.

137. Wang, S.; Jiang, F.; Xu, X.; Kuang, Y.; Fu, K.; Hitz, E.; Hu, L., Super‐strong, super‐stiff macrofibers with aligned, long bacterial cellulose nanofibers. *Advanced Materials* **2017,** *29* (35), 1702498.

138. Sasazaki, Y.; Shore, R.; Seedhom, B. B., Deformation and failure of cartilage in the tensile mode. *Journal of anatomy* **2006,** *208* (6), 681-694.

139. Benedict, J. V.; Walker, L. B.; Harris, E. H., Stress-strain characteristics and tensile strength of unembalmed human tendon. *Journal of Biomechanics* **1968,** *1* (1), 53-63.

140. Xue, R.; Xin, X.; Wang, L.; Shen, J.; Ji, F.; Li, W.; Jia, C.; Xu, G., A systematic study of the effect of molecular weights of polyvinyl alcohol on polyvinyl alcohol–graphene oxide composite hydrogels. *Physical Chemistry Chemical Physics* **2015,** *17* (7), 5431-5440.

141. Koshut, W. J.; Rummel, C.; Smoot, D.; Kirillova, A.; Gall, K., Flaw sensitivity and tensile fatigue of poly (vinyl alcohol) hydrogels. *Macromolecular Materials and Engineering* **2021,** *306* (3), 2000679.

142. Zhang, W.; Liu, X.; Wang, J.; Tang, J.; Hu, J.; Lu, T.; Suo, Z., Fatigue of double-network hydrogels. *Engineering Fracture Mechanics* **2018,** *187*, 74-93.

143. Kelly, C. N.; Francovich, J.; Julmi, S.; Safranski, D.; Guldberg, R. E.; Maier, H. J.; Gall, K., Fatigue behavior of As-built selective laser melted titanium scaffolds with sheet-based gyroid microarchitecture for bone tissue engineering. *Acta Biomaterialia* **2019,** *94*, 610-626.

144. Askew, M.; Mow, V., The biomechanical function of the collagen fibril ultrastructure of articular cartilage. **1978**.

145. Seedhom, B., Conditioning of cartilage during normal activities is an important factor in the development of osteoarthritis. *Rheumatology* **2006,** *45* (2), 146-149.

146. Freeman, M. A. R., *Adult articular cartilage*. Pitman Medical: 1979.

147. Freeman, M.; Meachim, G., Ageing, degeneration and remodelling of articular cartilage. In *Adult articular cartilage*, Pitman Medical London: 1973; pp 287-329.

148. Baumhauer, J. F.; Singh, D.; Glazebrook, M.; Blundell, C.; De Vries, G.; Le, I. L.; Nielsen, D.; Pedersen, M. E.; Sakellariou, A.; Solan, M.; Wansbrough, G.; Younger, A. S.; Daniels, T.; for; on behalf of the, C. M. S. G., Prospective, Randomized, Multi-centered Clinical Trial Assessing Safety and Efficacy of a Synthetic Cartilage Implant Versus First Metatarsophalangeal Arthrodesis in Advanced Hallux Rigidus. *Foot Ankle Int* **2016,** *37* (5), 457-69.

149. Falah, M.; Nierenberg, G.; Soudry, M.; Hayden, M.; Volpin, G., Treatment of articular cartilage lesions of the knee. *International Orthopaedics* **2010,** *34* (5), 621-630.

150. Levy, Y. D.; Gortz, S.; Pulido, P. A.; McCauley, J. C.; Bugbee, W. D., Do fresh osteochondral allografts successfully treat femoral condyle lesions? *Clin Orthop Relat Res* **2013,** *471* (1), 231-7.

151. McCulloch, P. C.; Kang, R.; Cole, B. J., Osteochondral allografts for large defects in the knee. *Techniques in Knee Surgery* **2006,** *5* (3), 165.

152. Farr, J.; Gracitelli, G. C.; Shah, N.; Chang, E. Y.; Gomoll, A. H., High Failure Rate of a Decellularized Osteochondral Allograft for the Treatment of Cartilage Lesions. *Am J Sports Med* **2016,** *44* (8), 2015-22.

153. Nathwani, D.; McNicholas, M.; Hart, A.; Miles, J.; Bobic, V., Partial Resurfacing of the Knee with the BioPoly Implant: Interim Report at 2 Years. *JB JS Open Access* **2017,** *2* (2), e0011.

154. Bollars, P.; Bosquet, M.; Vandekerckhove, B.; Hardeman, F.; Bellemans, J., Prosthetic inlay resurfacing for the treatment of focal, full thickness cartilage defects of the femoral condyle: a bridge between biologics and conventional arthroplasty. *Knee Surg Sports Traumatol Arthrosc* **2012,** *20* (9), 1753-9.

155. Bowland, P.; Ingham, E.; Jennings, L.; Fisher, J., Review of the biomechanics and biotribology of osteochondral grafts used for surgical interventions in the knee. *Proc Inst Mech Eng H* **2015,** *229* (12), 879-88.

156. Diermeier, T.; Venjakob, A.; Byrne, K.; Burgkart, R.; Foehr, P.; Milz, S.; Imhoff, A. B.; Vogt, S., Effects of focal metallic implants on opposing cartilage – an in-vitro study with an abrasion test machine. *BMC Musculoskeletal Disorders* **2020,** *21* (1), 261.

157. Martinez-Carranza, N.; Berg, H. E.; Hultenby, K.; Nurmi-Sandh, H.; Ryd, L.; Lagerstedt, A. S., Focal knee resurfacing and effects of surgical precision on opposing cartilage. A pilot study on 12 sheep. *Osteoarthritis and Cartilage* **2013,** *21* (5), 739-745.

158. Fuchs, A.; Eberbach, H.; Izadpanah, K.; Bode, G.; Sudkamp, N. P.; Feucht, M. J., Focal metallic inlay resurfacing prosthesis for the treatment of localized cartilage defects of the femoral condyles: a systematic review of clinical studies. *Knee Surg Sports Traumatol Arthrosc* **2018,** *26* (9), 2722-2732.

159. Kempson, G. E., Relationship between the tensile properties of articular cartilage from the human knee and age. *Annals of the Rheumatic Diseases* **1982,** *41*, 508-511.

160. Sabatini, M.; Pastoureau, P.; De Ceuninck, F., *Cartilage and osteoarthritis*. Springer: 2004; Vol. 2.

161. Flahiff, C.; Feldman, D.; Saltz, R.; Huang, S., Mechanical properties of fibrin adhesives for blood vessel anastomosis. *Journal of biomedical materials research* **1992,** *26* (4), 481-491.

162. Siedentop, K. H.; Harris, D. M.; Sanchez, B., Autologous fibrin tissue adhesive: factors influencing bonding power. *The Laryngoscope* **1988,** *98* (7), 731-733.

163. Nomori, H.; Horio, H.; Morinaga, S.; Suemasu, K., Gelatin-resorcinol–formaldehyde-glutaraldehyde glue for sealing pulmonary air leaks during thoracoscopic operation. *The Annals of thoracic surgery* **1999,** *67* (1), 212-216.

164. Sanders, L.; Stone, R.; Webb, K.; Mefford, T.; Nagatomi, J., Mechanical characterization of a bifunctional Tetronic hydrogel adhesive for soft tissues: Society for Biomaterials Student Award Winner in the Graduate Degree Category, 2015 Annual Meeting and Exposition, Charlotte, NC, April 15–18, 2015. *Journal of Biomedical Materials Research Part A* **2015,** *103* (3), 861-868.

165. Yuan, L.; Wu, Y.; Fang, J.; Wei, X.; Gu, Q.; El-Hamshary, H.; Al-Deyab, S. S.; Morsi, Y.; Mo, X., Modified alginate and gelatin cross-linked hydrogels for soft tissue adhesive. *Artificial cells, nanomedicine, biotechnology* **2017,** *45* (1), 76-83.

166. Okino, H.; Nakayama, Y.; Tanaka, M.; Matsuda, T., In situ hydrogelation of photocurable gelatin and drug release. *Journal of Biomedical Materials Research: An Official Journal of The Society for Biomaterials, The Japanese Society for Biomaterials, the Australian Society for Biomaterials, the Korean Society for Biomaterials* **2002,** *59* (2), 233-245.

167. Raja, S. T. K.; Thiruselvi, T.; Sailakshmi, G.; Ganesh, S.; Gnanamani, A., Rejoining of cut wounds by engineered gelatin–keratin glue. *Biochimica et Biophysica Acta -General Subjects* **2013,** *1830* (8), 4030-4039.

168. Lu, D.; Zhang, Y.; Li, Y.; Wang, H.; Shen, Z.; Wei, Q.; Lei, Z., The synthesis and tissue adhesiveness of temperature-sensitive hyperbranched poly (amino acid) s with functional side groups. *Polymer Chemistry* **2016,** *7* (10), 1963-1970.

169. Nie, W.; Yuan, X.; Zhao, J.; Zhou, Y.; Bao, H., Rapidly in situ forming chitosan/ε-polylysine hydrogels for adhesive sealants and hemostatic materials. *Carbohydrate polymers* **2013,** *96* (1), 342-348.

170. Oh, D. X.; Kim, S.; Lee, D.; Hwang, D. S., Tunicate-mimetic nanofibrous hydrogel adhesive with improved wet adhesion. *Acta biomaterialia* **2015,** *20*, 104-112.

171. Bochyńska, A. I.; Sharifi, S.; van Tienen, T. G.; Buma, P.; Grijpma, D. W. In *Development of Tissue Adhesives Based on Amphiphilic Isocyanate‐Terminated Trimethylene Carbonate Block Copolymers*, Macromolecular symposia, Wiley Online Library: 2013; pp 40-48.

172. Balcioglu, S.; Parlakpinar, H.; Vardi, N.; Denkbas, E. B.; Karaaslan, M. G.; Gulgen, S.; Taslidere, E.; Koytepe, S.; Ates, B., Design of xylose-based semisynthetic polyurethane tissue adhesives with enhanced bioactivity properties. *applied materials interfaces* **2016,** *8* (7), 4456-4466.

173. Zhang, H.; Zhao, T.; Duffy, P.; Dong, Y.; Annaidh, A. N.; O'Cearbhaill, E.; Wang, W., Hydrolytically Degradable Hyperbranched PEG‐Polyester Adhesive with Low Swelling and Robust Mechanical Properties. *Advanced healthcare materials* **2015,** *4* (15), 2260-2268.

174. Ninan, L.; Stroshine, R.; Wilker, J.; Shi, R., Adhesive strength and curing rate of marine mussel protein extracts on porcine small intestinal submucosa. *Acta biomaterialia* **2007,** *3* (5), 687-694.

175. Fan, C.; Fu, J.; Zhu, W.; Wang, D.-A., A mussel-inspired double-crosslinked tissue adhesive intended for internal medical use. *Acta biomaterialia* **2016,** *33*, 51-63.

176. Flachsmann R; Broom ND; Hardy AE; G., M., Why is the adolescent joint particularly susceptible to osteochondral shear fracture? *Clin Orthop Relat Res.* **2000,** *381*, 212-221.

177. Albes, J. M.; Krettek, C.; Hausen, B.; Rohde, R.; Haverich, A.; Borst, H.-G., Biophysical properties of the gelatin-resorcinformaldehyde/glutaraldehyde adhesive. *The Annals of thoracic surgery* **1993,** *56* (4), 910-915.

178. Kandalam, U.; Bouvier, A.; Casas, S.; Smith, R.; Gallego, A.; Rothrock, J.; Thompson, J.; Huang, C.-Y.; Stelnicki, E., Novel bone adhesives: a comparison of bond strengths in vitro. *International Journal of Oral Maxillofacial Surgery* **2013,** *42* (9), 1054-1059.

179. Kirillova, A.; Kelly, C.; von Windheim, N.; Gall, K., Bioinspired mineral–organic Bioresorbable bone adhesive. *Advanced Healthcare Materials* **2018,** *7* (17), 1800467.

180. Shao, H.; Bachus, K. N.; Stewart, R. J., A Water-Borne Adhesive Modeled after the Sandcastle Glue of P. californica. *Macromolecular Bioscience* **2009,** *9* (5), 464-471.

181. Zhang, J.; Liu, W.; Schnitzler, V.; Tancret, F.; Bouler, J.-M., Calcium phosphate cements for bone substitution: Chemistry, handling and mechanical properties. *Acta Biomaterialia* **2014,** *10* (3), 1035-1049.

182. Gbureck, U.; Barralet, J. E.; Spatz, K.; Grover, L. M.; Thull, R., Ionic modification of calcium phosphate cement viscosity. Part I: hypodermic injection and strength improvement of apatite cement. *Biomaterials* **2004,** *25* (11), 2187-2195.

183. Martin, R. I.; Brown, P. W., Mechanical properties of hydroxyapatite formed at physiological temperature. *Journal of Materials Science: Materials in Medicine* **1995,** *6* (3), 138-143.

184. Barralet, J. E.; Hofmann, M.; Grover, L. M.; Gbureck, U., High-Strength Apatitic Cement by Modification with α-Hydroxy Acid Salts. *Advanced Materials* **2003,** *15* (24), 2091-2094.

185. TenHuisen, K. S.; Brown, P. W., Formation of calcium-deficient hydroxyapatite from α-tricalcium phosphate. *Biomaterials* **1998,** *19* (23), 2209-2217.

186. Fukumori, T.; Nakaoki, T., High-tensile-strength polyvinyl alcohol films prepared from freeze/thaw cycled gels. *Journal of Applied Polymer Science* **2014,** *131* (15).

187. Lespasio, M. J.; Piuzzi, N. S.; Husni, M. E.; Muschler, G. F.; Guarino, A.; Mont, M. A., Knee Osteoarthritis: A Primer. *Perm. J.* **2017,** *21*, 16-183.

188. Hunter, W., VI. Of the structure and diseases of articulating cartilages. *Philosophical Transactions of the Royal Society of London* **1743,** *42* (470), 514-521.

189. Malda, J.; Groll, J.; van Weeren, P. R., Rethinking articular cartilage regeneration based on a 250-year-old statement. *Nature Reviews Rheumatology* **2019,** *15* (10), 571-572.

190. Makris, E. A.; Gomoll, A. H.; Malizos, K. N.; Hu, J. C.; Athanasiou, K. A., Repair and tissue engineering techniques for articular cartilage. *Nature Reviews Rheumatology* **2015,** *11* (1), 21-34.

191. Murphy, M. P.; Koepke, L. S.; Lopez, M. T.; Tong, X.; Ambrosi, T. H.; Gulati, G. S.; Marecic, O.; Wang, Y.; Ransom, R. C.; Hoover, M. Y., Articular cartilage regeneration by activated skeletal stem cells. *Nature medicine* **2020,** *26* (10), 1583-1592.

192. Levy, Y. D.; Gortz, S.; Pulido, P. A.; McCauley, J. C.; Bugbee, W. D., Do fresh osteochondral allografts successfully treat femoral condyle lesions? *Clin. Orthop. Relat. Res.* **2013,** *471*, 231-7.

193. McCulloch, P. C.; Kang, R.; Cole, B. J., Osteochondral allografts for large defects in the knee. *Techniques in Knee Surgery* **2006,** *5*, 165.

194. Bayliss, L. E.; Culliford, D.; Monk, A. P.; Glyn-Jones, S.; Prieto-Alhambra, D.; Judge, A.; Cooper, C.; Carr, A. J.; Arden, N. K.; Beard, D. J.; Price, A. J., The effect of patient age at intervention on risk of implant revision after total replacement of the hip or knee: a population-based cohort study. *The Lancet* **2017,** *389*, 1424-1430.

195. Vanlommel, J.; De Corte, R.; Luyckx, J. P.; Anderson, M.; Labey, L.; Bellemans, J., Articulation of Native Cartilage Against Different Femoral Component Materials. Oxidized Zirconium Damages Cartilage Less Than Cobalt-Chrome. *J. Arthroplasty* **2017,** *32*, 256-262.

196. Ling, D.; Bodugoz-Senturk, H.; Nanda, S.; Braithwaite, G.; Muratoglu, O. K., Quantifying the lubricity of mechanically tough polyvinyl alcohol hydrogels for cartilage repair. *Proc. Inst. Mech. Eng. H* **2015,** *229*, 845-852.

197. Chan, S. M. T.; Neu, C. P.; Komvopoulos, K.; Reddi, A. H.; Di Cesare, P. E., Friction and Wear of Hemiarthroplasty Biomaterials in Reciprocating Sliding Contact With Articular Cartilage. *J. Tribol.* **2011,** *133*.

198. Fuchs, A.; Eberbach, H.; Izadpanah, K.; Bode, G.; Sudkamp, N. P.; Feucht, M. J., Focal metallic inlay resurfacing prosthesis for the treatment of localized cartilage defects of the femoral condyles: a systematic review of clinical studies. *Knee Surg. Sports. Traumatol. Arthrosc.* **2018,** *26*, 2722-2732.

199. Capadona, J. R.; Shanmuganathan, K.; Tyler, D. J.; Rowan, S. J.; Weder, C., Stimuli-responsive polymer nanocomposites inspired by the sea cucumber dermis. *science* **2008,** *319* (5868), 1370-1374.

200. Capadona, J. R.; Van Den Berg, O.; Capadona, L. A.; Schroeter, M.; Rowan, S. J.; Tyler, D. J.; Weder, C., A versatile approach for the processing of polymer nanocomposites with self-assembled nanofibre templates. *Nature Nanotechnology* **2007,** *2* (12), 765-769.

201. Holloway, J. L.; Lowman, A. M.; Palmese, G. R., The role of crystallization and phase separation in the formation of physically cross-linked PVA hydrogels. *Soft Matter* **2013,** *9*, 826-833.

202. Cha, W.-I.; Hyon, S.-H.; Ikada, Y., Transparent poly(vinyl alcohol) hydrogel with high water content and high strength. *Macromol. Chem. Phys.* **1992,** *193*, 1913-1925.

203. Koshut, W. J.; Smoot, D.; Rummel, C.; Kirillova, A.; Gall, K., Tensile Fatigue of Poly(Vinyl Alcohol) Hydrogels with Bio-Friendly Toughening Agents. *Macromol. Mater. Eng.* **2020,** *305*, 1900784.

204. Yokoyama, F.; Masada, I.; Shimamura, K.; Ikawa, T.; Monobe, K., Morphology and structure of highly elastic poly(vinyl alcohol) hydrogel prepared by repeated freezing-and-melting. *Colloid Polym. Sci.* **1986,** *264*, 595-601.

205. Cha, W.-I.; Hyon, S.-H.; Oka, M.; Ikada, Y., Mechanical and wear properties of poly(vinyl alcohol) hydrogels. *Macromol. Symp.* **1996,** *109*, 115-126.

206. Oliveira, A. S.; Schweizer, S.; Nolasco, P.; Barahona, I.; Saraiva, J.; Colaço, R.; Serro, A. P., Tough and Low Friction Polyvinyl Alcohol Hydrogels Loaded with Anti-inflammatories for Cartilage Replacement. *Lubr.* **2020,** *8*.

207. Hassan, C. M.; Peppas, N. A., Structure and morphology of freeze/thawed PVA hydrogels. *Macromolecules* **2000,** *33*, 2472-2479.

208. Mavraki, A.; Cann, P., Friction and lubricant film thickness measurements on simulated synovial fluids. *Proc. Inst. Mech. Eng. J* **2009,** *223*, 325-335.

209. Nelson, A. E.; Allen, K. D.; Golightly, Y. M.; Goode, A. P.; Jordan, J. M. In *A systematic review of recommendations and guidelines for the management of osteoarthritis: the chronic osteoarthritis management initiative of the US bone and joint initiative*, Semin. Arthritis Rheum., Elsevier: 2014; pp 701-712.

210. Myant, C.; Cann, P., In contact observation of model synovial fluid lubricating mechanisms. *Tribol. Int.* **2013,** *63*, 97-104.

211. Gong, J. P.; Kagata, G.; Osada, Y., Friction of Gels. 4. Friction on Charged Gels. *J. Phys. Chem. B* **1999,** *103*, 6007-6014.

212. Vercaigne, S.; Wolke, J. G. C.; Naert, I.; Jansen, J. A., Histomorphometrical and mechanical evaluation of titanium plasma-spray-coated implants placed in the cortical bone of goats. *Journal of Biomedical Materials Research* **1998,** *41* (1), 41-48.

213. Susi, H., [17] The strength of hydrogen bonding: Infrared spectroscopy. In *Methods in Enzymology*, Elsevier: 1972; Vol. 26, pp 381-391.

214. Zhou, Q.; Lyu, J.; Wang, G.; Robertson, M.; Qiang, Z.; Sun, B.; Ye, C.; Zhu, M., Mechanically Strong and Multifunctional Hybrid Hydrogels with Ultrahigh Electrical Conductivity. *Advanced Functional Materials* **2021,** *31* (40), 2104536.

215. Caligaris, M.; Ateshian, G. A., Effects of sustained interstitial fluid pressurization under migrating contact area, and boundary lubrication by synovial fluid, on cartilage friction. *Osteoarthr. Cartil.* **2008,** *16*, 1220-1227.

216. Li, F.; Wang, A.; Wang, C., Analysis of friction between articular cartilage and polyvinyl alcohol hydrogel artificial cartilage. *J. Mater. Sci. Mater. Med.* **2016,** *27*, 87.

217. Katta, J.; Jin, Z.; Ingham, E.; Fisher, J., Biotribology of articular cartilage—A review of the recent advances. *Med. Eng. Phys.* **2008,** *30*, 1349-1363.

218. Oungoulian, S. R.; Durney, K. M.; Jones, B. K.; Ahmad, C. S.; Hung, C. T.; Ateshian, G. A., Wear and damage of articular cartilage with friction against orthopedic implant materials. *J. Biomech.* **2015,** *48*, 1957-1964.

219. Custers, R.; Dhert, W.; van Rijen, M.; Verbout, A.; Creemers, L.; Saris, D., Articular damage caused by metal plugs in a rabbit model for treatment of localized cartilage defects. *Osteoarthr. Cartil.* **2007,** *15* (8), 937-945.

220. Du, P. Z.; Markolf, K. L.; Levine, B. D.; McAllister, D. R.; Jones, K. J., Differences in the Radius of Curvature Between Femoral Condyles: Implications for Osteochondral Allograft Matching. *J. Bone Jt. Surg.* **2018,** *100*, 1326-1331.

Biography

Jiacheng Zhao graduated from Nanjing University in 2018 before he attended Duke University for his Ph.D. degree. He was studying chemistry at Kuangyaming Honors School before coming to Duke and thus, he also majored in chemistry for the past four years.

By the time this dissertation was finished, he published the following paper as first or co-first author:

1) F. Yang; J. Zhao; W. J. Koshut; J. Watt; J. C. Riboh; K. Gall; et al. A Synthetic Hydrogel Composite with The Mechanical Behavior and Durability of Cartilage. Adv. Funct. Mater. 2020 Vol. 30 Pages 2003451

2) J. Zhao; A. Kirillova; C. N. Kelly; H. Xu; W. J. Koshut; F. Yang; et al. High-Strength Hydrogel Attachment through Nanofibrous Reinforcement. Adv. Healthc. Mater. 2021 Vol. 10 Issue 4 Pages 2001119

3) W. J. Koshut; N. Kwon; J. Zhao; A. Amendola; et al. Flaw Sensitivity and Tensile Fatigue of A High-strength Hydrogel. Int. J. Fatigue 2022 Vol. 163 Pages 107071

He also received the following fellowship from Duke:

1) Duke Graduate Travel Award